Dissertation

ALTERNATIVE COILED COIL ELECTROSTATIC INTERFACES FROM SIDE CHAIN LENGTH VARIANCE

Submitted by

Shannon John Ryan

Department of Chemistry

In partial fulfillment of the requirements for the

Degree of Doctor of Philosophy

Colorado State University

Fort Collins, Colorado

Summer 2006

Colorado State University

May 24, 2006

WE HEREBY RECOMMEND THAT THE DISSERTATION PREPARED UNDER OUR SUPERVISION BY SHANNON JOHN RYAN ENTITLED ALTERNATIVE COILED COIL ELECTROSTATIC INTERFACES FROM SIDE CHAIN LENGTH VARIANCE BE ACCEPTED AS FULFILLING IN PART REQUIREMENTS FOR THE DEGREE OF DOCTOR OF PHILOSOPHY

Committee on Graduate Work

Prof. Robert Williams

Prof. Anthony Rappé

Prof. C. Michael Elliot

Prof. Robert Woody

Advisor: Prof. Alan Kennan

Department Head: Prof. Anthony Rappé

ABSTRACT OF DISSERTATION

ALTERNATIVE COILED COIL ELECTROSTATIC INTERFACES FROM SIDE CHAIN LENGTH VARIANCE

The alpha helical coiled coil is a ubiquitious structural element found throughout nature and is comprised of two or more α-helical strands bundled via a left handed superhelical twist. These structures are attractive scaffolds for molecular recognition studies due to their regular primary sequence heptad repeat denoted *abcdefg*. The folding of component strands is primarily directed by hydrophobic interactions between residues at positions *a* and *d*. In addition, residues at positions *e* and *g* comprise the hydrophilic interface and can confer additional specificity, generally via electrostatic interactions.

Hydrophilic contacts have been shown to contribute to orientation and oligomerization specificity, primarily through the minimization of Coulombic repulsion. We sought to investigate the role of sidechain length and functionality on homodimer and heterodimer specificity. In particular, chain length variants of glutamic acid and lysine with one to four methylenes were desired. The lysine analogs were commercially available and the glutamic acid variants were synthesized utilizing an olefin cross metathesis strategy between a bis-protected allyl glycine and Grubbs' first and second generation ruthenium catalysts. This modular approach allows access to different amino acid analogs by choice of metathesis partners as well as choice of protecting group. Solid phase peptide synthesis can proceed utilizing alpha amino acids protected with a Boc or

Fmoc group. Initial attempts using a Boc strategy were unsuccessful and discarded in favor of an Fmoc one.

These amino acids were incorporated into a sequence based on the coiled coil domain of GCN4 with persubstitution of *e* and *g* positions with the appropriate carboxylic acid or amine residues. Pure component solutions bearing chain length extended carboxylate side chains contain a helical signal as measured by circular dichroism (CD) spectroscopy, while corresponding amines do not. Equimolar heterodimeric complexes contain a range of stabilities as measured by CD. These stability differences can be exploited to control complex formation. Most notably, the native glutamic acid – lysine interaction can be exchanged to form the more stable side chain length extended carboxylate - lysine complex.

Shannon John Ryan
Department of Chemistry
Colorado State University
Fort Collins, CO 80523
Summer 2006

I would first like to thank Alan Kennan for being a great advisor. Alan, your open door allowed for many enjoyable discussions about chemistry and life, both of which were incredibly instructive. I look forward to hearing updates about lab happenings and the latest triumphs in darts. I would also like to thank my former labmate Nate, for his assistance and guidance as the senior graduate student. I learned a great deal from you and enjoyed our conversations. To my current labmates Phil, Maria, and Brent I have enjoyed working with you and hope I have taught you as much as you have taught me. The great friends I have made during graduate school have made this process all the more enjoyable, Collin, Javier and Chris our long bicycle rides eased the stress and gave us the necessary time to vent. My entire family has always understood my need to be a "Professional Student" and none of this would be possible without your love and support. A special thanks to my parents, who always stressed the importance of education and hard work.

I have left the person I owe the deepest gratitude for last. To my wife Sarah, you have been there through the ups and downs in graduate school and life. I appreciate the many sacrifices you have made for me. You have been my confidante and friend and I look forward to opening the next chapter of our lives together. I love you.

Table of Contents

Chapter 1

Background

1-1 Molecular Recognition and Biological Assemblies

The control of biological assemblies remains a difficult task within the area of molecular design. The impacts of interface variation within these macromolecules is difficult to ascertain in a global approach. To gain a better understanding of these interactions, minimization of the gross interactions to a single subset may provide valuable information regarding these interfaces. One attractive scaffold in the study of molecular recognition utilizing biological assemblies is the α-helical coiled coil. This

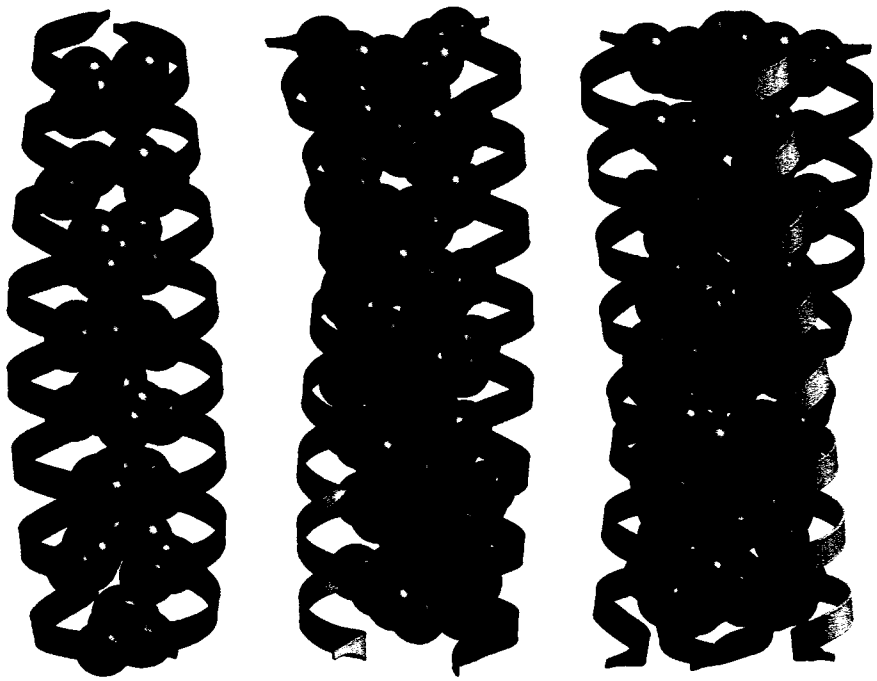

Figure 1. Coiled coil structures for dimer, trimer, and tetramer. Helix backbones represented as colored ribbons. Interior residues shown as grey spheres. Exterior residues omitted for clarity.

structural motif is ubiquitous throughout nature, found in such things as structural support proteins, recognition domains, and membrane fusion proteins. Work in this field has led to a general understanding of protein-protein interactions, but has been limited to

proteinogenic amino acids. The use of unnatural amino acids will allow for the design of novel assemblies that cannot be constructed using current methods.

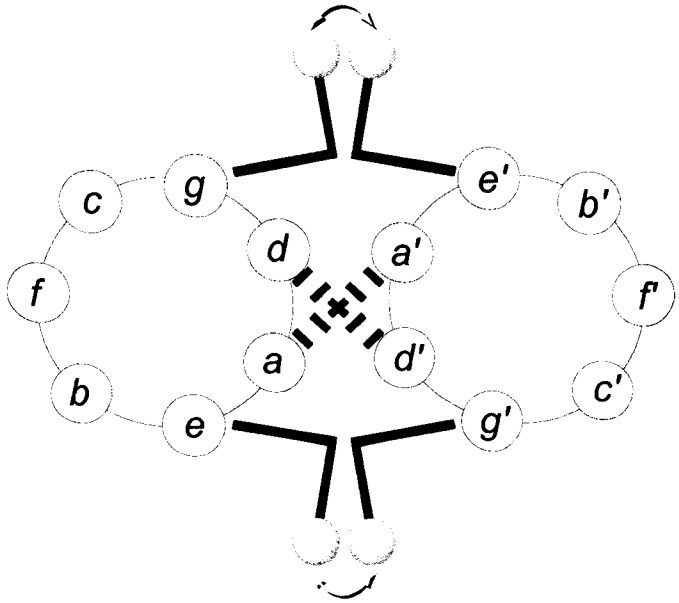

Figure 2. Schematic diagram of coiled coil heptad positions. Hydrophobic residues at *a* and *d* positions control assembly (interaction indicated by dashes). Core flanking *e* and *g* positions contribute to specificity (interaction depicted by grey spheres). Remaining positions *b, c,* and *f* are largely solvent exposed in lower order oligomers.

1-2 Alpha Helical Coiled Coil

The alpha helical coiled coil is a common structural element and is comprised of two or more α-helical strands bundled via a left handed superhelical twist in a parallel or anti-parallel manner (Figure 1). These structures contain a primary sequence heptad repeat denoted *abcdefg*, with residues containing hydrophobic side chains found primarily at positions *a* and *d* (Figure 2). The burial of these hydrophobes is the largest driving force for coiled coil assembly. There are also potential interactions at positions flanking the hydrophobic core, namely between residues found at positions *e* and *g*. These interactions can determine orientation and oligomerization specificity, primarily through reduction of electrostatic repulsion. The remaining positions (*b, c,* and *f*) are

largely solvent exposed and contain residues that are helix promoting such as lysine, glutamine, and alanine.[1] The high level of sequence regularity found in α-helical coiled coils make them an attractive scaffold for studies in molecular recognition.

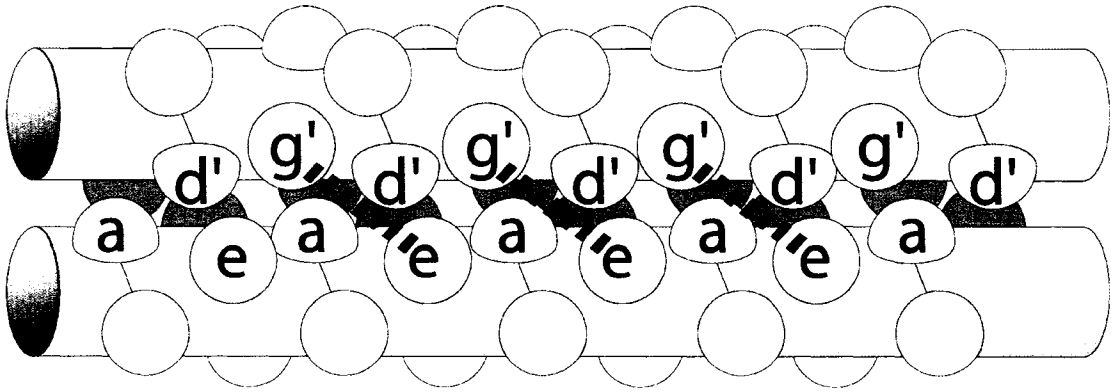

Figure 3. Schematic representation of "knobs into holes" core packing. Cylinders represent helical backbone. Hydrophilic interface interactions shown as dashed lines. Solvent exposed residues in white.

As stated previously, the burial of hydrophobic residues is the largest driving force for coiled coil assembly. Upon folding, these residues exhibit a "knobs into holes" arrangement where the sidechain from an *a* residue on one helix packs against an *a* residue on the opposing strand and between residues *d, e* and *g* (Figure 3).[2] The antiparallel orientation packs in a similar fashion, except *a* residues pack against *d* residues. This packing motif is well characterized and its use to control orientation and oligomerization will be discussed (*vida infra*).

The interaction between residues found at positions *e* and *g* comprise another recognition element that plays a role in determining coiled coil specificity. These interactions are comprised primarily of electrostatic interactions between positively charged ammonium or guanidinium groups and negatively charged carboxylates. This control element has been implicated in specificity determination in a variety of natural

and designed systems.[3] Although this interface is well regarded as a specificity determinant, its role in stabilizing coiled coils has been hotly contested.[4] Irrespective of the stability imparted by the hydrophilic interface, its stability contribution is small when compared to the hydrophobic interface. Assembly strategies utilizing the hydrophilic interface will be discussed at length in subsequent chapters.

Coiled coils have garnered much recent interest and their importance in biological assemblies is well documented. Their simplicity and regular sequence make them attractive templates for design studies in molecular recognition. The remainder of this chapter will highlight several examples of design principles that are particularly relevant, leading to current efforts in this field.

1-3 Coiled Coil Design – Oligomerization

The largest body of work in α-helical coiled coils has focused on the naturally occurring protein GCN4, a yeast transcription factor that contains a basic DNA binding region and a coiled coil region. The crystal structure of the coiled coil region indicates conserved hydrophobic residues with the exception of a central polar asparagine residue, in an *a* position, which forms a buried hydrogen bond to the corresponding asparagine residue in the opposing helix.[5] Investigation of the importance of this residue, as well as positional effects of hydrophobic substitution in the core, was completed by Kim and coworkers. They removed the core asparagine, and per-substituted the *a* or *d* position with leucine, valine or isoleucine. Depending on the substitution pattern of these amino acids, stable complexes with various oligomerization states were formed (Table 1).[6] Analysis of the crystal structures indicated three different packing motifs, defined by the position of the core sidechain Cα-Cβ bond relative to the vector connecting Cα of

residues on the opposing helix. The three types of packing are: perpendicular, where the Cα-Cβ bond is at a 90° angle; parallel, when the Cα-Cβ bond is parallel; and acute, where the Cα-Cβ bond is at a 60° angle (Figure 4). Utilizing these broad geometric packing constraints, some general rules could be ascertained as follows: β-branched amino acids found at *d* positions disfavor dimer formation, at *a* positions disfavor tetramer formation, and substitution at *a* and *d* positions favors trimer formation.

Table 1. Oligomerization dependence on hydrophobic pattern.[6]

Position *a*	Position *d*	Tm (°C)	No. Helices
GCN4-p1	GCN4-p1	53	2
I	L	>100	2
I	I	>100	2
L	I	>100	4
V	I	73	NA
L	V	81	3
V	L	95	(2,3)
L	L	>100	3

As shown by the work outlined above, the removal of this central asparagine residue leads to the formation of various oligomerization states. This polar residue in the hydrophobic core specifies for oligomerization state as a result of the increased solvation of dimeric systems versus trimeric or tetrameric. Substitution of this central asparagine with other polar residues such as lysine, glutamine, serine or threonine results in various oligomerization states.[7] Replacement of asparagine with lysine forms a dimeric complex with intermediate stability (Tm=45°C), whereas glutamine replacement forms complexes with greater stability (Tm=60°C) but results in a mixture of dimers and trimers.[8] In a comprehensive study by Hodges and co-workers, all twenty amino acids were substituted in a central *a* position. In this study they report that glutamine substitution results solely in trimer formation.[9] The disparity between these two studies could arise from a

difference in overall sequence or the use of covalently linked peptides in the Hodges study.

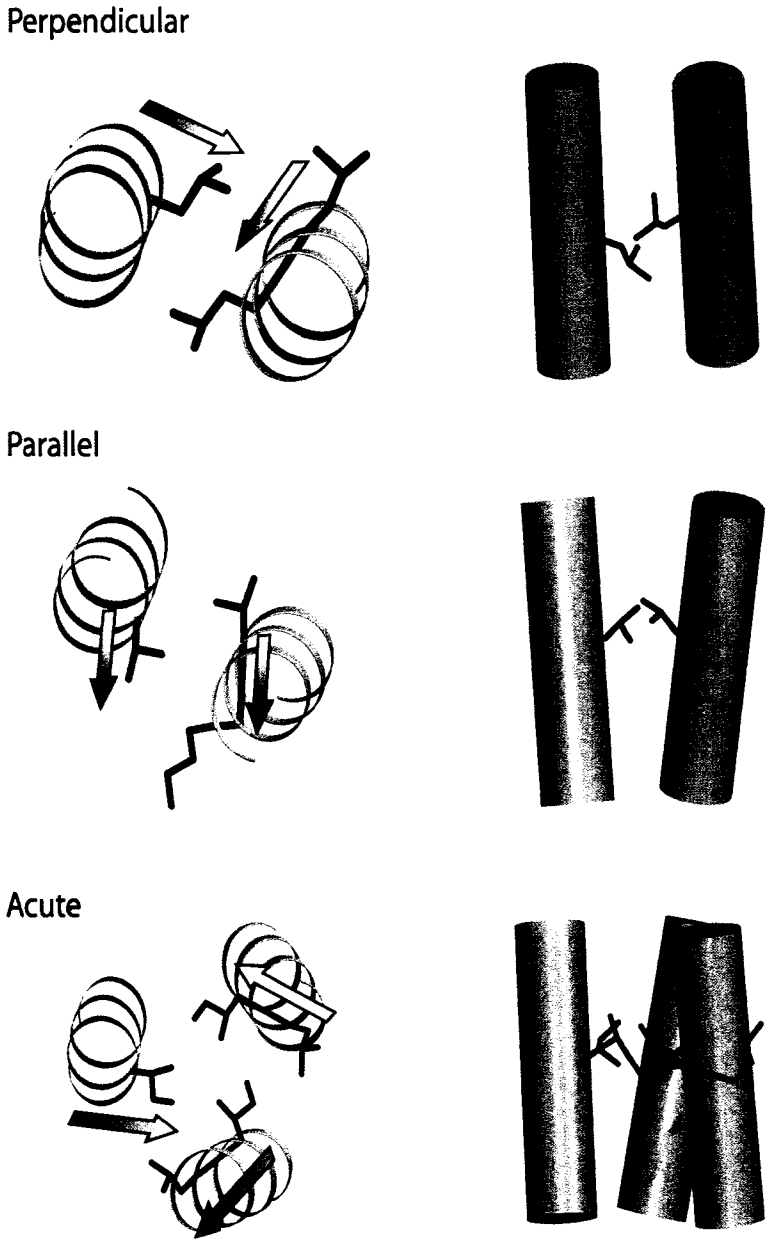

Figure 4. Hydrophobic core packing angles. Participating residues shown from both a top down orientation and side view. Hydrophobic residues are shown in red and blue with orientation of bond of interest and Cα- Cα vector in green.

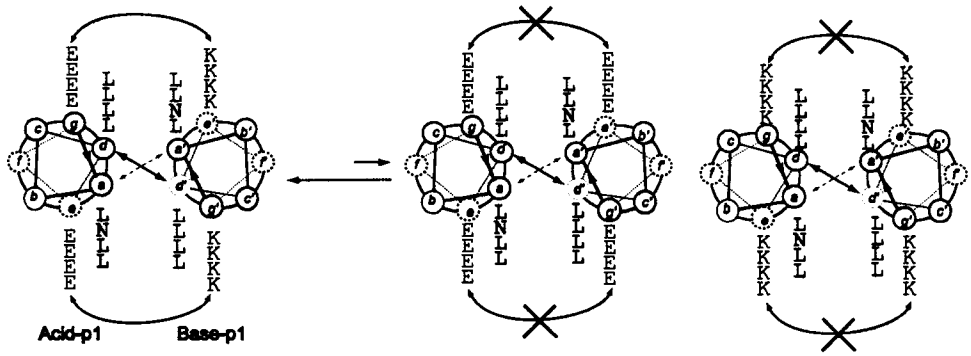

Figure 5. Persubstituted Acid-p1 and Base-p1 peptides. Electrostatic repulsions in homodimeric complexes (Acid-p1:Acid-p1 or Base-p1:Base-p1, right) should favor formation of heterodimer (Acid-p1:Base-p1, left). Non interacting residues omitted for clarity.

In general, mutation of a central asparagine residue leads to a decrease in specificity. In contrast, utilizing the hydrophilic interface, Kim and coworkers were able to form complexes with a high level of specificity. They used the GCN4 sequence with a central asparagine reside and persubstituted the *e* and *g* residues with lysine (Base-p1) or glutamic acid (Acid-p1, Figure 5). They reasoned the equilibrium should favor heterodimer formation, because of electrostatic repulsions present in each homodimer. Analysis of an equimolar solution indicated the formation of a stable heterodimer (Figure 6). In order to further investigate the effects of electrostatics, specifically on the Acid-p1 and Base-p1 homodimers, these peptides were covalently linked through a disulfide

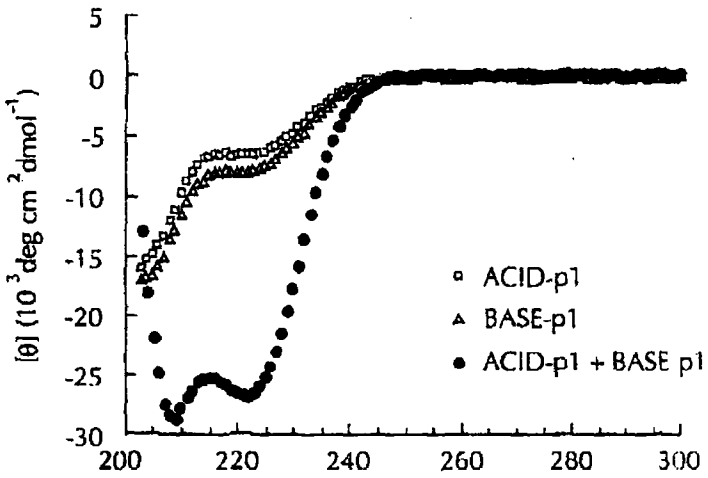

Figure 6. Wavelength scan of **Acid-p1** (squares), **Base-p1** (triangles) and **Acid-p1:Base-p1** (circles). Figure taken from O'Shea, E.K. et al. 1993.[10]

bond. This disulfide linkage works to stabilize coiled coil formation, so that these complexes can be further investigated. Initial experiments tested the effects of pH on these complexes. As the pH is lowered, the stability of the covalently linked Acid-p1 increases. In contrast, the opposite trend is observed with the covalently linked Base-p1 peptide, where an increase in pH leads to increased stability (Figure 7). These results support that electrostatic repulsion destabilizes potential homodimers: as the charge is

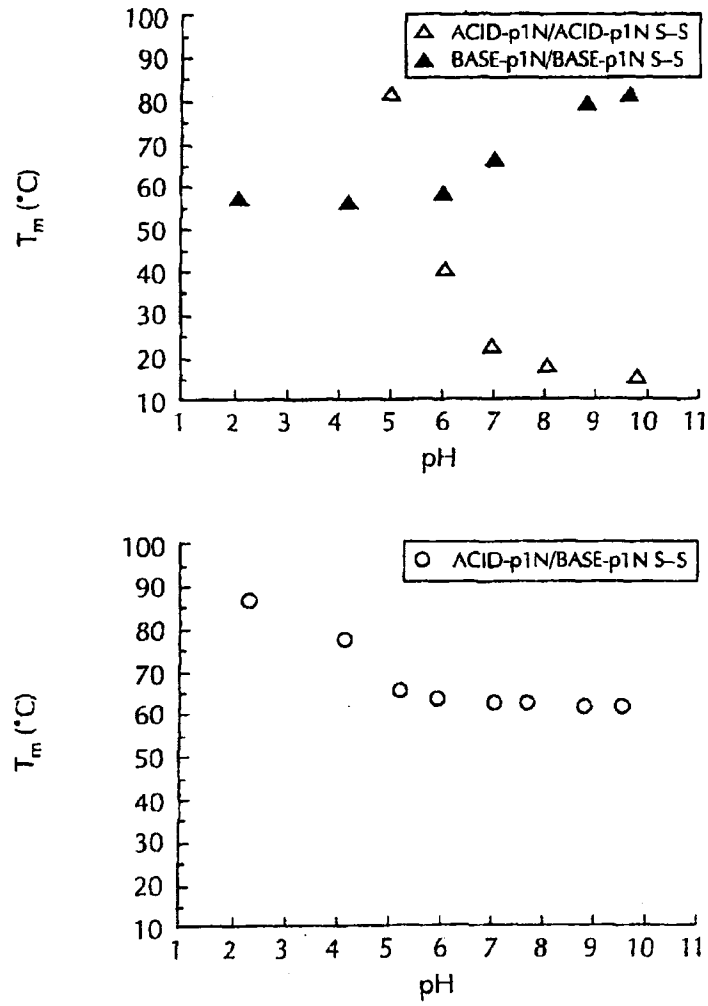

Figure 7. Effect of pH on melting temperatures (Tm) of covalently linked homodimers (top) and covalently linked heterodimer (bottom). Figure from O'Shea et al. 1993.[10]

removed through protonation of the acid or deprotonation of the amine, the complex gains stability. In agreement with these results, changes in pH minimally affect the covalently linked heterodimer, which exhibits only a slight increase in stability at low pH (Figure 7). In addition, if complementary electrostatics are playing a stabilizing role, increasing salt concentration should effectively lower complex stability. The change in stability of the Acid-p1:Base-p1 heterodimer with increased concentrations of NaCl is negligible (Figure 8), indicating that specificity results from minimization of electrostatic repulsions.[10] Further investigation into specificity determinants using the Acid-p1:Base-p1 heterodimer found that mutation of the central asparagine to leucine results in an increase in stability, but loss of specificity, forming parallel and antiparallel heterotetramers. These studies indicate the critical role a central asparagine plays with regard to specificity, albeit at the cost of stability.[11]

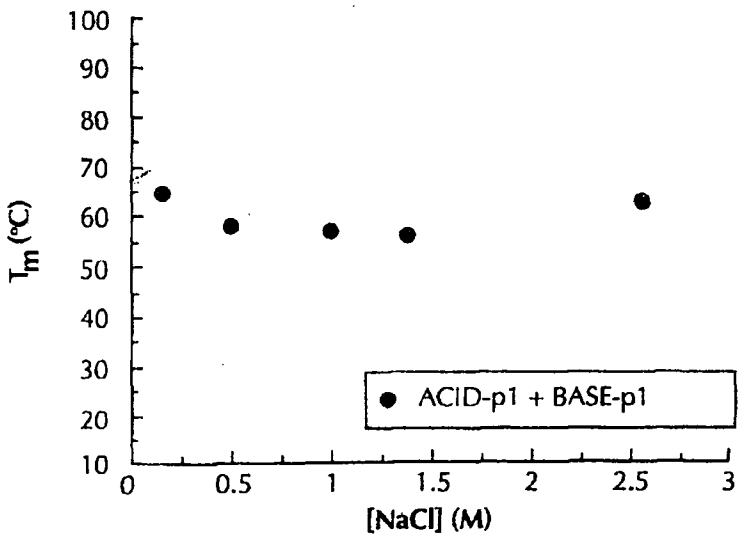

Figure 8. Effect of salt concentration on melting temperature (Tm) in heterodimeric complexes. Figure taken from O'Shea et al. 1993.[10]

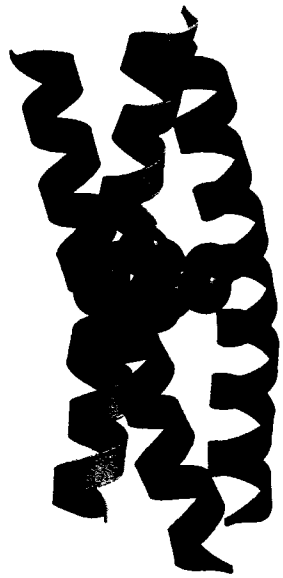

Figure 9. Crystal structure of GCN4 alanine core mutant. Benzene molecule, shown in gray, is tightly bound in the hydrophobic core, stabilizing trimer.

Further investigation of the hydrophobic core, led Alber and co-workers to design a model system that could be regulated by addition of a small molecule ligand. In this system, they mutated the central asparagine residue of GCN4-p1 to an alanine residue. With this mutation, dimeric oligomerization was favored but not exclusively. They reasoned that trimer formation should be disfavored as a result of the steric void caused by the small methyl side chain of alanine, but trimer formation could be stabilized by addition of a small molecule that would fill this void (Figure 9). Modeling studies suggested that benzene or cyclohexane would be appropriate ligands to test this theory. Indeed, addition of benzene increased the thermal stability of these complexes by 9 °C and favored trimer formation. Analysis of the crystal structure indicates the benzene bound in the cavity formed by methyl side chain of each alanine residue.[12]

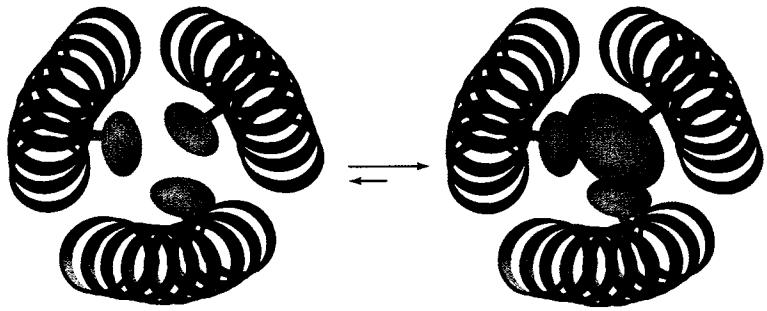

Figure 10. Diagram of first generation system. Homomeric complex (left) contains a steric void as a result of three alanine residues packed against each other. Heteromeric complex (right) contains a 2:1 mixture of alanine:cyclohexyl alanine. Cyclohexyl alanine packs in void left by alanine residues.

Mindful of this work by Alber and coworkers, our group has utilized the idea of size complementarity to control oligomerization specificity. Whereas Alber and coworkers utilized a small molecule ligand, early studies in our group wanted to incorporate the ligand into the participating peptides. By matching two small residues with one large residue, the steric matching of these residues results in complex formation. To accomplish this, two peptides were used, one containing an alanine residue and the other containing a cyclohexyl alanine at a central *a* position in each peptide (Figure 10).

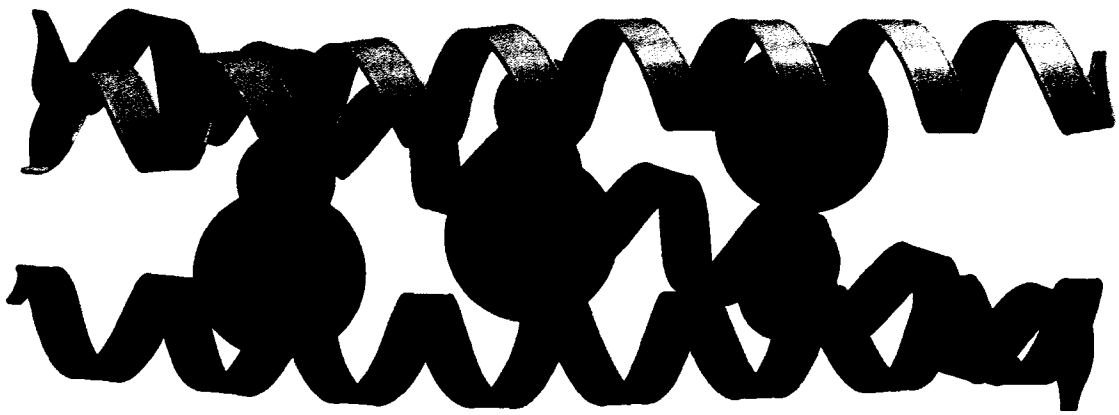

Figure 11. Crystal structure representation of second generation system. Each peptide contains 2 alanine residues and 1 cyclohexyl alanine residue. Heteromeric complex formation is successful when each peptide bears the correct orientation of alanine and cyclohexyl alanine residues.

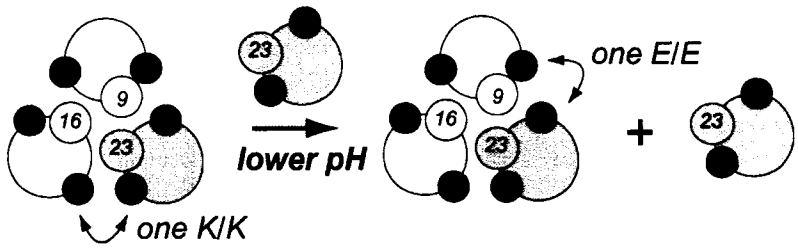

Figure 12. Initial complex contains a mis-matched Lys-Lys interaction. Decreasing the pH results in single peptide exchange, where a single Glu-Glu interaction is tolerated due to low pH.

Utilizing these peptides a hetero-trimeric coiled coil was preferentially formed. These studies also indicated that specificity was lost if the cyclohexyl alanine sidechain was changed to contain napthyl alanine or cyclopropyl alanine. These results demonstrate that specific interaction occurs between the alanine and cyclohexyl alanine groups, while the napthyl group is likely too large and the cyclopropyl group is too small.[13,14] Although this initial system validated the idea of utilizing steric matching to control specificity, the cyclohexyl alanine peptide formed a homotrimeric complex with greater stability than the designed trimer. A second generation system was then developed, such that the designed complex would be more stable than component peptide homotrimers. This system contained substitution at three distinct *a* layers, with each peptide containing a cyclohexyl alanine and two alanines in different sequences. An equimolar mixture of these peptides forms a 1:1:1 heterotrimer with each peptide contributing the cyclohexyl group for one core layer (Figure 11).[14] More control over these systems was achieved by exploiting electrostatic interactions at the hydrophilic interface. Analysis of these heterotrimers revealed that in the presence of a sterically matched core, an electrostatic repulsion between peptides containing a lysine-lysine interface was tolerated at neutral pH. Similarly, when all hydrophilic interfaces were matched, a single mismatched core layer

containing alanine was tolerated.[15] Utilizing these orthogonal interfaces and effects of environmental changes, namely pH, control of complex formation can be achieved. In these experiments a preformed trimer with a mis-matched hydrophilic interface was used. Modification of the pH to disfavor the initial trimer results in replacement of one strand from the complex with a new strand that may contain a different mis-matched interface allowing for further manipulation (Figure 12). Utilizing these mis-matches and pH changes, multiple peptide exchanges could take place.[16]

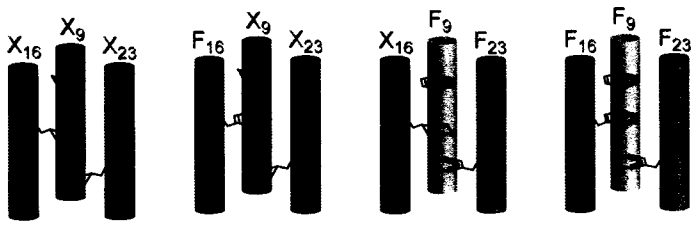

Figure 13. Substitution of central *a* positions with cyclohexyl alanine or phenyalanine. Each layer also contains two alanine side chains (not shown). Other core layers and non core positions omitted for clarity.

More recent efforts in our lab have shown that phenylalanine is also a suitable steric matching partner when matched with alanine residues in the hydrophobic core. It is interesting to note however that substitution in a similar fashion to the cyclohexyl alanine system results in a trimer with decreased stability. Mixing of the core layers between phenylalanine and cyclohexyl alanine results in increased stability as more cyclohexyl alanine residues are added (Figure 13). These results indicate that phenylalanine is a suitable replacement for cyclohexyl alanine in 2:1 steric matching schemes.[17] In addition, the use of phenylalanine allows for native expression of these complexes, allowing for widespread use of this recognition domain in more intricate systems.

1-4 Coiled Coil Design – Orientation

The relative position of N and C termini, or strand orientation, in coiled coils has received much attention recently as an increasing number of naturally occurring anti-parallel coiled coils have been discovered.[18] Orientation specificity, like oligomerization specificity, has been controlled through hydrophobic and hydrophilic elements. Early studies to control orientation employed careful repositioning of the central asparagine residue so that in the antiparallel orientation an asparagine-asparagine interaction could occur, but in the parallel orientation a repulsive asparagine-leucine interaction would occur in the hydrophobic core (Figure 14).[19] To determine relative helix orientation in this system, an equilibrium thiol-disulfide exchange assay was performed. In this experiment a Gly-Gly-Cys linker is placed at the N or C-terminus of the investigated peptide, which allows for covalent linkage via a disulfide bond. Peptides are then mixed in an inert atmosphere and can equilibrate to form the most stable complex. The HPLC spectra analyzing the appropriately functionalized Acid-a1 and Base-a1 indicate that the

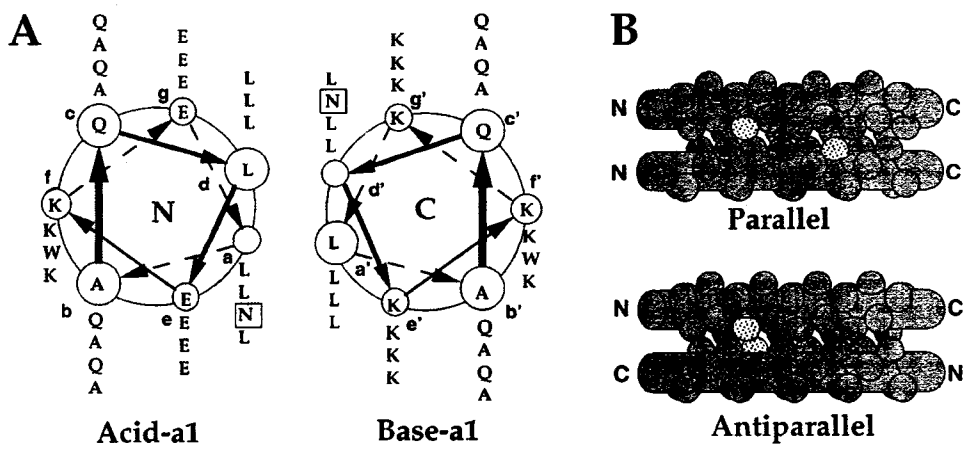

Figure 14. Helical wheel diagram (**A**) of the antiparallel Acid-a1:Base-a1 complex. Schematic view (**B**) of Asn interaction in hydrophobic core in parallel (destabilizing) or antiparallel orientation. Figure from Oakley et al. 1998.[19]

antiparallel orientation is preferred (Figure 15). Interestingly, covalently linked peptides with both orientations are helical, with the antiparallel orientation exhibiting greater stability. Unfortunately, a single asparagine is unable to confer complete specificity, and due to the destabilizing nature of polar substitution in the hydrophobic core, additional asparagine substitution cannot be utilized. Therefore, other interactions will need to be exploited.

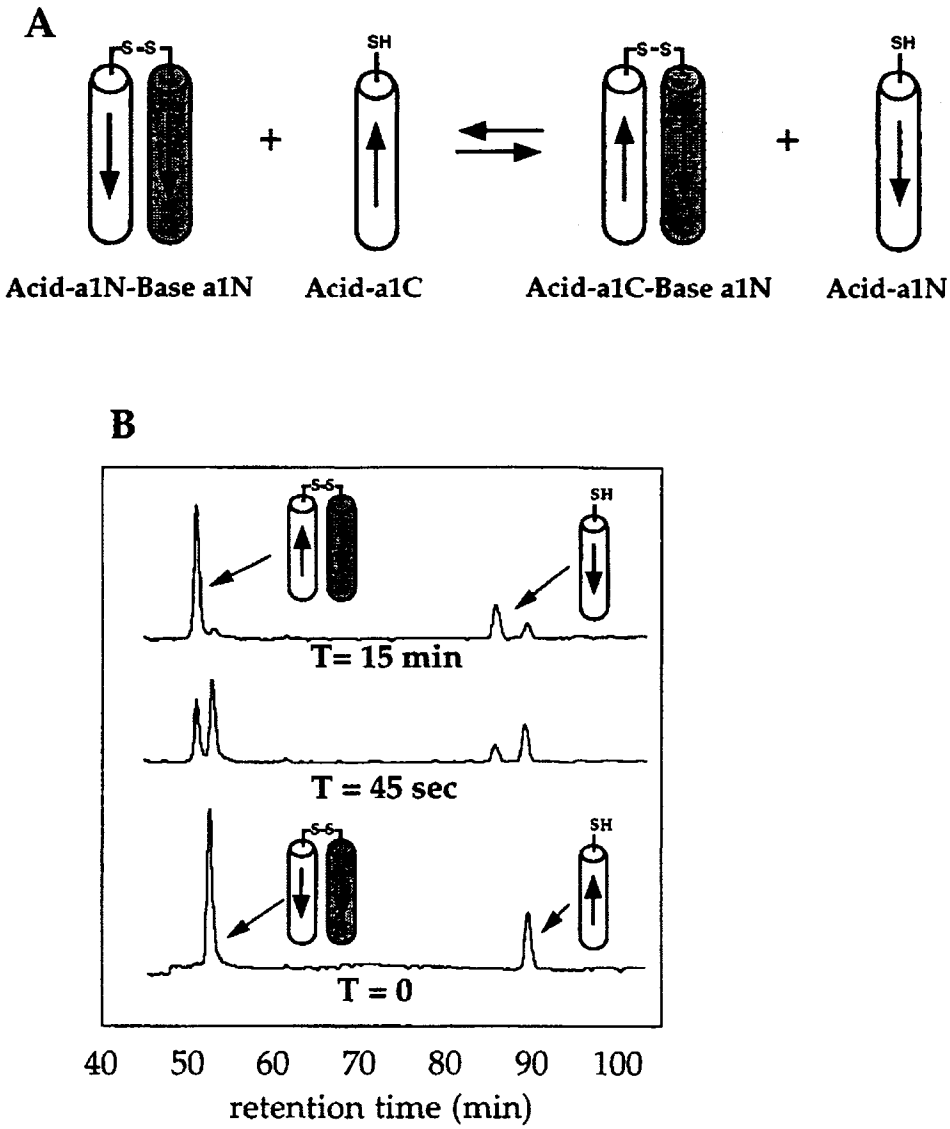

Figure 15. Schematic representation (**A**) of disulfide exchange assay. HPLC spectra (**B**) of disulfide exchange. Initial complex (bottom trace) contains parallel heterodimer. Disulfide exchange results in formation of new heterodimer (middle trace) as evidenced by new peak. Complete exchange occurs to form antiparallel complex (back trace) Figure from Oakley and Kim 1998.[19]

The issue of antiparallel specificity has been addressed by Oakley and coworkers in two studies where they separately report on formation of a heterodimeric and homodimeric antiparallel coiled coils. In the heterodimeric example, orientation specificity was obtained by modification of the hydrophilic interface such that the parallel orientation results in electrostatic repulsions that are diminished in the antiparallel orientation.[20] Further investigations indicate that a buried polar interaction and avoidance of two repulsive electrostatic interactions contribute similarly to coiled coil orientation.[21] More recently, Oakley and coworkers have developed a homodimeric antiparallel coiled coil by utilizing design elements at the hydrophobic core and hydrophilic interface. In the core, isoleucine substitutions at *d* positions could favorably pack against alanine residues at *a* positions in the antiparallel orientation, while the parallel orientation is disfavored as a result of destabilizing alanine-alanine interactions. A single arginine residue was placed in the hydrophobic core to specify for dimer formation.[22] At the

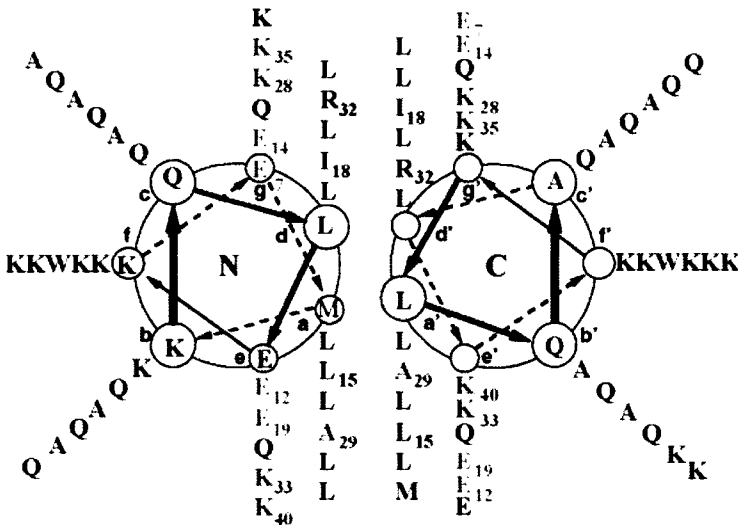

Figure 16. Helical wheel diagram of homodimeric antiparallel coiled coil. In antiparallel orientation, potential for 8 coulombic attractions at the hydrophilic interface, whereas 8 coulombic repulsions would result in the parallel orientation. Placement of an arginine residue imparts dimerization specificity. Figure from Gurnon et al. 2003.[23]

hydrophilic interface the judicious placement of glutamic acid and lysine residues results in eight attractions in the antiparallel orientation, but eight potential repulsions in the parallel orientation (Figure 16).[23] Utilizing these design elements, Oakley and coworkers successfully designed a homodimeric antiparallel coiled coil.

Hodges and coworkers developed a similar system utilizing core constraints to specify orientation. In this system alternating pairs of alanine and leucine at central core positions direct strand orientation by avoiding all alanine core layers. Each relevant level consisted of an Ala-Leu-Ala-Leu core composition. Interestingly, electrostatics were degenerate in this system, indicating that the preference for the antiparallel orientation was solely the result of hydrophobic core organization.[24]

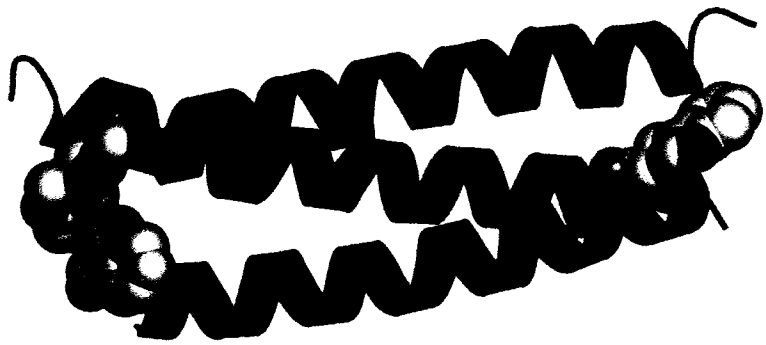

Figure 17. Crystal structure showing helix backbone (green) and N-terminal tryptophan residues (space filling). All other residues omitted for clarity.

DeGrado and coworkers designed a study meant to produce a parallel dimeric species, but inadvertently created an antiparallel trimer. The hydrophobic core contains leucine at all positions with the exception of a tryptophan residue at the N-terminus. This single tryptophan residue is competent to drive orientation in this system, as neither the remainder of the hydrophobic core nor interactions at the hydrophilic interface should provide a driving force for antiparallel formation. In addition, the crystal structure indicates that an all tryptophan layer may not be stericly tolerated (Figure 17).[25]

Work in our group to control strand orientation has been built on the knowledge we have gained using steric matching to drive oligomerization *(vida supra)*. In these initial studies, the core layer on one of the peptides was changed such that the alanine, cyclohexylalanine, alanine substitutions were positioned at *d* residues. In order for proper steric matching to occur, the complex would need to form in the antiparallel orientation (Figure 18). Thiol-disulfide equilibrium exchange studies confirmed the preference for the antiparallel orientation of these complexes. In addition, through use of mismatched interfaces and changes in pH, it is possible to control complex formation between the parallel orientation and the antiparallel orientation through changes in pH.[26]

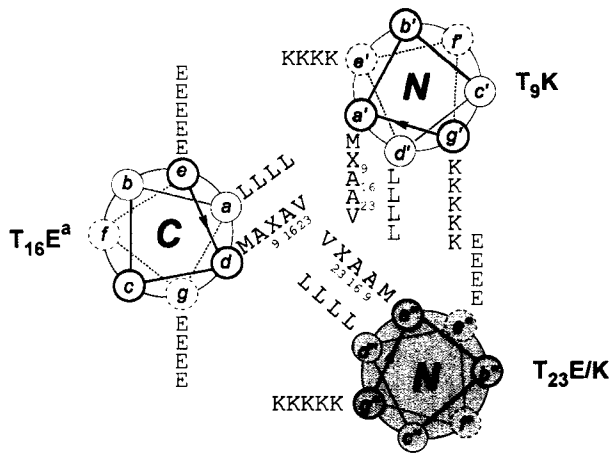

Figure 18, Helical wheel projection of anti-parallel complex. $T_{16}E$ contains alanine and cyclohexyl alanine residues substituted at *d* positions. T_9K and $T_{23}E/K$ contain alanine and cyclohexyl alanine residues at *a* positions. Proper steric matching results in antiparallel orientation.

1-5 Side Chain Length and Functionality

Work in our lab to this point has focused largely on controlling orientation and oligomerization though steric matching in the hydrophobic core. Investigation of orientation and oligomerization based on interactions at the hydrophilic interface, in our

lab as well as others, has been largely limited to the twenty natural amino acids. In the early study using covalently linked homodimers Acid-p1 and Base-p1, Kim and coworkers postulated that the stability difference at neutral pH was a function of the tether length between the peptide backbone and charged functional group. This was supported by studies they completed using covalently linked peptides persubstituted with lysine analogs: ornithine (3 methylenes) and diaminobutyric acid (2 methylenes). In both cases these peptides did not show evidence for structure at 0 °C.[10] We started this project with a simple question: what role does sidechain length and functional group play in controlling coiled coil assembly? The ensuing chapters will describe, in detail, our progress towards answering this question.

1-6 Literature Cited

1 (a) O'Neil, K.T.; DeGrado, W.F. *Science*, **1990,** *250*, 646-651. (b) Bryson, J.W.; Betz, S.F.; Lu, H.S.; Suich, D.J.; Zhou, H.X.; O'Neil, K.T.; Degrado, W.F. *Science*, **1995,** *270,* 935-941. (c) Engel, D.E.; DeGrado, W.F. *J. Mol. Biol.* **2004**, *337*, 1195-1205.

2 Crick, F. *Acta Crystallogr.* **1953,** *6*, 689-697.

3 (a) Meier, M.; Lustig, A.; Aebi, U.; Burkhard, P.J. *J. Struct. Biol.* **2002**, *137*, 65-72. (b) Litowski, J.R.; Hodges, R.S.; *J. Biol. Chem.* **2002**, *277*, 37372-37279. (c) Burkhard, P.J.; Ivaninskii, S.; Lustig, A.J. *J. Mol. Biol.* **2002**, *318*, 901-910.

4 (a) Lumb, K.J.; Kim, P.S. *Science*, **1995**, *268*, 436-438. (b) Lavigne, P.; Sonnichsen, F.D.; Kay, C.M.; Hodges, R.S. *Science,* **1996,** *271,* 1136-1137. (c) Lumb, K.J.; Kim, P.S. *Science*, **1996**, *271,* 1138. (d) Wendt, H; Leder, L.; Harma, H.; Jelesarov, I.; Baici, A.; Bosshard, H.R. *Biochemistry*, **1997**, *36*, 204-213. (e) Durr, E.; Jelesarov, I.; Bosshard, H.R. *Biochemistry*, **1999**, *38*, 870-880. (f) Marti, D.; Jelesarov, I.; Bosshard,

H.R. *Biochemistry*, **2000**, *39*, 12804-12818. (g) Phelan, P.; Gorfe, A.A.; Jelesarov, I.; Marti, D.N.; Warwicker, J.; Bosshard, H.R. *Biochemistry*, **2002**, *41*, 2998-3008. (h) Marti, D.N.; Bosshard, H.R. *Biochemistry*, **2004**, *43*, 12436-12447.

5 O'Shea, E.K.; Klemm, J.D.; Kim, P.S.; Alber, T. *Science*, **1991**, *254*, 539-544.

6 Harbury, P.D.; Zhang, T.; Kim, P.S.; Alber, T. *Science*, **1993**, *262*, 1401-1407

7 (a)Eckert, D.M.; Masahkevich, V.N.; Kim, P.S. *J. Mol. Biol.* **1998**, 284, 859-865, (b)Gonzalez, L.; Woolfson, D.N.; Alber, T.A. *Nat. Struct. Biol.* **1996**, 3, 1011-1018

8 (a)Gonzalez, L.; Woolfson, D.N.; Alber, T. *Nat. Struct. Biol.* **1996,** *13*, 1011-1018. (b) Akey, D.L.; Malashkevich, V.N.; Kim, P.S. *Biochemistry*, **2001,** *40*, 6352-6360. (c) Campbell, K.M.; Sholders, A.J.; Lumb, K.J. *Biochemistry,* **2002**, *41*, 4866-4871. (d) Campbell, K.M.; Lumb, K.J. *Biochemistry*, **2002**, *41*, 7169-7175.

9 Wagschal, K,. Tripet, B.; Lavigne, P.; Mant, C.; Hodges, R.S. *Protein Science*, **1999**, *8*, 2312-2329.

10 O'Shea, E.K.; Lumb, K.J.; Kim, P.S. *Curr. Biol*, **1993**, *3*, 658-667.

11 Lumb, K.J.; Kim, P.S. *Biochemistry,* **1995**, *34*, 8642-8648.

12 Gonzales, L.; Plecs, J.J.; Alber, T. *Nat. Struct. Bio.* **1996**, *3*, 510-514.

13 Schnarr, N.A.; Kennan, A.J. *J. Am. Chem. Soc.* **2001**, *123*, 11081-11082

14 Schnarr, N.A.; Kennan, A.J. *J. Am. Chem. Soc.* **2002**, *124*, 9779-9783.

15 Schnarr, N.A.; Kennan, A.J. *J. Am. Chem. Soc.* **2003**, *125*, 667-671.

16 (a) Schnarr, N.A.; Kennan, A.J. *J. Am. Chem. Soc.* **2003**, *125*, 6364-6365. (b) Schnarr, N.A.; Kennan, A.J. *J. Am. Chem. Soc.* **2003**, *125*, 13046-13051.

17 Travisano, P.; Kennan, A.J. *Org. Lett.* **2004**, *6*, 4219-4222.

18 Add Reference about Natually occurring antiparallel Coiled coils

19 Oakley, M.G.; Kim, P.S. *Biochemistry* **1998**, *37*, 12603-12610.

20 McClain, D.L.; Woods, H.L.; Oakley, M.G. *J. Am. Chem. Soc.* **2001**, *123*, 3151-3152.

21 McClain, D.L.; Binfet, J.P.; Oakley, M.G. *J. Mol. Biol.* **2001**, *313*, 371-383.

22 McClain, D.L.; Gurnon, D.G.; Oakley, M.G. *J. Mol. Biol.* **2002**, *324*, 257-270.

23 Gurnon, D.G.; Whitaker, J.A.; Oakley, M.G. *J. Am. Chem. Soc.* **2003**, *125*, 7518-7519.

24 Monera, O.D.; Zhou, N. E.; Lavigne, P.; Kay, C.M.; Hodges, R.M. *J. Biol. Chem.* **1996**, 3995-4001.

25 Lovejoy, B.; Choe, S.; Cascio, D.; McRorie, D.K.; DeGrado, W.F.; Eisenberg, D. *Science* **1993**, *259*, 1288-1293.

26 (a) Schnarr, N.A.; Kennan, A.J. *J. Am. Chem. Soc.* **2004**, *126*, 14447-14451. (b) Schnarr, N.A.; Kennan, A.J. *Org. Lett.* **2005**, *7*, 395-398.

Chapter 2

Unnatural Amino Acid Synthesis and Peptide Incorporation

2-1 Introduction

One objective in our studies of α-helical coiled coil model systems is the development of orthogonal interfaces for increased control of peptide complexes. Initial efforts in our lab targeted the hydrophobic core via a steric matching strategy (*vida supra*). As the hydrophilic interface also plays an important role in controlling coiled coil assembly, the study of this interface may prove instructive. Previous efforts to probe this interface have focused on the proteinogenic amino acids. This limits analysis of this interface to a relatively small subset of possible functional groups. The use of electrostatic interactions between glutamic acid – lysine pairs has been studied in oligomerization and orientation studies.[1] Of particular interest is the work completed by Kim and coworkers, where persubstition of the hydrophilic interface led to heterodimer specificity. Furthermore, in this study they examined the effects of covalently linking peptides persubstituted with lysine analogs: diaminobutyric acid (two methylenes) and ornithine (three methylenes). These covalently linked homodimers did not show any evidence for complex formation.[2] Mindful of these studies, an appropriate starting point for analysis of the hydrophilic interface is using the natural carboxylate – ammonium interaction and varying the number of methylenes separating the functional group and peptide backbone. In order to study these complexes a number of glutamic acid and lysine analogs were needed (Figure 1). The appropriate lysine analogs are readily commercially available, but the glutamic acid analogs must be independently synthesized. As such, we explored several alternatives, hoping to identify a route that

was sufficiently modular to permit preparation of several different targets, efficient enough to generate multigram quantities, and compatible with standard side chain protecting groups for direct use in solid-phase peptide synthesis.

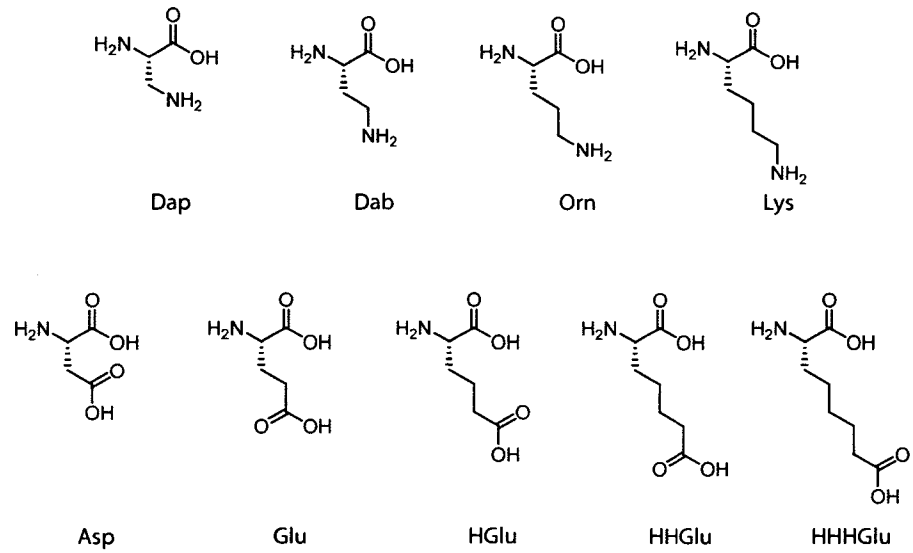

Figure 1. Desired sidechain analogs of lysine and glutamic acid to probe effects of sidechain length on coiled coil stability

Olefin metathesis has been utilized in a variety of contexts, from simple molecules to those of incredible complexity.[3] We sought to utilize olefin cross metathesis as a modular approach to various unnatural amino acids. Allyl glycine is an attractive common synthetic intermediate as it can be easily prepared on gram scale from readily available starting materials and further elaborated via olefin cross metathesis. Allyl glycine has been utilized in diverse metathesis reactions, and the facile access to suitable coupling partners further supports the viability of this route.[4,5]

2-2 Allyl Glycine Synthesis

The synthesis of properly protected glutamic acid analogs was envisioned to proceed through olefin cross metathesis of protected allyl glycine and a corresponding coupling partner. The synthesis of allyl glycine followed the route developed by Myers

and co-workers and was completed in four steps (Scheme 1).[6] The first step, a condensation of glycine methyl ester hydrochloride (**2**) with (R,R)-(-)-pseudoephedrine hydrochloride (**1**) proceeds in moderate yield (67%, crystallized) to form the glycinamide (**3**). Diastereoselective alkylation of glycinamide (**3**) with allyl bromide proceeds in excellent yield (96%) and diastereoselectivity (96% d.e.). A single recrystallization increases the diastereoselectivity (>99% d.e.) with a loss in overall yield (61%). Hydrolytic removal of the chiral auxiliary and Boc or Fmoc protection proceeds in moderate to good yields (69% and 89%, respectively). Benzylation of the resultant free acid proceeded in moderate yields (Fmoc 63%, Boc 56%). Attempts to increase the yield through modification of reaction conditions met with limited success. Alternative reaction conditions such as pre-formation of the cesium salt and reaction with benzyl bromide (51%), as well as Fisher esterification (25%) did not improve overall yields.[7] Modification of the initial reaction conditions resulted in the best yields and was utilized. Benzylation provided the bis-protected allyl glycine (**5, 6**) suitable for olefin cross metathesis.

Solvent	Benzyl Bromide (eq)	Sodium Bicarbonate (eq)	Yield (%)
DMF	3	3	27
DMF	5	3	47
DMF	8	3	40
DMF	10	3	35
DMF	2	5	63
Dioxane	10	3	0

Table 1. Modification of Benzylation reaction conditions using Fmoc-Allylglycine-OH.

Scheme 1. Synthesis of allyl glycine derivative.

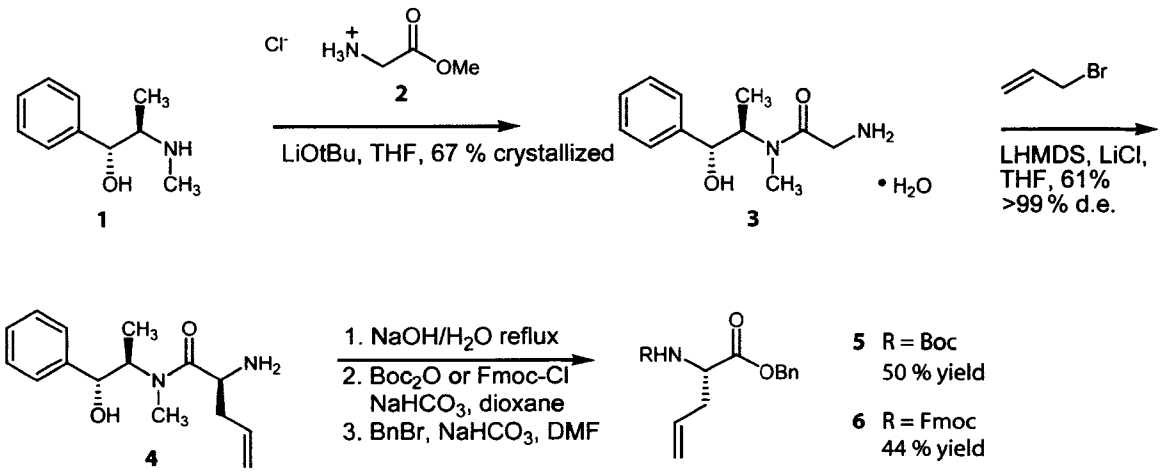

2-3 Homoglutamic Acid synthesis[8]

Our initial target was homoglutamic acid (HGlu) which contains an additional methylene in its sidechain, and we preferred a derivative compatible with Boc peptide synthesis methods (Scheme 2). Reaction of commercially available cyclohexyl acrylate with (**5**) in the presence of Grubbs' second generation catalyst (**7**), followed by hydrogenation of the olefin and benzyl protecting group, produced HGlu (**8**) in good

Scheme 2. Synthesis of Boc HGlu.

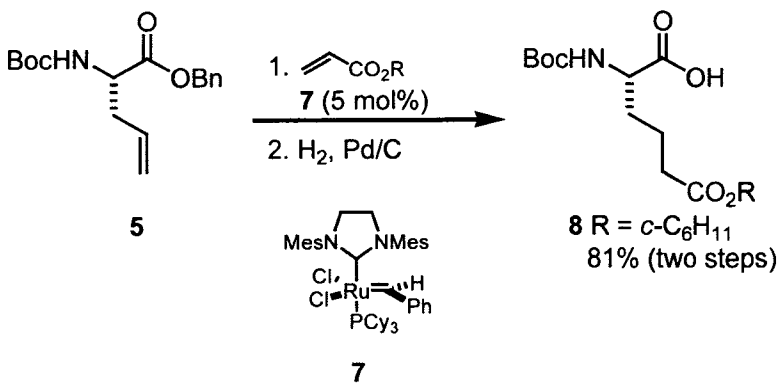

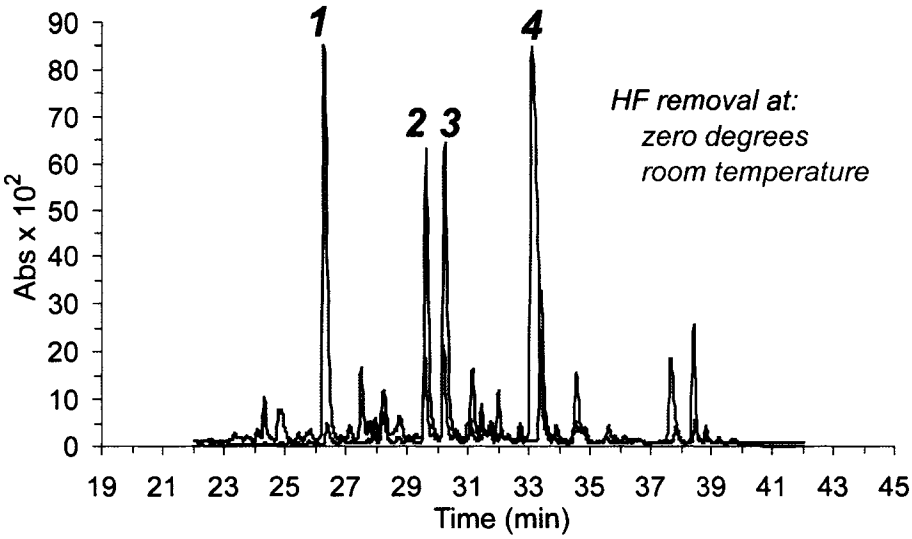

Figure 2. Crude HPLC of Boc-HGlu test peptide (Aba-LKALE*KE*LAL-NH_2, E* = HGlu) with HF removed at zero degrees (green) or room temperature (red) Collection and electrospray mass spectrometry analysis reveals: Peak 4 (MW_{obs} = 1495.9), Peak 2,3 (MW_{obs} = 1405.7), Peak 1 (MW_{obs} = 1315.6)

yield and high optical purity (methyl ester formed with diazomethane is >99% ee by chiral HPLC). Having prepared Boc-HGlu with the sidechain protected as its cyclohexyl ester (a standard protecting group for Boc peptide synthesis), we undertook its incorporation into a short test peptide containing two HGlu monomers (Figure 2, red trace). The synthesis of this test peptide appeared to proceed smoothly, producing a single dominant peak in the crude HPLC. Analysis of the isolated major product

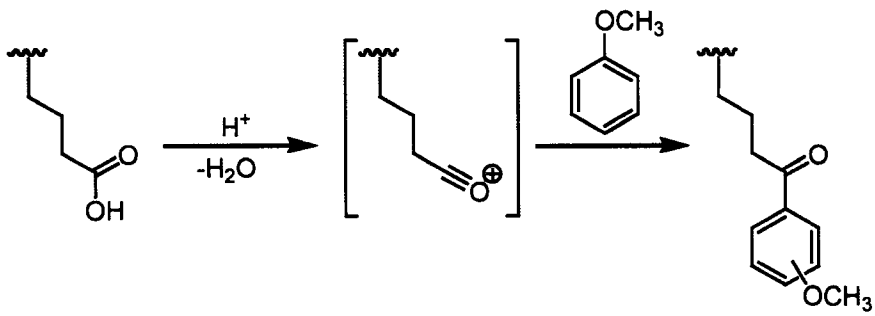

Figure 3. Possible explanation for unsuccessful Boc synthesis. Acylium ion formation and capture with anisole produces a peptide whose molecular weight is 90 mass units high per alkylation.

revealed that its molecular weight was 180 mass units too high (MW_{obs} = 1495.9, MW_{calc} = 1315.6). This increase in mass is consistent with bis-alkylation of HGlu-derived acylium ions by the anisole scavenger used during cleavage with anhydrous HF (Figure 3), a result similar to known side reactions of glutamic acid residues.[9]

It is not clear why conditions that routinely produce only minor if any glutamic acid alkylation should favor near complete modification of HGlu. During the cleavage procedure, the vessel had warmed to room temperature during HF removal, and a repeat experiment using an ice bath throughout did improve matters, affording the desired peptide as the major peak. Unfortunately, significant contamination remained from two other peaks with identical masses corresponding to mono-alkylation (MW_{obs} = 1405.73, Figure 1, green trace). As a result the Boc strategy was abandoned in favor of an Fmoc one.

Scheme 3. Synthesis of Fmoc HGlu

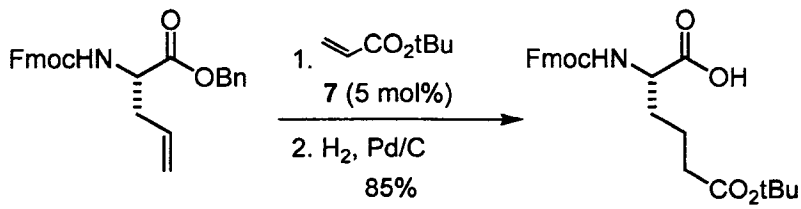

6 **10**

Peptide synthesis using the Fmoc strategy necessitates a change in the side chain acid protecting group to *tert*-butyl rather than cyclohexyl ester. Thus, HGlu preparation requires commercially available *tert*-butyl acrylate as a metathesis coupling partner. Again, cross metathesis followed by hydrogenation provides Fmoc-HGlu (**10**) suitable for Fmoc solid phase peptide synthesis (Scheme 3). To determine the feasibility of peptide synthesis using this glutamic acid homolog, a second test sequence was used. This shorter sequence was designed with only one modified residue, to aid in deciphering

possible side products. Fortunately, the synthesis gave the desired peptide as the dominant peak in the crude HPLC (Figure 4).

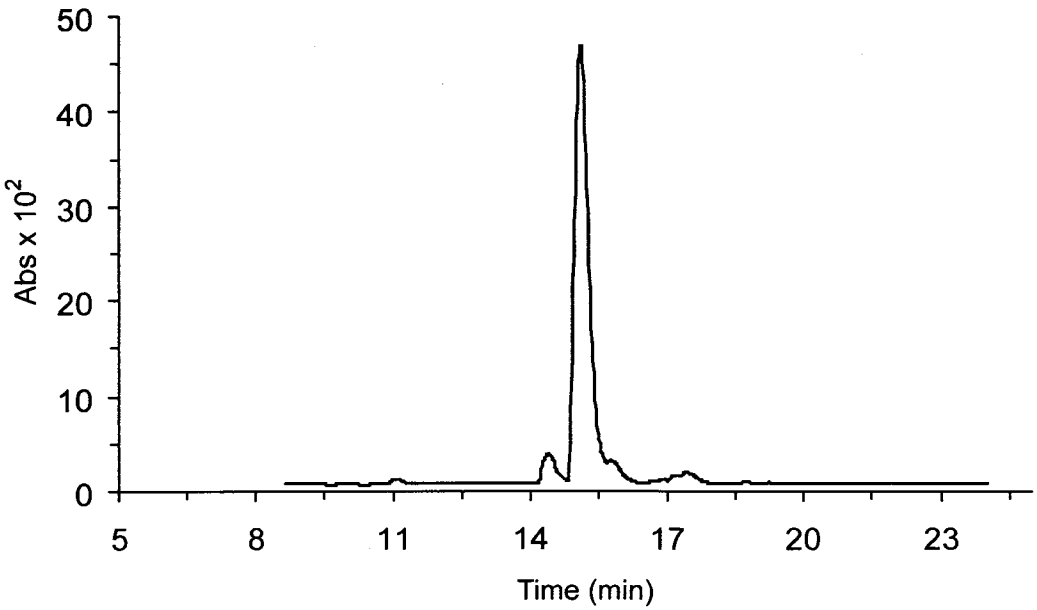

Figure 4. HPLC analysis of crude peptide (Aba-KLE*KG-NH_2, E* = HGlu). Dominant peak is desired peptide (MW_{calc} = 747.4, MW_{obs} = 748.4)

2-4 Extended Side Chain Length Analogs

Upon completion of the HGlu monomer synthesis and successful incorporation into test peptide sequences, synthesis of the four and five methylene sidechain analogs of glutamic acid (**17, 18**) were investigated. In order to synthesize these higher order homologues, suitable cross metathesis partners are required. Conveniently, both vinyl and allyl acetic acid (**11, 12**) can be converted to the corresponding *tert*-butyl esters (**13, 14**) by reaction with isobutylene and catalytic sulfuric acid in methylene chloride (Scheme 4).[10] Although the yields are only moderate, the low cost starting materials make this a feasible route to multigram quantities of the desired esters.

Scheme 4. Synthesis of Metathesis substrates

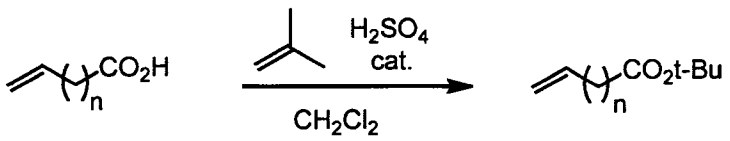

11 n = 1
12 n = 2

13 n = 1, 42 %
14 n = 2, 40 %

With the alkene substrates available, investigation of the cross metathesis using Grubbs' first generation catalyst was investigated. The electron deficient nature of the olefins found in *tert*-butyl and cyclohexyl acrylate precluded the use of this less active catalyst in the synthesis of HGlu. However, previous work had shown that Grubbs' first generation catalyst afforded higher yields than the second generation one with allylglycine (**6**) and a functionalized carbohydrate.[5] Initial attempts using the first generation catalyst (**15**) proceeded in moderate overall yields (Table 1). Attempts to optimize reaction conditions, including varying the catalyst loading and increasing the equivalents of alkene substrate, resulted in slight increases in yield. Adding additional catalyst (10 mole percent) after an initial reaction time (6 h), did not significantly improve yields as previously suggested.[5] In addition, pre-formation of the alkene dimer did not lead to increased yields as previously reported in other systems.[11] Although the alkene dimer

Scheme 5. Cross Metathesis using first generation catalyst.

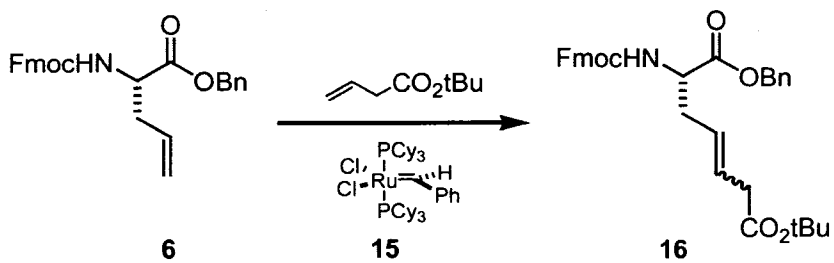

6 **15** **16**

was a competent cross metathesis partner in this reaction, the alkene monomer was quickly consumed, putatively forming the reaction product and slower reacting homodimer. Modified reaction conditions that provided the greatest overall yield proceeded by initial addition of five mole percent catalyst and two equivalents of alkene. Monitoring the reaction demonstrated that after two hours, formation of product had slowed, and at this time an additional aliquot of catalyst and alkene were added. This procedure was repeated twice more, significantly increasing the catalyst loading and alkene concentration, leading to enhanced yields.

Monomer (Eq)	Catalyst (mol %)	Yield
2	5	36
2	20	38
5	20	44
5	20[a]	44
2[b]	5	24
8[c]	20	81

Table 1. Optimization of cross metathesis reaction utilizing Grubbs' first generation catalyst. (a) Initial addition of 10 mol % catalyst followed by additional 10 mol % catalyst (b) preformation of alkene dimer (c) sequential addition of 2 equivalents of alkene and 5 mol % catalyst

Further investigation into the cross metathesis found that Grubbs' second generation catalyst (**7**) was more active, leading to similar yields (73%) in an operationally simpler manner. Concomitant deprotection of the benzyl ester and olefin reduction (Scheme 5) was accomplished through hydrogenation, providing the four methylene analog of glutamic acid (**17,** HHGlu). The five methylene analog of glutamic acid (HHHGlu) can be synthesized in a similar strategy utilizing the *tert*-butyl ester of allyl acetic acid (**14**), providing an analog (**18**) suitable for Fmoc solid phase peptide

synthesis. Each product was optically pure, as judged by chiral HPLC evaluation of the corresponding methyl ester.

Scheme 6. Synthesis of Fmoc derivatives

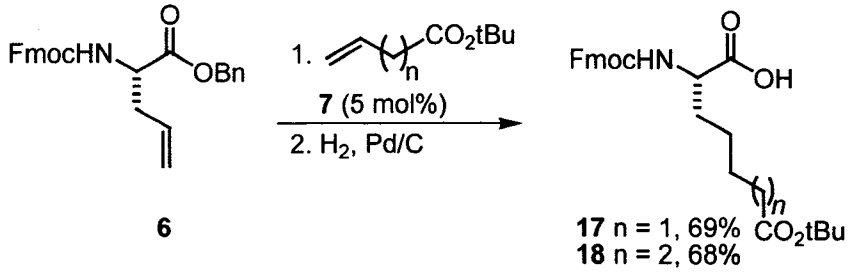

6

17 n = 1, 69%
18 n = 2, 68%

With the HHGlu and HHHGlu analogs in hand, we proceeded to incorporate them into test peptides. Utilizing the monosubstituted test peptide sequence, these amino acids were successfully incorporated, yielding the dominant peak in the crude HPLC (Figure 5). We then sought to incorporate these monomers in the context of a more realistically useful sequence, in particular one that contained multiple copies of the new amino acid. This sequence is derived from GCN4, a natural coiled coil, and contains eight copies of the unnatural amino acid among its thirty residues. The synthesis of this peptide proceeded smoothly, as indicated by HPLC analysis of the crude peptide (Figure 6).

This modular approach has proven to be an efficient means by which to obtain chain-extended glutamic acid analogues that are suitable for Fmoc solid phase peptide synthesis. These derivatives can be prepared on multigram scale, allowing for the inclusion of multiple copies into relatively long model peptides.

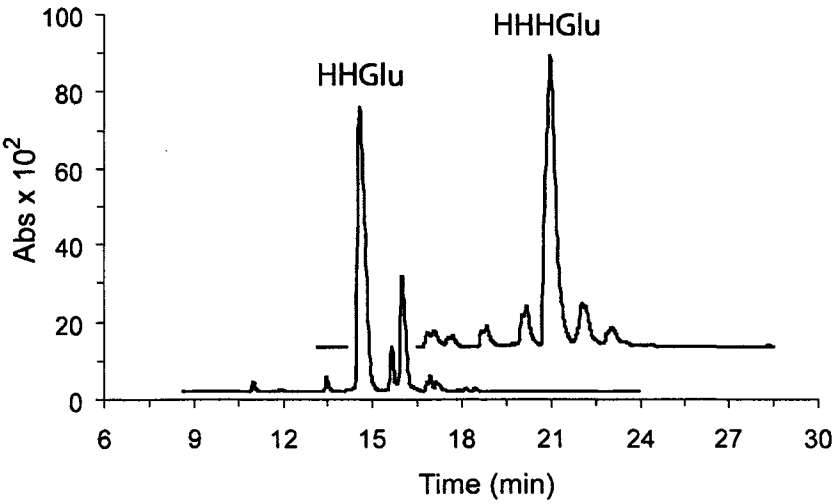

Figure 5. HPLC analysis of crude peptide (HHGlu - Aba-KLE**KG-NH_2, E** = HHGlu; HHHGlu Aba-KLE***KG-NH_2, E*** = HHHGlu). Dominant peaks are desired peptide (HHGlu MW_{calc} = 761.4, MW_{obs} = 762.5; HHHGlu MW_{calc} = 775.5, MW_{obs} = 776.5)

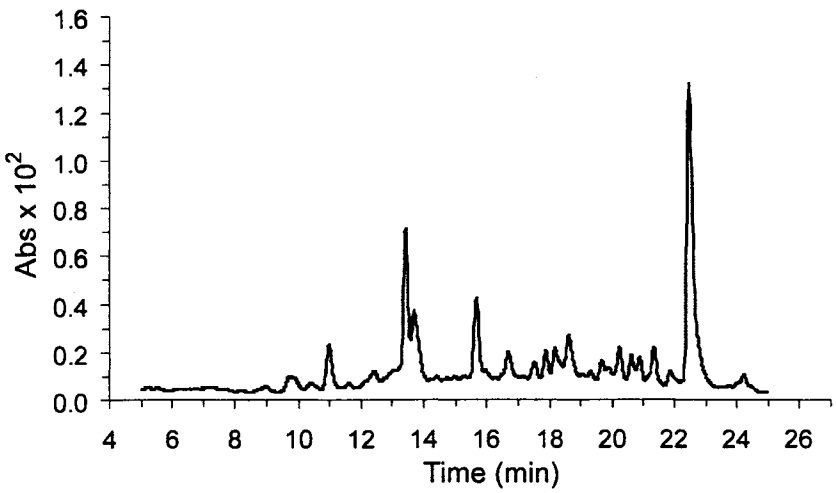

Figure 6. Crude HPLC trace of peptide containing 8 copies of the unnatural HGlu residue (Ac-AQLE*KE*LQALE*KE*NAQLE*KE*LQALE*KE*LAQ-NH_2, underlined lysine contains acetamidobenzoic acid attached to the sidechain as a spectroscopic tag. The desired peptide is the dominant peak

2-5 Experimental

General Methods. Tetrahydrofuran was freshly distilled from sodium-benzophenone ketyl. Methylene chloride was degassed with argon and passed through two columns of

neutral alumina. Column chromatography was performed on EM Science silica gel 60 (230 – 400 Mesh). Thin layer chromatography was performed on EM Science 0.25 mm silica gel 60-F plates. Visualization was accomplished with UV light or $KMnO_4$ followed by heating. All chemicals were obtained from Sigma-Aldrich (Milwaukee, WI) unless noted.

Infrared spectra were obtained on a Nicolet Avatar 320 FT-IR spectrometer. ^1H NMR spectra were obtained on a Varian 400 MHz spectrometer at ambient temperature. Data are reported as follows: chemical shift in parts per million (δ, ppm) from an internal standard [tetramethylsilane (TMS) or deuterated chloroform ($CDCl_3$)], multiplicity (s = singlet, d = doublet, t = triplet, q = quartet, and m = multiplet), coupling constant (Hz), and integration. ^{13}C NMR was recorded on a 100 MHz spectrometer at ambient temperature. Chemical shifts are reported in ppm from $CDCl_3$, taken as 77.0 ppm. Mass spectra were obtained on a Fisons VG Autospec. High performance liquid chromatography (HPLC) was performed on an Agilent model 1100 equipped with a diode array detector using the indicated Chiracel columns.

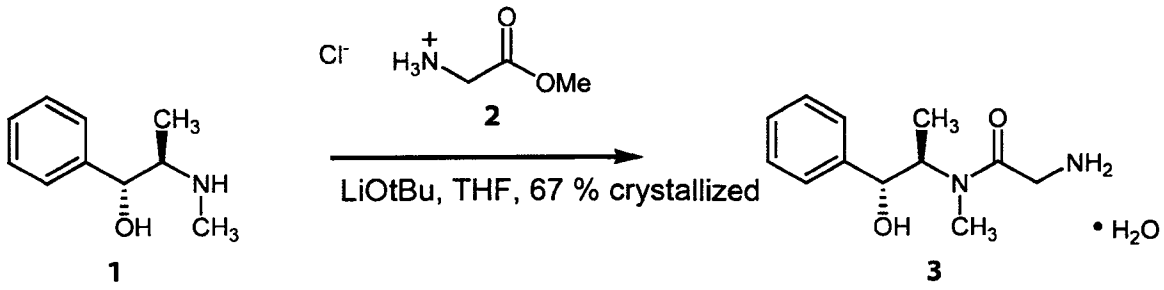

A round bottom flask was equipped with a stir bar and flame dried. The flask was charged with pseudoephedrine (20.0 g, 121.12 mmol) and glycine methyl ester (19.7 g, 157.46 mmol, 1.3 equiv.) To this, freshly distilled tetrahydrofuran (150 mL) was added

and allowed to stir for twenty minutes. After this time, lithium *tert*-butoxide (13.6 g, 169.57 mmol, 1.4 equiv.) was added and allowed to stir for two hours. Following this period, water (130 mL) was added and the tetrahydrofuran was removed *in vacuo*. The remaining aqueous phase was extracted with methylene chloride (330 mL). The aqueous phase was saturated with sodium chloride and re-extracted with methylene chloride (4 x 80 mL). The combined organic phases were dried over sodium sulfate and concentrated *in vacuo,* resulting in a yellow oil. This oil was dissolved in hot tetrahydrofuran (100 mL) and water (4 mL) was added. The solution was allowed to stand at room temperature overnight, whereupon crystals were present. The resulting mixture was cooled to -20°C for 4 hours then washed with cold (-20°C) ether (2 x 75 mL). Resulting crystals were dried *in vacuo*. All spectroscopic data agree with those previously reported.[6]

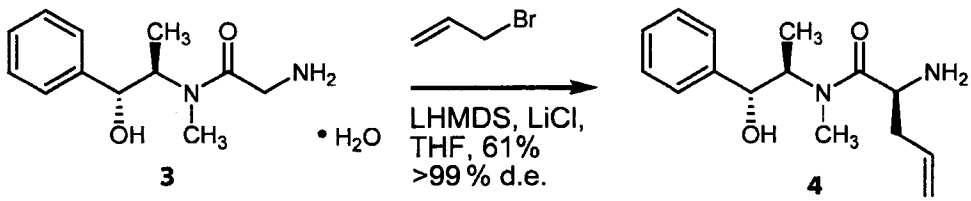

A flame-dried three necked round bottom flask equipped with a stir bar and a pressure equalizing addition funnel was charged with lithium chloride (7.0 g, 166.32 mmol, 4.0 equiv) and freshly distilled tetrahydrofuran (125 mL). After stirring for 20 minutes, pseudoephedrine glycinamide (10.0 g, 41.58 mmol) was added portionwise over a period of five minutes, and the resulting slurry was stirred in an ice bath for 20 minutes. Lithium hexamethyldisilizane (LHMDS, 66 mL of a 1 M solution in THF, 66 mmol, 1.6 equiv) was added dropwise by addition funnel over 20 minutes followed by stirring in an

ice bath for 20 minutes. Additional LHMDS (66 mL of a 1 M solution in THF, 66 mmol, 1.6 equiv) was then added in one portion. The reaction was allowed to cool in an ice bath for an additional 20 minutes, followed by allyl bromide addition (3.8 mL, 43.7 mmol, 1.1 equiv) over 3 minutes, and stirring at 0 °C for one hour. Water (100 mL) was added, and the solution was acidified to pH 0 with 6N HCl. This biphasic solution was then washed with 200 mL of ethyl acetate. The resulting organic layer was sequentially extracted with 3N HCl and 1N HCl (100 mL each). The combined aqueous layers were cooled in an ice bath and basified to pH 14 with a 50% sodium hydroxide solution. This solution was then extracted with dichloromethane (200 mL, then 3 x 75 mL). The resulting organic layers were dried over sodium sulfate and concentrated *in vacuo* resulting in a yellow oil which solidified upon standing *in vacuo* (9.37 g, 96% yield). The yellow solid was dissolved in hot toluene (20 mL) and allowed to cool to room temperature and stand overnight at which time crystals were present. The solution was cooled to -20 °C for 6 hours then washed sequentially with 10 mL cold (-20 °C) toluene and four 20 mL portions of ether. The crystals were then dried *in vacuo*. All spectroscopic data agree with those previously reported.[6]

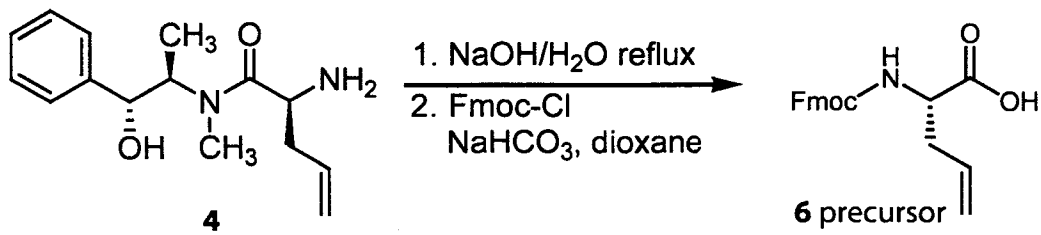

4 **6** precursor

A round bottom flask equipped with a stir bar and condenser, and charged with allylglycinamide (9.85 g, 37.6 mmol), aqueous 1 M sodium hydroxide (75.2 mL, 75.2 mmol, 2 equiv.) and water (75 mL) was heated to reflux for 2 hours. Upon cooling,

pseudoephedrine was observed to crystallize from the solution. The aqueous solution was extracted with dichloromethane (100 mL, then 50 mL) to remove residual pseudoephedrine. Each organic layer was individually back extracted with water (50 mL) and the aqueous layers were combined with the original aqueous solution and concentrated *in vacuo* to a volume of 75 mL. Dioxane (75 mL) and sodium bicarbonate (6.3 g, 75.2 mmol, 2 equiv) were added to this solution, followed by cooling in an ice bath for 20 minutes and subsequent addition of 9-fluorenylmethoxychloride (10.7 g, 41.3 mmol, 1.1 equiv). After stirring for three hours (the first hour at 0 °C, then room temperature) water (250 mL) was added, and the solution was washed with 1:1 ethyl acetate:ether (400 mL). The resulting organic layer was washed with a 2% sodium bicarbonate solution (100 mL). The combined aqueous layers were acidified to pH 1 with 1 N HCl and extracted with ethyl acetate (2 x 200 mL). The organic layers were dried over sodium sulfate and concentrated *in vacuo*. Residual dioxane was removed by dissolving the residue in toluene (50 mL) and concentrating *in vacuo*, followed by dissolving in chloroform (2 x 50 mL) and concentrating *in vacuo,* yielding an amorphous solid (8.78 g, 69% yield). All spectroscopic data agree with those previously reported.[6]

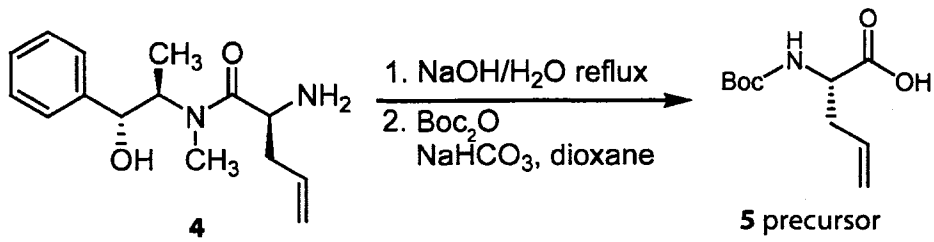

4 **5** precursor

A round bottom flask equipped with a stir bar and condenser, and charged with 1 M NaOH (49.6 mL), water (50 mL) and allyl glycinamide (6.5 g, 24.8 mmol) was heated to reflux for two hours. The solution was then allowed to cool to room temperature at

which point pseudoephedrine crystallized from the solution. The solution was extracted with CH_2Cl_2 (100 mL then 50 mL). These organic layers were back extracted with water and all aqueous layers were combined and concentrated to a volume of 50 mL. Dioxane (50 mL) and sodium bicarbonate (4.2 g, 49.6 mmol, 2.0 equiv.) were added, and the mixture was cooled in an ice bath for 20 minutes. Boc anhydride (6.5 g, 29.76 mmol, 1.2 equiv.) was added, and the mixture was stirred for three hours (1.5 hours in an ice bath and 1.5 hours at room temperature). The reaction mixture was washed with ethyl acetate (200 mL, then 100 mL), and the combined ethyl acetate layers were then washed with NaOH (0.1 M, 50 mL). All aqueous layers were combined, ethyl acetate was added (50 mL) and the solution was acidified to pH 1 with 1M HCl. After separation, the aqueous layer was extracted with ethyl acetate (2 x 100 mL) and the combined ethyl acetate layers were dried with sodium sulfate and concentrated *in vacuo* yielding a colorless oil (4.73 g, 21.97 mmol, 89%). All spectroscopic data agree with those previously recorded.[6]

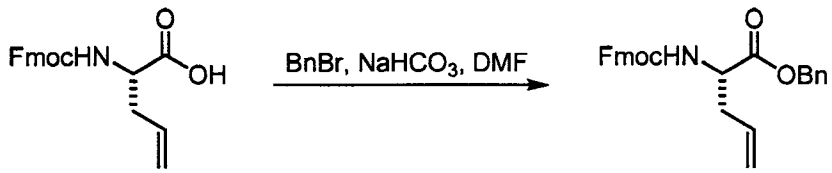

6

A round bottom flask equipped with a stir bar was charged with Fmoc-allyl glycine-OH (4.12 g, 12.2 mmol), N,N-dimethyl formamide (20.6 mL), sodium bicarbonate (5.1 g, 61.1 mmol, 5 equiv) and benzyl bromide (3.0 mL, 24.4 mmol, 2.0 equiv) and stirred overnight. Water (75 mL) was added, and the reaction was extracted with ethyl acetate (2 x 100 mL). The combined organic layers were dried over sodium sulfate, concentrated *in vacuo* and purified by silica gel chromatography (80:20 hexanes:ethyl acetate) affording 3.30 g (63%) of a colorless oil A white crystalline solid

was obtained by slow evaporation from chloroform. **^{1}H NMR** ($CDCl_3$, 400 MHz) δ 7.73 (d, 7.6 Hz, 2H), 7.56 (d, 7.4 Hz, 2H), 7.24 (m, 9H), 5.57 (m, 1H), 5.31 (d, 8 Hz, 1H), 5.05 (m, 4H), 4.48 (m, 1H), 4.35 (d, 7.2 Hz, 2H), 4.18 (t, 8 Hz, 1H), 2.47 (m, 2H) **^{13}C NMR** ($CDCl_3$, 100 MHz) δ 171.7, 155.9, 143.8, 141.6, 132.3, 128.8, 128.8, 128.6, 127.9, 127.3, 125.3, 120.2, 67.5, 67.3, 47.3, 36.9 **IR** (cm^{-1}) 3337, 3066, 2950, 1715, 1519, 1450, 1215, 1048 **HRMS** m/z calculated for $C_{27}H_{25}NO_4$ [M+H] = 428.1784; found 428.1856

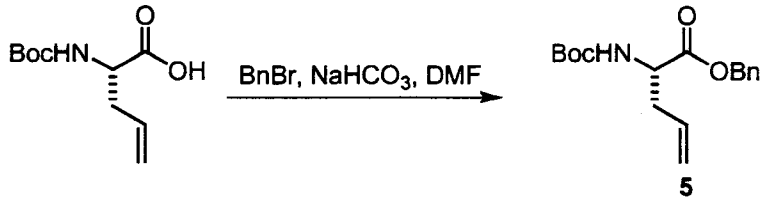

5

A round bottom flask equipped with a stir bar was charged with N,N-dimethyl formamide (15 mL), sodium bicarbonate (5.9 g, 69.73 mmol, 5.0 equiv.) and Boc-allyl Gly-OH (3 g, 13.95 mmol). Benzyl bromide (3.4 mL, 27.89 mmol, 2.0 equiv) was then added, and the solution was stirred overnight. Water (100 mL) was added, and the mixture was extracted with ethyl acetate (2 x 100 mL). The combined organic layers were dried with sodium sulfate, concentrated *in vacuo* and purified by silica gel chromatography (90:10 hexanes:ethyl acetate) to yield 2.4 g (56%) of a colorless oil. **^{1}H NMR** ($CDCl_3$, 400 MHz) δ 7.36 (s, 5H), 5.59 (m, 1H), 5.07 (m, 4H), 4.41 (m, 1H), 2.45 (m, 2H), 1.44 (s, 9H) **^{13}C NMR** ($CDCl_3$, 100 MHz) δ 172.2, 155.3, 135.5, 132.4, 128.8, 128.6, 128.5, 119.5, 80.1, 67.3, 53.1, 36.9, 28.5 **IR** (cm^{-1}) 3368, 2979, 1716, 1499, 1161 **HRMS** *m/z* calculated for $C_{17}H_{23}NO_4$ [M+H] = 306.1621; found 306.1701

General Procedure for esterification: A flame-dried 150 mL roundbottom flask equipped with a stir bar was charged with CH_2Cl_2, sulfuric acid and starting material.

After cooling in an ice bath for 20 minutes, isobutylene was bubbled into the solution for 10 minutes and the solution was left under positive pressure. The reaction was allowed to stir for 5 days, upon which time isobutylene pressure is released and the reaction solution is neutralized with sodium carbonate (10%, 100 mL), and extracted with ethyl acetate (2 x 50 mL). Combined organic layers were washed with brine (2 x 50 mL), dried over sodium sulfate and concentrated in vacuo, yielding a clear liquid.

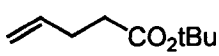

14

According to the general procedure vinyl acetic acid (25 g, 290 mmol), CH_2Cl_2 (100 mL), and sulfuric acid (0.6 mL, 18M) were mixed and cooled. Standard workup yielded 16.09 g (42%). **^{1}H NMR** ($CDCl_3$, 400 MHz) δ 5.81 (m, 1H), 5.07 (m, 2H), 2.95 (m, 2H), 1.41 (s, 9H) **^{13}C NMR** ($CDCl_3$, 100 MHz) δ 171.0, 131.1, 118.1, 80.7, 40.5, 28.2 **IR** (cm^{-1}) 2981, 2933, 1735, 1643, 1369, 1156

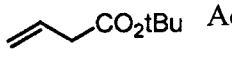

13

According to the general procedure allyl acetic acid (25 g, 249 mmol), CH_2Cl_2 (100 mL), and sulfuric acid (0.6 mL, 18M) were mixed and cooled. Standard workup yielded 15.8 g (40%). **^{1}H NMR** ($CDCl_3$, 400 MHz) δ 5.75 (m, 1H), 4.95 (m, 2H), 2.27 (m, 4H), 1.41 (s, 9H) **^{13}C NMR** ($CDCl_3$, 100 MHz) δ 172.6, 137.1, 115.4, 80.4, 34.9, 29.2, 28.2 IR (cm^{-1}) 2980, 2933, 1732, 1368, 1257, 1154

General Procedure for olefin cross metathesis: A round bottom flask equipped with a stir bar is flame-dried and charged with Fmoc-allylglycine-OBn, Grubbs' second-generation catalyst (5 mol %), and the corresponding ester (5 equivalents). A condenser

is added and the reaction is heated to reflux for two hours under an atmosphere of argon. The solution is then adsorbed onto silica gel and chromatographed.

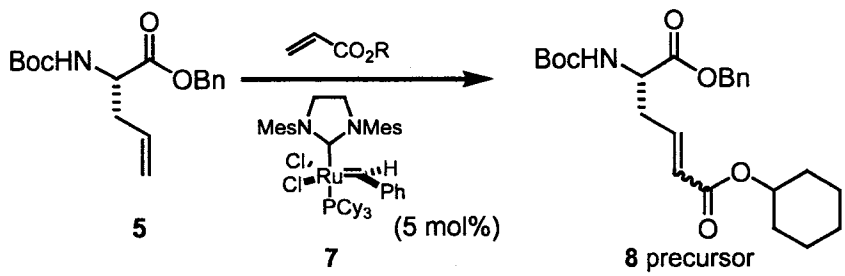

According to the general procedure Boc-allylglycine-OBn (1.0 g, 3.27 mmol, 1 equiv.), cyclohexyl acrylate (2.6 mL, 16.37 mmol, 5.0 equiv, Lancaster Synthesis), Grubbs catalyst (139.0 mg, 0.16 mmol, 5 mol %) and CH_2Cl_2 (20 mL) were mixed. Standard reaction conditions, workup and chromatography (85:15 hexanes:ethyl acetate) yielded 1.25 g (89%).. Only *E* isomer based on splitting of vinylic proton found at 5.81 ppm **^{1}H NMR** ($CDCl_3$, 400 MHz) δ 7.34 (m, 5H), 6.74 (m, 1H), 5.81 (d, 15.6 Hz, 4H), 5.09 (m, 3H), 4.77 (m, 1H), 4.49 (m, 1H), 2.68 (m, 1H), 2.56 (m, 1H), 1.85 (m, 2H), 1.71 (m, 2H), 1.54 (m, 2H), 1.44 (s, 9H), 1.39 (m, 2H), 1.36 (m, 2H), 1.25 (m, 2H) **^{13}C NMR** ($CDCl_3$, 100 MHz) δ 171.7, 165.6, 155.3, 141.8, 128.9, 128.8, 128.6, 125.8, 80.5, 72.9, 67.6, 52.7, 35.4, 31.8, 28.5, 25.6, 24 **IR** (cm^{-1}) 3358, 2936, 1716, 1258, 1166 **HRMS** *m/z* calculated for $C_{24}H_{33}NO_6$ [M+H] = 432.5220; found 432.2386

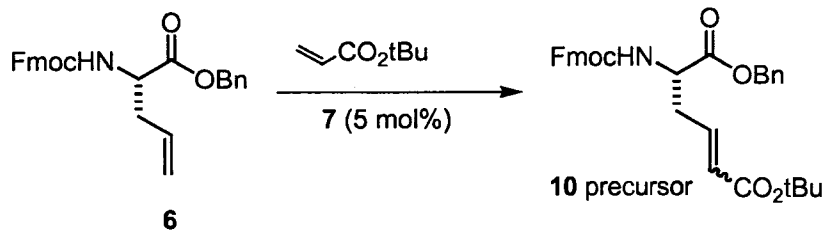

According to the general procedure Fmoc-allylglycine-OBn (1 g, 2.34 mmol, 1.0 equiv.), tert-butyl acrylate (1.7 mL, 11.70mmol, 5.0 equiv.), Grubbs catalyst (99.3 mg,.0.12 mmol, 5 mol %) and CH_2Cl_2 (20 mL) were mixed. Standard reaction conditions, workup and chromatography (80:20 hexanes:ethyl acetate) yielded 1.04 g (87%). **^{1}H NMR** ($CDCl_3$, 400 MHz) δ 7.74 (d, 7.4 Hz, 2H), 7.56 (d, 7.4 Hz, 2H), 7.29 (m, 9H), 5.75 (d, 12 Hz, 1H), 5.43 (d, 8 Hz, 1H), 5.16 (d, 6.8 Hz, 3H), 4.54 (m, 1H), 4.36 (m, 2H), 4.18 (t, 8 Hz, 1H) **^{13}C NMR** ($CDCl_3$, 100 MHz) δ 171.2, 165.3, 156.2, 143.9, 141.5, 140.6, 135.2, 128.9, 128.9, 128.7, 128, 127.3, 127.2, 125.3, 120.2, 80.8, 67.8, 67.4, 53.2, 43.7, 35 **IR** (cm^{-1}) 3337, 3065, 1715, 1519, 1450, 1215,1048 **HRMS** *m/z* calculated for $C_{32}H_{33}NO_6$ [M+H] = 428.1784; found 428.1856

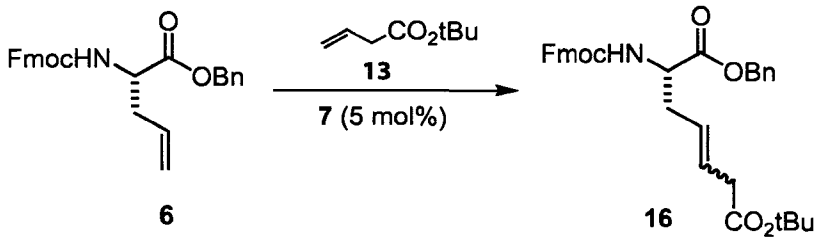

According to the general procedure Fmoc-Allylglycine-OBn (1 g, 2.34 mmol, 1.0 equiv.), vinyl acetic acid t-butyl ester (1.7 g, 11.70mmol, 5.0 equiv.), Grubbs catalyst (99.3 mg,.0.12 mmol, 5 mol %) and CH_2Cl_2 (20 mL) were mixed. Standard reaction conditions, workup and chromatography (80:20 hexanes:ethyl acetate) yielded 950 mg (73%). 4:1 *E:Z* ratio based on splitting of methylene found at 2.5 ppm **^{1}H NMR** ($CDCl_3$, 400 MHz) δ 7.74 (d, 7.6 Hz, 2H) , 7.58 (d, 7.4 Hz, 2H), 7.29 (m, 9H), 5.56 (m, 1H), 5.42 (d, 8 Hz, 1H), 5.31 (m, 1H), 5.13 (m, 2H), 4.46 (m, 1H), 4.35 (m, 2H), 4.21 (m, 1H), 2.94* (d, 10 Hz, 0.44H), 2.88* (d, 8 Hz, 1.56H), 2.35 (m, 2H), 1.43 (s, 9H) **^{13}C NMR** ($CDCl_3$, 100 MHz) δ 171.8, 171.2, 156.1, 143.9, 141.5, 135.6, 128.9, 128.7, 128.6, 128.6,

127.9, 127.3, 125.4, 120.2, 80.9, 67.5, 67.3, 53.6, 47.3, 39.3, 35.6, 28.3 **IR** (cm^{-1}) 3343, 2976, 1727, 1521, 1150, 740.2 **HRMS** *m/z* calculated for $C_{33}H_{35}NO_6$ [M+H] = 542.2464; found 542.2524 * cis-trans isomers

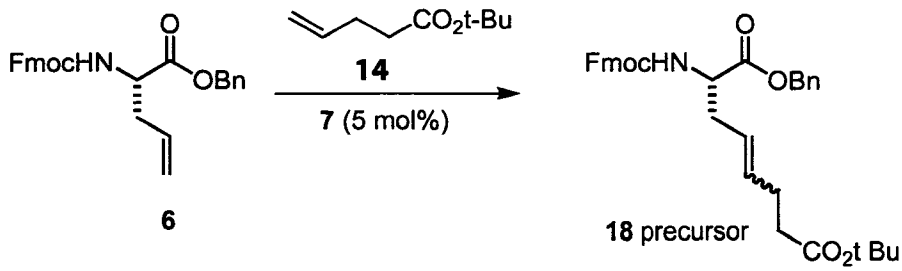

According to the general procedure Fmoc-allylglycine-OBn (1 g, 2.34 mmol, 1.0 equiv.), allyl acetic acid t-butyl ester (1.9 g, 11.70mmol, 5.0 equiv.), Grubbs catalyst (99.3 mg, 0.12 mmol, 5 mol %) and CH_2Cl_2 (20 mL) were mixed. Standard reaction conditions, workup and chromatography (80:20 hexanes:ethyl acetate) yielded 960 mg (74%). 5.7:1 *E:Z* ratio based on splitting of methylene found at 2.9 ppm **^{1}H NMR** ($CDCl_3$, 400 MHz) δ 7.74 (d, 7.4 Hz, 2H), 7.57 (d, 7.4 Hz, 2H), 7.29 (m, 9H), 5.45 (d, 16 Hz, 1H), 5.35 (d, 8 Hz, 1H), 5.12 (m, 3H), 4.43 (m, 1H), 4.35 (m, 1H), 4.19 (t, 8 Hz, 1H), 2.47 (m, 2H), 2.21 (m, 4H), 1.42 (s, 9H), 2.35 (m, 2H), 1.43 (s, 9H) **^{13}C NMR** ($CDCl_3$, 100 MHz) δ 172.5, 171.9, 155.9, 144.1, 141.5, 135.5, 134.0, 128.8, 128.7, 128.6, 127.9, 127.3, 125.4, 124.3, 120.2, 80.5, 67.4, 67.3, 53.7, 47.3, 35.6, 35.3, 28.3, 28.2*, 23.0 **IR** (cm^{-1}) 3343, 2976, 1725, 1150, 740 **HRMS** *m/z* calculated for $C_{34}H_{37}NO_6$ [M+H] = 556.2621; found 556.2699 * t-butyl rotamer

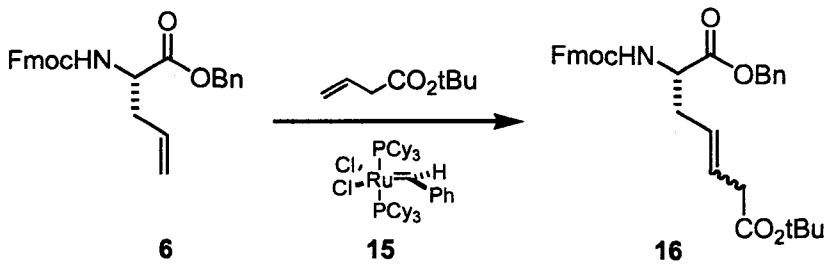

6 15 16

A round bottom flask equipped with a stir bar is flame-dried and charged with Fmoc-allylglycine-OBn (1 g, 2.34 mmol), vinyl acetic *t*-butyl ester (665.3 mg, 4.68 mmol, 2.0 equiv), Grubbs' first generation catalyst (96.3 mg, 0.12 mmol, 5 mol %), and CH_2Cl_2 (20 mL). A reflux condenser is added and the reaction is heated to reflux for two hours. The reaction is monitored by thin layer chromatography (80:20 hexanes:ethyl acetate). When the product is no longer forming (about 2 hrs.) as monitored by thin layer chromatography, reaction cooled and an additional aliquot of Grubbs' first generation catalyst (96.3 mg, 0.12 mmol, 5 mol %) and vinyl acetic *t*-butyl ester (665.3 mg, 4.68 mmol, 2.0 equiv) were added and the solution was heated to reflux. This procedure is repeated twice more for a catalyst loading of 20 mol % and 8.0 equivalents vinyl acetic *t*-butyl ester. Resulting solution adsorbed onto silica gel and chromatographed (80:20 hexanes:ethyl acetate) yielded 1.05 g (81%)

General Procedure for Hydrogenation: A round bottom flask equipped with a stir bar is charged with the cross metathesis product, Pd/C (10% by weight), and ethanol. A hydrogen balloon is used to purge the system for 30 seconds and the reaction is left under positive hydrogen pressure for 1 hour. The solution is filtered through celite and concentrated *in vacuo*. For *ee* determination the corresponding methyl ester was

generated by treatment with $TMSCHN_2$ (2.0M in Et_2O) in 2-5 mL of $MeOH:CH_2Cl_2$ at 23 °C for 5 min. followed by quenching with AcOH and concentration *in vacuo*.

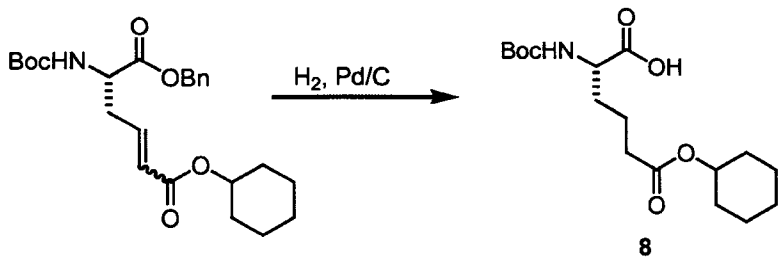

8

According to the general procedure, **8** precursor (1.25 g, 2.90 mmol), Pd/C (125 mg, 10 weight %) and ethanol (35 mL) were mixed. Standard reaction and workup yielded 920 mg (92%) **^{1}H NMR** ($CDCl_3$, 400 MHz) δ 8.33 (brs, 1H), 5.13 (d, 8 Hz, 1H), 4.72 (m, 1H), 4.3 (m, 0.7H), 4.1 (m, 0.3H), 2.31 (m, 2H), 1.81 (m, 3H), 1.69 (m, 5H), 1.51 (m, 1H), 1.44 (s, 9H), 1.33 (m, 5H) **^{13}C NMR** ($CDCl_3$, 100 MHz) δ 176.8, 173.1, 155.9, 80.3, 73.1, 53.2, 34.2, 31.8, 28.5, 25.5, 23.9, 21 **IR** (cm^{-1}) 3342, 2937, 2861, 1717.4, 1167 **HRMS** *m/z* calculated for $C_{17}H_{29}NO_6$ [M+Na] = 366.4051; found 366.1892 Corresponding methyl ester used for ee determination. HPLC analysis (Chiracel ADH, 9:1 hex/*i*-PrOH, 1.0 mL/min, 210 nm): t_r (minor) = N.D., t_r (major) = 9.75 min. >99% ee.

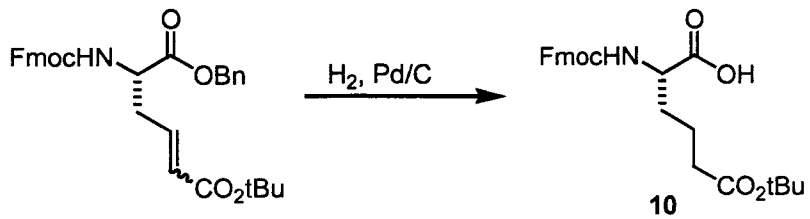

10

According to the general procedure, **10** precursor (990 mg, 1.83 mmol,), Pd/C (99 mg, 10 weight %) and ethanol (35 mL) were added. Standard reaction and workup

yielded 770 mg (96%). **^{1}H NMR** (CDCl3, 400 MHz) δ 8.71 (brs, 1H), 7.76 (d, 7.4 Hz, 2H), 7.56 (d, 8 Hz, 2H), 7.3 (m, 4H), 5.56 (d, 8 Hz, 1H), 4.52 (m, 1H), 4.41 (m, 2H), 4.22 (t, 8 Hz, 1H), 2.29 (t, 8 Hz, 2H), 1.92 (m, 1H), 1.68 (m, 3H), 1.47 (s, 9H) **^{13}C NMR** ($CDCl_3$100 MHz) δ 176.6, 173.2, 156.4, 144, 143.9, 141.5, 130.2, 127.9, 127.3, 125.3, 120.2, 81, 67.4, 53.7, 47.3, 34.9, 31.6, 28.3, 20.8, 47.3 **IR** (cm^{-1}) 3323, 2976, 1715, 1519, 1368,1152 **HRMS** *m/z* calculated for $C_{25}H_{29}NO_6$ [M+H] = 440.1995; found 440.2073. Corresponding methyl ester used for ee determination. HPLC analysis (Chiracel ADH, 9:1 hex/*i*-PrOH, 1.0 mL/min, 254 nm): t_r (minor) = 11.12 min., t_r (major) = 19.31 >99% ee.

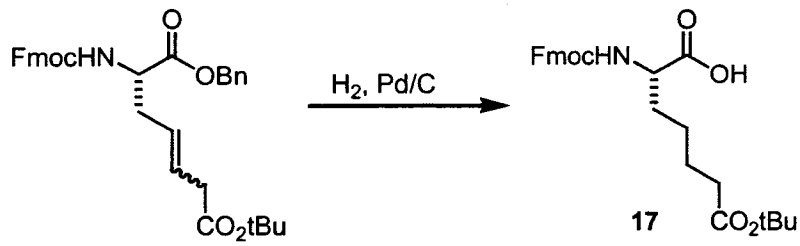

According to the general procedure, **17** precursor (1.08 g, 2.00 mmol,), Pd/C (108 mg, 10 weight %) and ethanol (40 mL) were added. Standard reaction and workup yielded 850 mg (94%) **^{1}H NMR** ($CDCl_3$, 400 MHz) δ 9.65 (brs, 1H), 7.77 (d, 7.4 Hz, 2H), 7.6 (d, 6 Hz, 2H), 7.3 (m, 4H), 5.48 (d, 8 Hz, 1H), 4.52 (m, 1H), 4.42 (d, 6 Hz, 2H), 4.22 (t, 8 Hz, 1H), 2.23 (t, 8 Hz, 2H), 1.91 (m, 1H), 1.54 (m, 3H), 1.47 (s, 9H), 1.29 (m, 2H) **^{13}C NMR** ($CDCl_3$, 100 MHz) δ 177.0, 173.4, 156.4, 144, 143.9, 141.5, 127.9, 127.3, 125.3, 120.2, 80.7, 67.3, 53.8, 47.3, 35.4, 32.2, 28.3, 24.9, 24.8 **IR** (cm^{-1}) 3323, 2877, 1715, 1525, 1367, 1250, 1156 **HRMS** *m/z* calculated for $C_{26}H_{31}NO_6$ [M+H] = 454.2151; found 454.2233. Corresponding methyl ester used for ee determination.

HPLC analysis (Chiracel ADH, 9:1 hex/*i*-PrOH, 1.0 mL/min, 254 nm; t_r (minor) = 11.05 min., t_r (major) = 18.25 >99% ee.

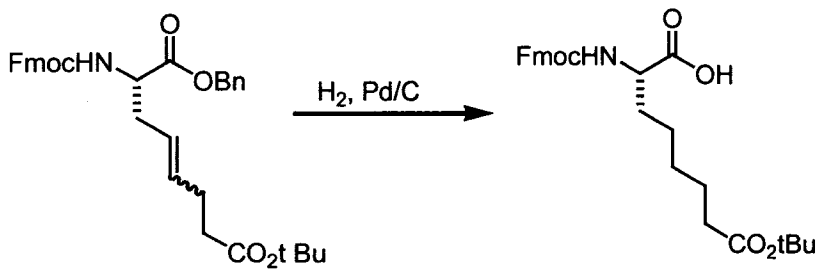

18

According to the general procedure, **18** precursor (1.03 g, 1.90 mmol,), Pd/C (103 mg, 10 weight %) and ethanol (35 mL) were added. Standard reaction and workup yielded 820 mg (92%) **^{1}H NMR** ($CDCl_3$, 400 MHz) δ 9.45 (brs, 1H), 7.75 (d, 7.6 Hz, 2H), 7.59 (d, 8 Hz, 2H), 7.3 (m, 4H), 5.43 (d, 8 Hz, 1H), 4.5 (m, 1H), 4.41 (d, 8 Hz, 2H), 4.22 (t, 8 Hz, 1H), 2.21 (t, 8 Hz, 2H), 1.89 (m, 1H), 1.66 (m, 1H), 1.56 (m, 2H), 1.45 (s, 9H), 1.27 (m, 4H) **^{13}C NMR** ($CDCl_3$, 100 MHz) δ 177.1, 173.4, 156.4, 144.1, 143.9, 141.5, 127.9, 127.3, 125.3, 120.2, 80.6, 67.3, 53.9, 47.3, 35.6, 32.3, 28.8, 28.3, 25.1, 25.0 **IR** (cm^{-1}) 3324, 2933, 1724, 1530, 1450, 1367, 1250, 1156 **HRMS** *m/z* calculated for $C_{27}H_{33}NO_6$ [M+H] = 468.2308; found 468.2380. Corresponding methyl ester used for ee determination. HPLC analysis (Chiracel ADH, 9:1 hex/*i*-PrOH, 1.0 mL/min, 254 nm; t_r (minor) = 11.30 min., t_r (major) = 17.62 >99% ee.

2-6 Literature Cited

1 (a) Lumb, K.J.; Kim, P.S. *Biochemistry* **1995**, *34*, 8642-8648. (b) Schnarr, N.A.; Kennan, A.J. *J. Am. Chem. Soc.* **2003**, *125*, 667-671. (c) Gurnon, D.G.; Whitaker, J.A.;

Oakley, M.G. *J. Am. Chem. Soc.* **2003**, *125*, 7518-7519. (d) Schnarr, N.A.; Kennan, A.J. *J. Am. Chem. Soc.* **2004**, *126*, 14447-144451.

2 O'Shea, E.K.; Lumb, K.J.; Kim, P.S. *Curr. Biol.* **1993**, *3*, 658-667.

3 (a) Nicolaou, K. C.; Bulger, P. G.; Sarlah, D. *Angew. Chem. Int. Ed.* **2005**, *44,* 4490-4527. (b) Grubbs, R. H. *Tetrahedron* **2004**, *60,* 7117-7140. (c) Schrock, R. R.; Hoveyda, A. H. *Angew. Chem. Int. Ed.* **2003**, *42,* 4592-4633.

4 (a) Nolen, E.G.; Kurish, A.J.; Potter, J.M.; Donahue, L.A.; Orlando, M.D. *Org. Lett.* **2005**, *7*, 3383-3386. (b) Boyle, T.P.; Bremner, J.B.; Coates, J.A.; Keller, P.A.; Pyne, S.G. *Tetrahedron* **2005**, *61*, 7271-7276. (c) Nolen, E.G.; Kurish, A.J.; Wong, K.A.; Orlando, M.D.; *Tetrahedron Lett.* **2003**, *44*, (d) (e) Dondoni, A.; Giovannini, P. P.; Marra, A. J. *J. Chem. Soc. Perkin Trans. I* **2001**, 2380-2388. (f) Bremner, J. B.; Keller, P. A.; Pyne, S. G.; Robertson, A. D.; Skelton, B. W.; White, A. H.; Witchard, H. M. *Aust. J. Chem.* **2000**, *53,* 535-540. (g) Biagini, S. C. G.; Gibson, S. E.; Keen, S. P. *J. Chem. Soc. Perkin Trans. I* **1998**, 2485-2499.

5 Biswas, K.; Coltart, D. M.; Danishefsky, S. J. *Tetrahedron Lett.* **2002**, *43,* 6107-6110.

6 (a) Myers, A. G.; Schnider, P.; Kwon, S.; Kung, D. W. *J. Org. Chem.* **1999**, *64,* 3322-3327. (b) Myers, A. G.; Gleason, J. L. *Org. Synth.* **1999**, *76,* 57-76. (c) Myers, A. G.; Gleason, J. L.; Yoon, T.; Kung, D. W. *J. Am. Chem. Soc.* **1997**, *119,* 656-673.

7 .Wang, S.-S.; Gisin, B.F.; winter, D.P.; Makofske, R.; Kulesha, I.D.; Tzougraki, C.; Meienhofer, J. *J. Org. Chem.* **1977**, *42*, 1286.

8 Ryan, S.J.; Zhang, Y.; Kennan, A.J. *Org. Lett.* **2005**, *7*, 4765-4767.

9 Miranda, L.P.; Jones, A.; Meutermans, W.F.; Alewood, P.F. *J. Am. Chem. Soc.* **1998**, *120*, 1410-1420.

10 Anderson, G.W.; Callahan, F.M. *J. Am. Chem. Soc.* **1960**, *82*, 3359.

11 (a) Blackwell, H.E.; O'Leary, D.J.; Chatterjee, A.K.; Washenfelder, R.A.; Bussmann, D.A.; Grubbs, R.H. *J. Am. Chem. Soc.* **2000**, *122*, 58-71. (b) Chatterjee, A.K.; Choi, T.-L.; Sanders, D.P.; Grubbs, R.H. *J. Am. Chem. Soc.* **2003**, *125*, 11360-11370.

Chapter 3

Effects of Sidechain Length and Electrostatics

3-1 Introduction

The study of protein-protein interactions has garnered much recent attention.[1] As a ubiquitous and tractable means for governing protein association, the α-helical coiled coil has been the focus of numerous investigations.[2] Although considerable data have been gathered on the structure-function relationships of natural core residues, the limited number of side chain candidates restricts the design of novel assemblies.[3] Here we investigate the effects of side chain length variation on natural functionality when substituted at the hydrophilic interface. These results point to the importance of sidechain length and functionality in regard to stabilization of coiled coils.

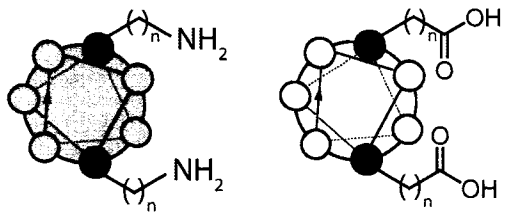

Figure 1. Substitution at hydrophilic interface (n = 1 – 4).

3-2 Homodimeric Complexes

Coiled coil formation can be controlled by both the hydrophobic core and hydrophilic interface. The current system describes the effects of sidechain length and functionality with regard to dimeric coiled coil formation and stability. To test this system we focused on the dimerization domain of GCN4, where substitution at the hydrophilic interface has been thoroughly studied.[4]

The peptides used here have a similar primary sequence to those used by Kim and co-workers in a study on the impacts of electrostatic matching[5], and are derived from GCN4. This system contains a hydrophobic core comprised of leucine at each *a/d* position, with the exception of a central asparagine residue at position 14. The inclusion of this central asparagine residue drives parallel orientation and dimer specificity. Residues found at positions *b, c,* and *f* are solvent exposed and contain helix promoting (Ala, Gln, Lys) or solubilizing (Lys, Gln) residues. The *e* and *g* interface is persubstituted with amino acids with sidechains bearing an amine or carboxylic acid and one, two, three or four methylene units separating the peptide backbone and functional group (Figure 2).

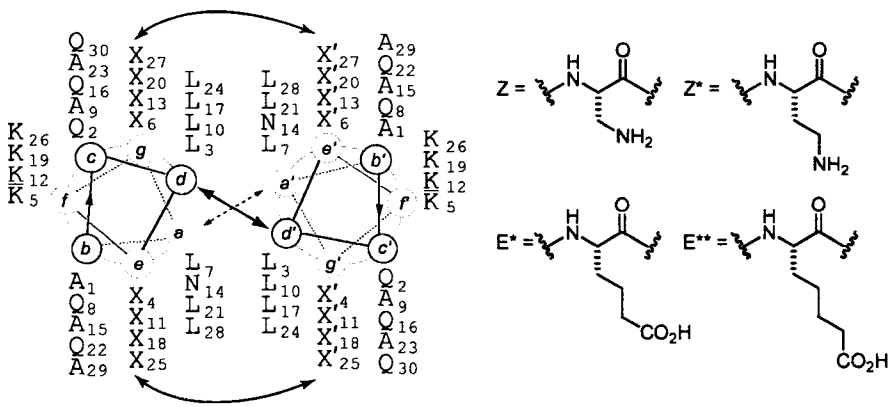

pAsp	Ac-AQLDKDLQALDKDNAQLDKDLQALDKDLAQ-NH_2
pGlu	Ac-AQLEKELQALEKENAQLEKELQALEKELAQ-NH_2
pHGlu	Ac-AQLE*KE*LQALE*KE*NAQLE*KE*LQALE*KE*LAQ-NH_2
pHHGlu	Ac-AQLE**KE**LQALE**KE**NAQLE**KE**LQALE**KE**LAQ-NH_2
pDap	Ac-AQLZKZLQALZKZNAQLZKZLQALZKZLAQ-NH_2
pDab	Ac-AQLZ*KZ*LQALZ*KZ*NAQLZ*KZ*LQALZ*KZ*LAQ-NH_2
pOrn	Ac-AQLOKOLQALOKONAQLOKOLQALOKOLAQ-NH_2
pLys	Ac-AQLKKKLQALKKKNAQLKKKLQALKKKLAQ-NH_2

Figure 2. Peptides employed. Each sequence contains substitution at all *e/g* residues with amine or carboxylic acid functional group. Each peptide is N-terminally acetylated (Ac) and C-terminally amidated (Am). Underlined lysine residue contains an acetimidobenzoate group as a spectroscopic tag.

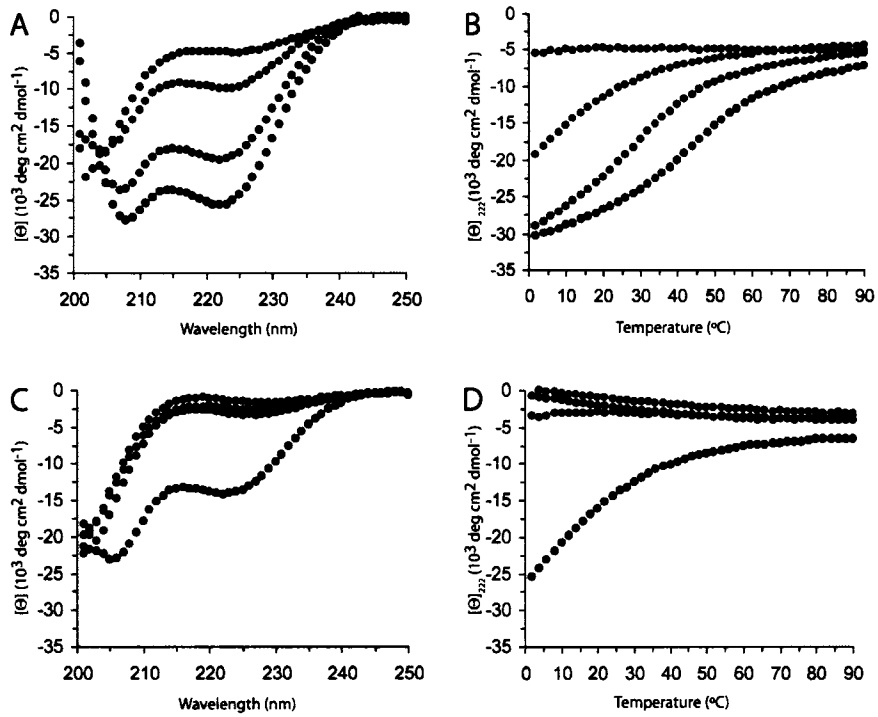

Figure 3. Wavelength scan (**A**) and thermal denaturation (**B**) CD data for solutions of Asp (●), Glu (●), HGlu (●), and HHGlu (●). Wavelength scan (**C**) and thermal denaturation (**D**) CD data for solutions of Dap (●), Dab (●), Orn (●), and Lys (●). All samples are 10 μM total peptide in PBS buffer (10 mM phosphate pH 7.0, 150 mM NaCl).

To evaluate the effects of side chain length and electrostatics on these peptides, pure solutions of each new sequence were analyzed by circular dichroism (CD) spectroscopy. It was not clear *a priori* what effect an extended sidechain would have on these pure component solutions, but based on literature demonstrations of like charge repulsion at *e/g* interfaces in similar systems, we expected these homodimers to be poor candidates for stable complex formation. The peptides containing shorter tethers bear this out, with the Asp, Dap, Dab, and Orn peptides exhibiting little if any helical characteristics (Figure 3). The Lys and Glu peptides exhibit a somewhat helical profile, but with a low absolute signal, and thermal denaturation demonstrates a non-cooperative unfolding transition in this regime.

Surprisingly, peptides containing the extended side chain length analogs of glutamic acid (HGlu and HHGlu) exhibit helical profiles and a cooperative thermal transition. These complexes exhibit thermal stabilities (Tm = 45 and 49°C, respectively) that are comparable with natural sequences (GCN4 Tm = 53°C).[6,7] Although these complexes contain a central asparagine, which has been shown to induce dimerization, we wanted to further characterize these complexes. Since varying oligomerization states (dimers, trimers, and higher oligomers) are predicted to be comparably helical, CD is not a good measure of specificity in aggregation number. Sedimentation equilibrium analysis reveals that these complexes exhibit dimer formation (Table 1). One plausible explanation for homodimer formation in these complexes, but not in peptides with amine termini with similar side chain lengths, is electron delocalization within the carboxylate. This delocalization of charge may allow for increased solvation, thus decreasing charge-charge repulsions and allowing complex folding.

Table 1. Molecular Weights from Sedimentation Equilibrium[a]

Sample	$MW_{r\ calcd}$	$MW_{r\ obsd}$
HGlu	7560	6839
HHGlu	7786	7701

[a] Conditions as in Figure 3.

3-3 Heterodimeric Complexes

Having shown the limited ability of these peptides to form stable homooligomers, we were then interested to see what effects complementary electrostatics would have in regard to complex formation and stability. Analysis of the full complement of possible heterodimers provides a variety of information.

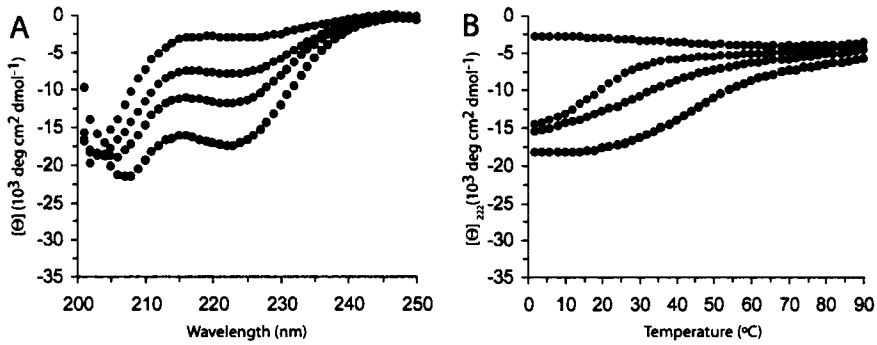

Figure 4. Wavelength scan (**A**) and thermal denaturation (**B**) CD data for equimolar solutions of Dap:Asp (●), Dap:Glu(●), Dap:HGlu(●), and Dap:HHGlu(●). Conditions as in Figure 3.

Focusing first on heterodimeric Dap complexes, we observe that both the Dap:Asp and Dap:Glu mixtures do not exhibit a helical profile, while the signal from the Dap:HGlu mixture is simply the average of the component signals (Figure 4). The final complex in this series, Dap:HHGlu, displays a signal that is minimally more helical than the weighted average of the component signals. As such, their thermal transitions are the result of the weighted average of the pure component solutions.

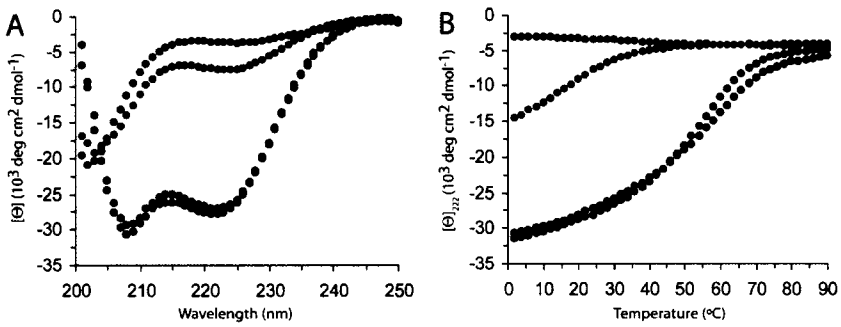

Figure 5. Wavelength scan (**A**) and thermal denaturation (**B**) CD data for equimolar solutions of Dab:Asp (●), Dab:Glu (●), Dab:HGlu (●)and Dab:HHGlu (●). Conditions as in Figure 3.

Increasing the amine sidechain length by one methylene unit (Dab) and mixing with the acidic peptides indicates some interesting results (Figure 5). The mixtures containing natural amino acids (Asp, Glu) show poor overall helicity and non cooperative thermal denaturation. In contrast, the Dab:HGlu and Dab:HHGlu

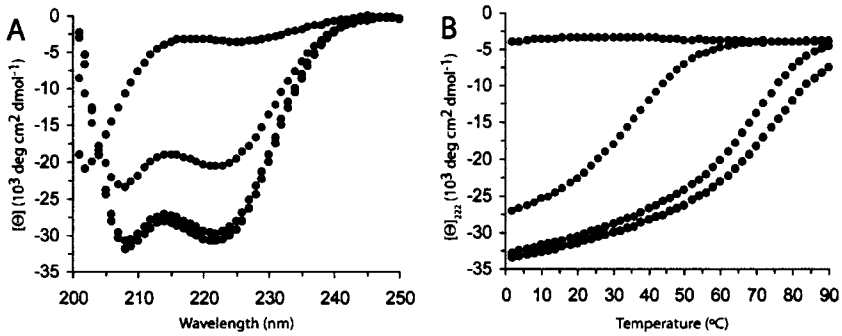

Figure 6. Wavelength scan (**A**) and thermal denaturation (**B**) CD data for equimolar solutions of Orn:Asp (•), Orn:Glu(•), Orn:HGlu(•), and Orn:HHGlu(•). Conditions as in Figure 3.

pairs are highly helical and thermally stable ($[\theta]_{222}$ = –27 774 deg cm^2 dmol^{-1}, Tm = 61°C and –31 190 deg cm^2 dmol^{-1}, Tm = 67°C, respectively). Analysis of the Orn peptide mixtures follows the trend of increasing the amine sidechain length and leads to increasingly stable complexes (Figure 6). Again the mixture containing the Asp peptide (Orn:Asp) shows little helicity and a non cooperative thermal denaturation. Extension of the amine side chain does allow for complex formation in the Orn:Glu mixture ($[\theta]_{222}$ = –20 614 deg cm^2 dmol^{-1}, Tm = 42°C), albeit a complex of marginal stability. Similarly to the Dab heterooligomers, the Orn:HGlu and Orn:HHGlu mixtures exhibit similar helical profiles of increased stability ($[\theta]_{222}$ = –29725 deg cm^2 dmol^{-1}, Tm = 75°C and $[\theta]_{222}$ = –30803 deg cm^2 dmol^{-1}, Tm = 81°C, respectively) relative to the analogous Dab complexes. The final set of complexes is formed upon mixing of the persubstituted lysine peptides with each of the acidic species and results in complexes of increased stability (Figure 7). Analysis of the Asp:Lys mixture indicates a slight helical profile that overlays with the statistical average of the two component signals. In addition, the thermal denaturation does not exhibit a cooperative unfolding. In contrast, the other three complexes: Glu:Lys,

HGlu:Lys, and HHGlu:Lys exhibit exceptional helicity and thermal stability ($[\theta]_{222}$ = - 28 690 deg cm^2 $dmol^{-1}$, Tm = 72°C, $[\theta]_{222}$ =- 30 338, Tm = > 90°C, and $[\theta]_{222}$ = - 30 280, Tm = > 90°C, respectively)

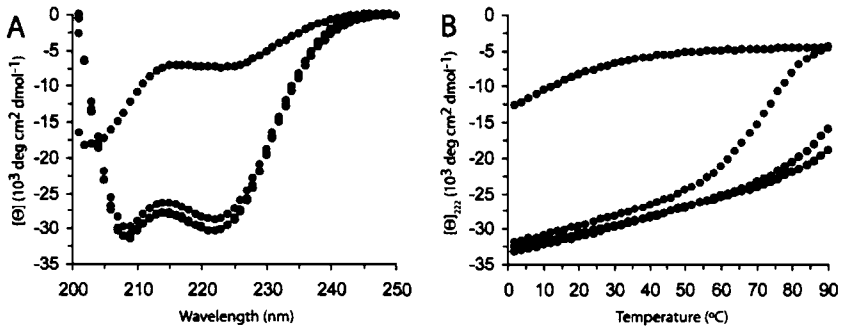

Figure 7. Wavelength scan (**A**) and thermal denaturation (**B**) CD data for equimolar solutions of Lys:Asp (•), Lys:Glu (•), Lys:HGlu (•), and Lys:HHGlu(•). Conditions as in Figure 3.

Characterization to confirm oligomerization state was completed using analytical equilibrium sedimentation analysis. Observed relative mass values were obtained for matched electrostatic pairs that indicated complex formation (Dab:HGlu, Dab:HHGlu, Orn:Glu, Orn:HGlu, Orn:HHGlu, Lys:Glu, Lys:HGlu, Lys:HHGlu) and are consistent with those calculated for the heterodimer (Table 2).

Table 2. Molecular Weights from Sedimentation Equilibrium[a]

Sample	$MW_{r\ calcd}$	$MW_{r\ obsd}$
Glu:Orn	7216	7062
Glu:Lys	8378	8147
HGlu:Dab	7216	7695
HGlu:Orn	7328	8177
HGlu:Lys	8378	8137
HHGlu:Dab	7329	8208
HHGlu:Orn	7441	8520
HHGlu:Lys	8491	8145

[a] Conditions as in Figure 3.

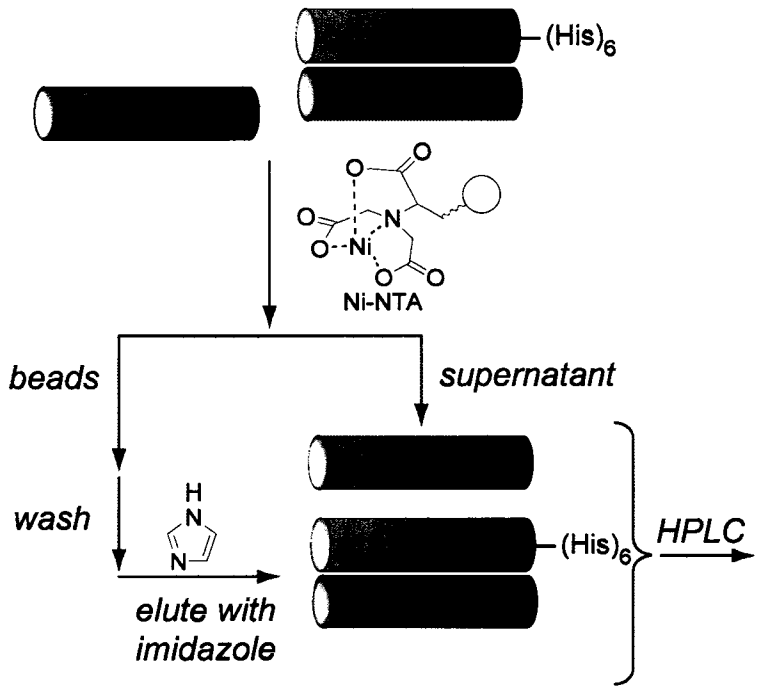

Figure 8. Ni-NTA affinity tag analysis scheme. Initially peptide **A** is specifically bound to peptide **C**, which bears an N-terminal Gly-Gly-$(His)_6$ affinity tag. Upon exposure to Ni-NTA agarose beads, **C** is bound through the His tag, and **A** is bound through its interaction with **C**. Only **B**, which does not interact with the beads or the tagged peptide, remains unbound. After supernatant removal and washing with blank buffer, bound material is eluted with treatment with imidazole. HPLC analysis reveals the identity of unbound (supernatant fraction) and bound (elution fraction) material. Peptides **A** and **B** are intended to represent all binding and nonbinding peptides, respectively. Thus any higher order aggregates are analyzed in the same manner.

An additional measure undertaken to confirm complex stoichometry was completed through the use of an affinity tag strategy. To facilitate this analysis additional basic peptides were prepared that contained an N-terminal Gly-Gly-$(His)_6$ affinity tag. This sequence binds specifically to Ni-nitrilotriacetic (Ni-NTA)-functionalized agarose beads.[8] This interaction is exploited according to the general scheme given in Figure 8. Upon exposure of a mixture to Ni-NTA beads, tagged peptides and their specific binding partners adhere to the solid support. The supernatant, containing unbound material, is removed, followed by washing with buffer to remove any nonspecific interactions. The bound material is eluted by

treatment with imidazole buffer. HPLC analysis reveals the identity of unbound and bound material, respectively.

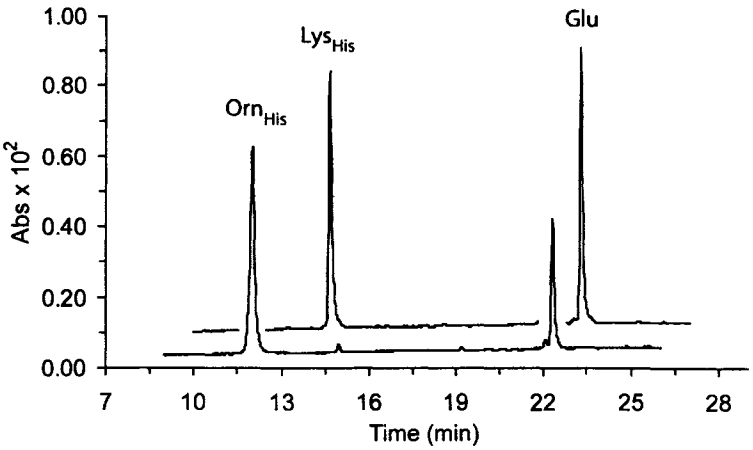

Figure 9. Ni-NTA affinity tag analysis of two equimolar solutions (Orn_{His}:Glu and Lys_{His}:Glu). Orn_{His}:Glu does not contain an equimolar fraction of tagged and untagged peptide in the elution fraction, while Lys_{His}:Glu does.

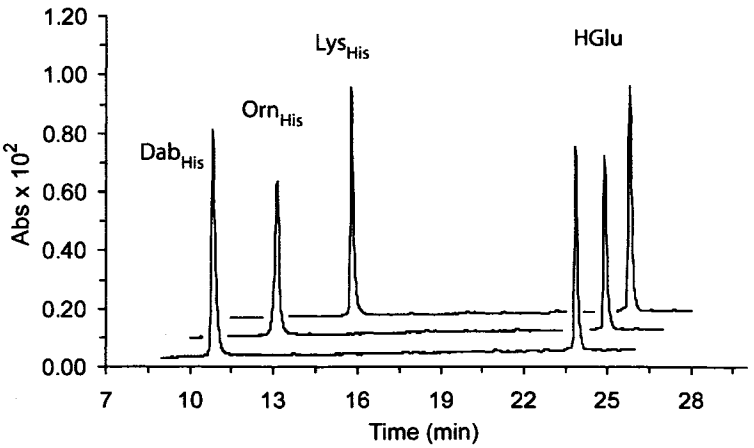

Figure 10. Ni-NTA affinity tag analysis of three equimolar solutions (Dab_{His}:HGlu, Orn_{His}:HGlu, and Lys_{His}:HGlu). Each elution fraction contains an equimolar ratio of tagged and untagged peptides.

With the exception of the Glu:Orn peptide mixture (Figure 9), each of the tagged peptides retain their binding partner in an equimolar mixture, adding an additional measure of certainty to the formation of dimeric complexes (Figure 10,11). The low thermal stability of the Glu:Orn complex may help to explain incomplete

retention in this case, perhaps indicating that there is a lower limit of complex stability required for this assay.

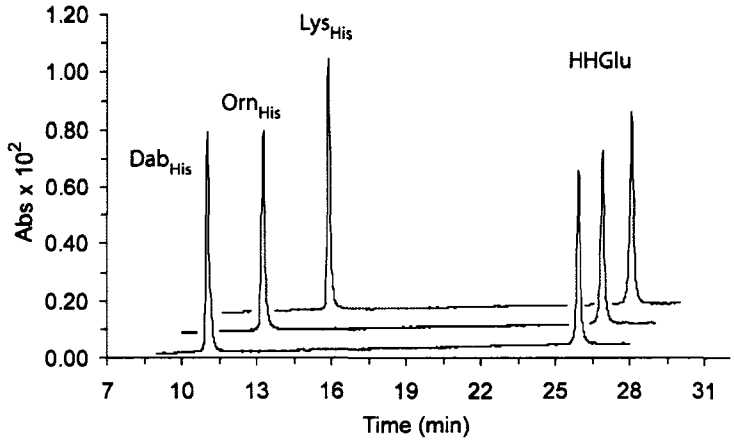

Figure 11. Ni-NTA affinity tag analysis of three equimolar solutions Dab_{His}:HHGlu, Orn_{His}:HHGlu, and Lys_{His}:HHGlu. Each elution fraction contains an equimolar ratio of tagged and untagged peptides.

In order to quantify complex stability, we generally use guanidine hydrochloride denaturation experiments at 25 °C. Unfortunately, chemical denaturation of the complexes studied here with this reagent cause peculiar results

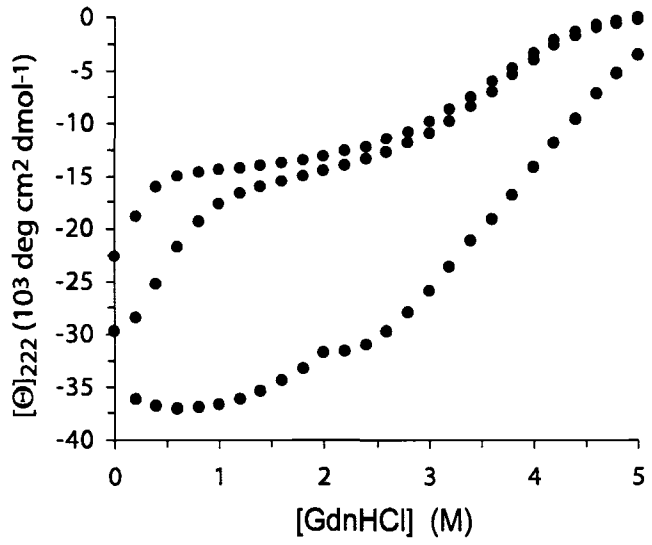

Figure 12. Representative guanidine hydrochloride denaturation profiles (25 °C) of Dab:HHGlu (•), Orn:HHGlu(•), and Lys:HHGlu (•). All solutions 10 μM total peptide.

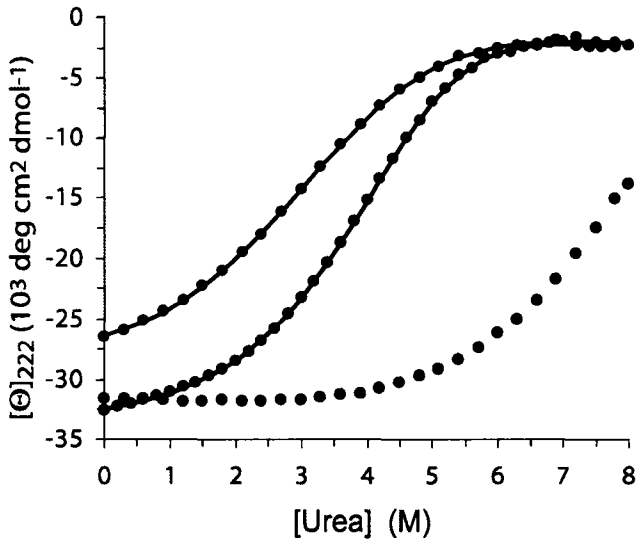

Figure 13. Representative urea denaturation profiles (25 °C) of Dab:HGlu (•), Orn:HGlu (•), and Lys:HGlu (•). Solid lines represent the fit of the data. All solutions 10 μM total peptide.

(Figure 12). As in thermal denaturation, an ideal spectrum contains a folded baseline, a transition region and an unfolded baseline. Unfortunately, utilizing guanidine hydrochloride results in spectra that do not cleanly exhibit these characteristics. We attributed these results to intrinsic increases in ionic strength found in this buffer, which may be shielding the electrostatics at the hydrophilic interface. As such, we exchanged chemical denaturants, and used urea to discern complex stability (Figure 13). Complexes with intermediate stability exhibit a cooperative unfolding pattern, while complexes with low stability (Glu:Orn, HGlu homodimer) are essentially noncooperative. In addition, complexes with very high stability are not denatured in the concentration regime examined here (HGlu:Lys, HHGlu:Lys). Complexes with cooperative unfolding were fit according to a monomer-dimer model that assumes

both folded and unfolded baselines are a linear function of denaturant concentration (Table 3).[9]

Table 3. Complex stability determined by Urea denaturation

Sample	ΔG_{unf} (kcal/mol)
Glu:Lys	11.50 ± 1.07
HGlu:Dab	8.60 ± 0.70
HGlu:Orn	10.53 ± 0.97
HHGlu:Dab	8.15 ± 0.56
HHGlu:Orn	11.03 ± 0.96
HHGlu	6.02 ± 0.33

All solutions 10 μM total peptide

Upon completion of the characterization of these various complexes, there appears to be both a minimum number of methylenes in each sidechain as well as a minimum combined number of methylenes required for successful complex formation. Irrespective of the sidechain length of their electrostatic partners, the Dap and Asp peptides are unable to form complexes. Similarly, peptide mixtures that contain two, three, or four combined methylene units in their sidechains are unable to form stable complexes (Figure 14). An incremental increase in the combined number of methylenes to five results in moderately stable complexes (Figure 15). The

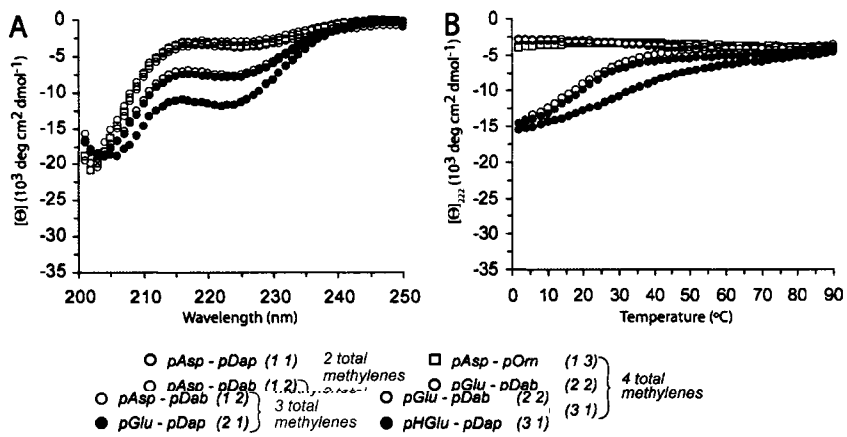

Figure 14. Wavelength scan (**A**) and thermal denaturation data (**B**) comparing 2-4 combined methylenes.

Glu:Orn and HGlu:Dab peptides both exhibit helical profiles, but disparate overall helicity and stability. These complexes contain a 2:3 or a 3:2 methylene number in regard to their acid or amine functionality. It is interesting that there appears to be a preference for the acid functionality to contain a longer tether between it and the peptide backbone.

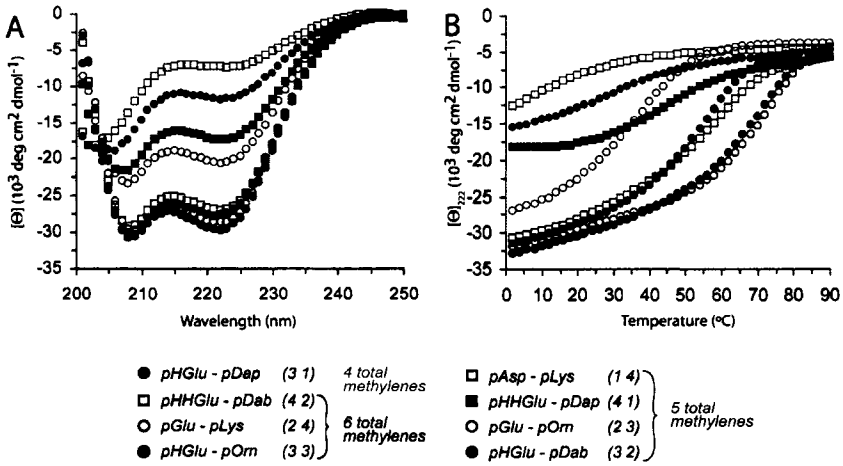

Figure 15. Wavelength scan (**A**) and thermal denaturation (**B**) comparing 5 and 6 methylenes. HGlu:Dap mixture added for perspective.

Unfortunately, this trend appears to be mitigated in peptides that contain six combined methylenes, ruling out the use of generalizations when characterizing the

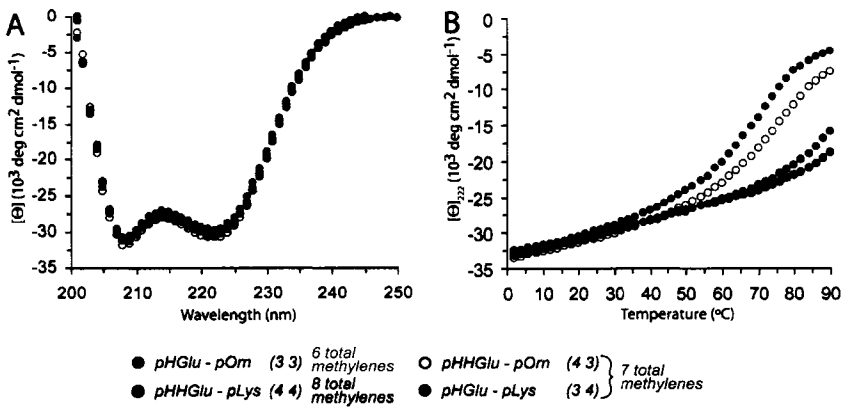

Figure 16. Wavelength scan (**A**) and thermal denaturation (**B**) comparing complexes containing 7 and 8 methylenes. **HGlu:Orn** complex added for perspective.

effects of functionality and sidechain length (Figure 15). These complexes all contain helical profiles and are of reasonable stability. Analysis of the HHGlu:Dab and Glu:Lys complexes, containing a 4:2 or 2:4 methylene count bears out that as the respective sidechains are lengthened, the preference for a certain side chain length orientation is lessened as the difference in stability between these complexes is not as large. Complexes that contain seven or eight methylenes among the two sidechains exhibit exceptional helicity and thermal stability (Figure 16). These three complexes have melting transitions greater than 80 °C and as a result, little comparative data can be ascertained from these spectra.

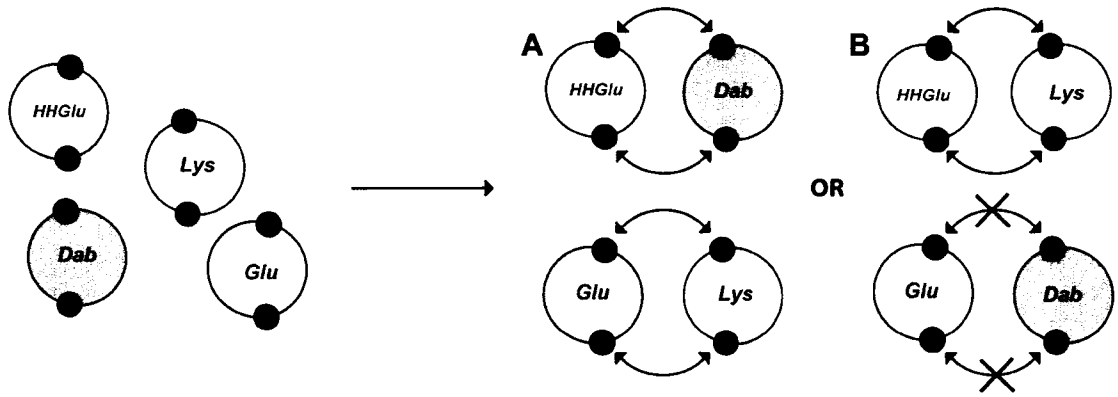

Figure 17. Competition between HHGlu, Glu, Dab, and Lys peptides. Equimolar mixture of these peptides can result in formation of two complexes (HHGlu:Dab and Glu:Lys) or formation of one complex (HHGlu:Lys), while the other two peptides (Glu and Dab) are unable to form a stable complex.

3-4 Complex Assembly - Peptide Partitioning

Having established the characteristics of these peptide complexes, we focused on more complex assembly problems. Control of component folding may provide insight into recognition events that control cellular processes. Furthermore, understanding folding events may lead to advances in biopolymer applications, such as peptide hydrogels. Initial experiments to determine the effects of varying complex stability focused on an equimolar peptide mixture containing HHGlu, Glu, Dab, and

Lys. These peptides can form two viable complexes (HHGlu:Dab and Glu:Lys) or one viable (HHGlu:Lys) and one non-viable complex (Glu:Dab) depending on peptide partitioning (Figure 17).

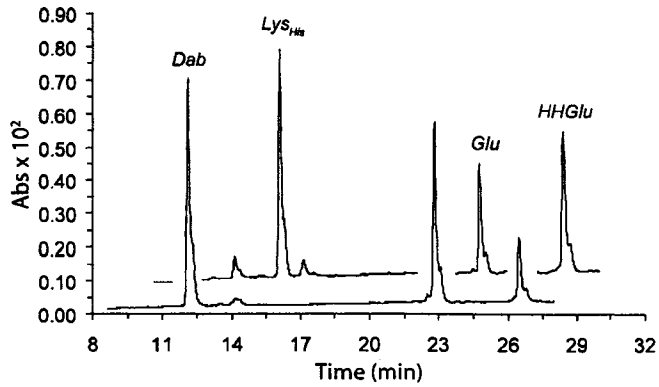

Figure 18. Ni-NTA affinity tag analysis of equimolar HHGlu, Glu, Dab, LysHis mixture. Supernatant fraction (front trace) contains Dab, Glu, and HHGlu, while elution fraction (back trace) contains tagged peptide (LysHis) and Glu and HHGlu. See Figure 17 for schematic diagram.

To determine complex formation, we used the previously described Ni-NTA affinity tag strategy (Figure 8). A Gly-Gly-$(His)_6$ sequence was appended to the N-terminus of the Lys peptide, this peptide was mixed in an equimolar fraction with the non tagged peptides. Analysis of the elution fraction should reveal tagged peptides

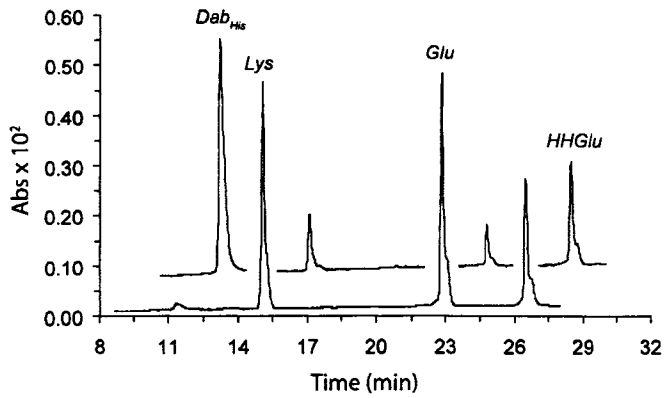

Figure 19. Ni-NTA affinity tag analysis of equimolar HHGlu, Glu, DabHis, Lys mixture. Supernatant fraction (front trace) contains Lys, Glu, and HHGlu. Elution fraction (back trace) contains tagged peptide (Dab His) and HHGlu. See Figure 17 for schematic diagram.

and their specific binding partners. Furthermore, in these experiments, the supernatant fraction is also instructive, as it should contain the rejected components. Unfortunately, the resulting traces do not contain the desired peak ratios (Figure 18). In this initial experiment the supernatant was expected to be enriched with Dab and HHGlu (Figure 17, scenario A), but instead was enriched with Dab and Glu. Similarly, the elution fraction was expected to be dominated by Glu by virtue of its association with the tagged Lys peptide, but instead HHGlu prevails. These experiments were also completed using DabHis (Figure 19) and GluHis (Figure 20) and the respective untagged peptides, to ensure that His tag placement was not interfering with complex formation. In each of these cases similar results were observed.

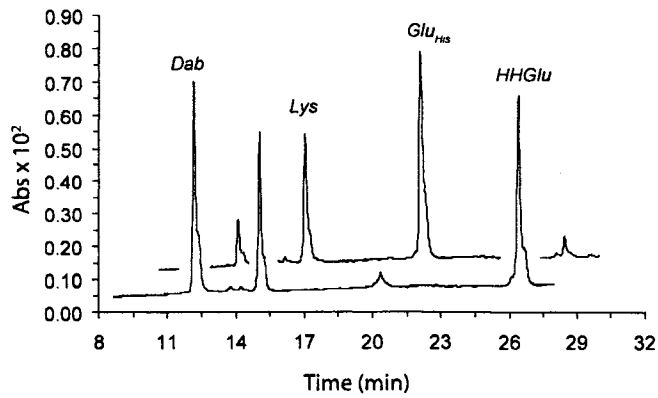

Figure 20. Ni-NTA affinity tag analysis of equimolar HHGlu, GluHis, Dab, Lys mixture. Supernatant fraction (front trace) contains Dab, Lys, and HHGlu. Elution fraction (back trace) contains tagged peptide (GluHis) and Lys. See Figure 17 for schematic diagram.

3-5 Complex Assembly – Peptide Exchange

Although peptide partitioning did not prove to be a viable option with these peptide complexes, the range of stability of these complexes may allow for peptide exchange to form a complex with greater stability. In these assays an initial complex would undergo a component exchange upon addition of a third peptide that would

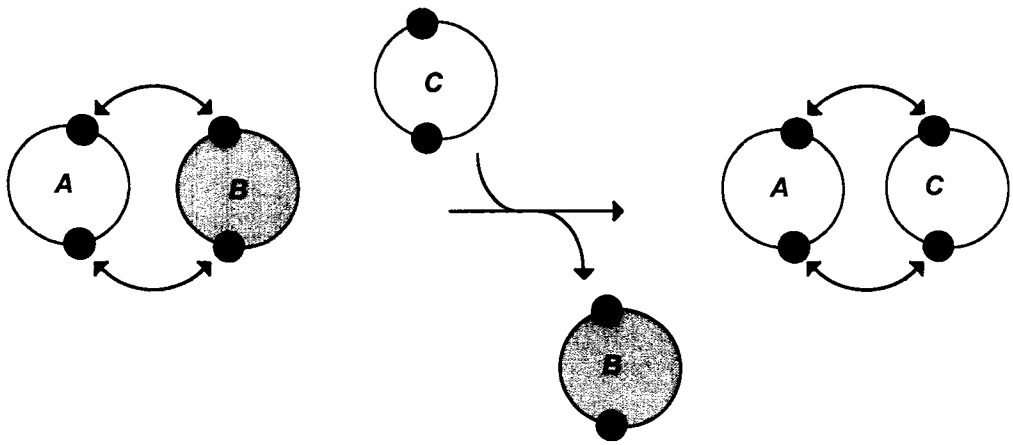

Figure 21. Peptide exchange experiment scheme. Initial complex contains equimolar mixture of peptides A and B. Introduction of peptide C, results in displacement of peptide B, forming new complex on increased stability between peptides A and C.

form a more stable heterodimer (Figure 21). Our initial efforts focused on complexes that would offer the greatest difference in stability between initial and exchanged complexes. Thus, our initial heterodimeric complexes contained mixtures of DabHis and HGlu (or HHGlu, Figure 22). Upon addition of the Lys peptide an exchange should occur with two results: formation of a new Lys:HGlu (or HHGlu) complex that does not contain a His tag and therefore should be located in the supernatant, and expulsion of the DabHis peptide from the complex, which results in only this peptide present in the elution fraction (Figure 23). As expected, observed peak ratios are consistent with an exchange from the initial complex upon addition of the Lys peptide, as both the Lys and HGlu (or HHGlu) peptides are significantly enriched in the supernatant fraction, while the elution fraction is dominated by DabHis. Although this experiment demonstrated the capacity for component exchange, it was completed with initial and final complexes that contained the greatest stability difference. To probe the limitations of peptide exchange, complexes with a smaller stability difference were analyzed. The initial complexes in these exchange reactions

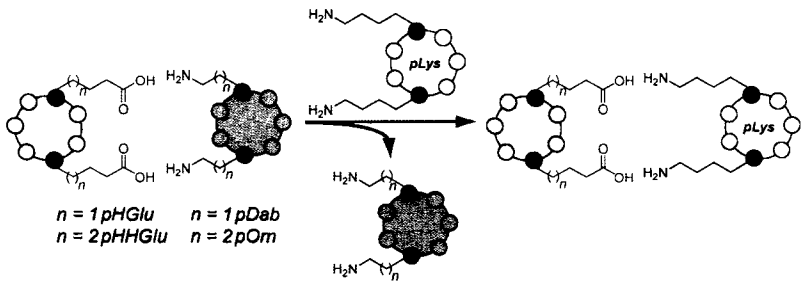

Figure 22. Exchange assay diagram for four different initial complexes DabHis:HGlu, DabHis:HHGlu, OrnHis:HGlu or OrnHis:HHGlu. In each case addition of Lys results in exchange of initial amine bearing component in favor of more stable Lys:HGlu or Lys:HHGlu complex.

contained OrnHis:HGlu (or HHGlu). The peptide exchange, if successful, should proceed in an analogous manner as outlined for the DabHis complexes (Figure 22). Analysis of the resulting HPLC spectra indicate that component exchange occurred as predicted (Figure 24). The supernatant fraction contains approximately equimolar ratios of the Lys and HGlu (or HHGlu) components. In addition, the elution fraction is dominated by the tagged OrnHis peptide, indicating that a smaller stability difference does not prevent component exchange. These results open the possibility of component exchange that disrupts native glutamic acid – lysine interactions.

In this experiment, the Lys peptide will bear an N-terminal Gly-Gly-$(His)_6$ affinity tag. The initial complex containing LysHis:Glu is exposed to the beads and then HGlu (or HHGlu) is added to the mixture. Successful exchange should again produce two results: the exchanged Glu peptide should be the dominant peak in the supernatant and the elution fraction should contain the newly formed LysHis:HGlu (or HHGlu) heterodimer (Figure 25). Scrutiny of the resulting spectra from these experiments indicates that the initial LysHis:Glu complex is susceptible to component exchange (Figure 26). The dominant peak in the supernatant fraction is Glu, while the elution fraction is considerably enriched in HGlu (or HHGlu).

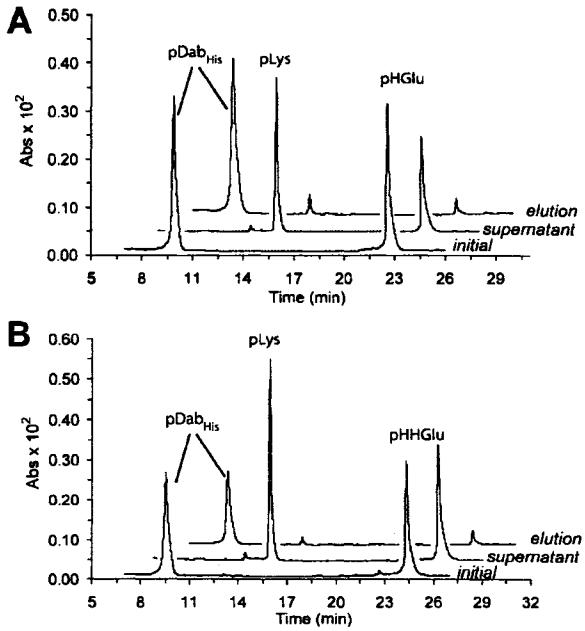

Figure 23. Ni-NTA affinity tag analysis of exchange assay. Initial complex (front trace) contains DabHis:HGlu (**A**) or DabHis:HHGlu (**B**). Addition of Lys results in component exchange with DabHis peptide, enriching the supernatant fraction (middle trace) with Lys:HGlu (**A**) or Lys:HHGlu (**B**). Remaining elution fraction (rear trace) enriched in DabHis. See Figure 22 for schematic diagram.

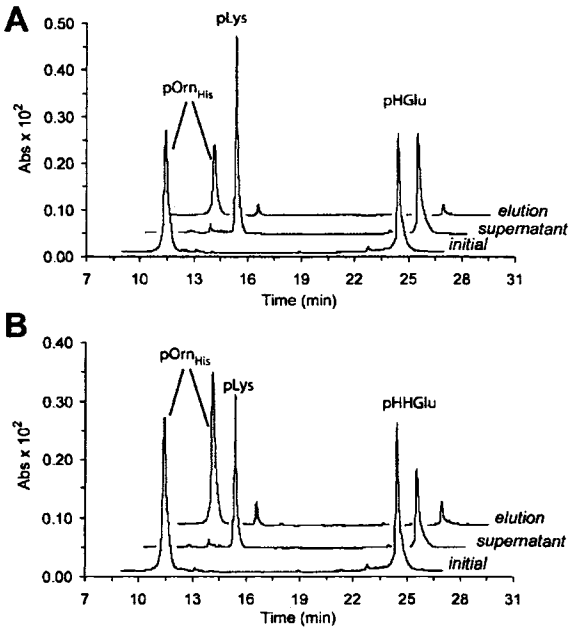

Figure 24. Ni-NTA affinity tag analysis of exchange assay. Initial complex (front trace) contains OrnHis:HGlu (**A**) or OrnHis:HHGlu (**B**). Addition of Lys results in component exchange with OrnHis peptide, enriching the supernatant fraction (middle trace) with Lys:HGlu (**A**) or Lys:HHGlu (**B**). Remaining elution fraction (rear trace) enriched in OrnHis. See Figure 22 for schematic diagram

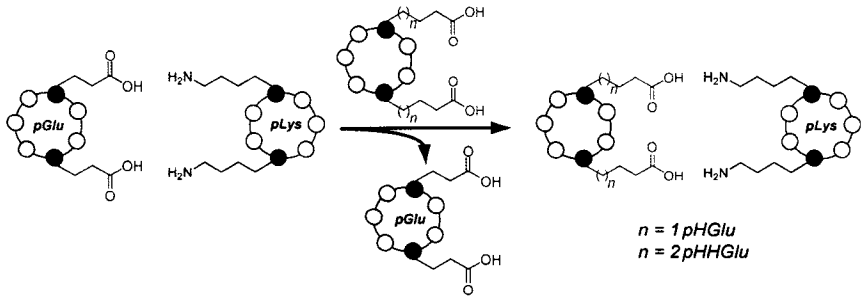

Figure 25. Exchange assay diagram for LysHis:Glu complex. In each case addition of HGlu or HHGlu results in exchange of Glu component in favor of more stable Lys:HGlu or Lys:HHGlu complex.

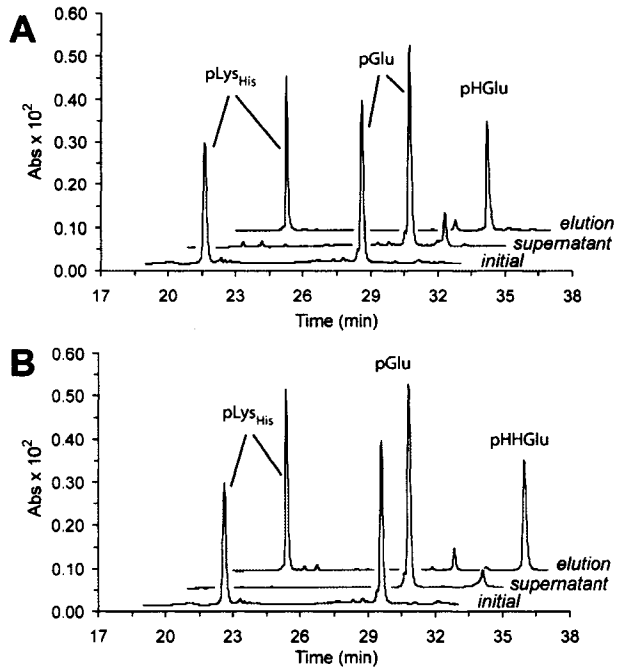

Figure 26. Ni-NTA affinity tag analysis of exchange assay. Initial complex (front trace) contains LysHis:Glu. Addition of HGlu (**A**) or HHGlu (**B**) results in component exchange, enriching the supernatant fraction (middle trace) with Glu. Remaining elution fraction (rear trace) enriched in LysHis:HGlu (**A**) or LysHis:HHGlu (**B**)

3-6 Conclusions

The data presented above demonstrate the importance of sidechain length and functionality to homodimer stability. The increased stability of the carboxylate

bearing complexes when compared to those with ammonium groups with similar sidechain length was unexpected and the exact cause of this is still unclear. Although generalizations about side chain length and functionality in heterodimeric complex stability cannot be made, there is a lower limit of combined methylenes required for complex formation. In addition, heteromers where one component peptide bears a single methylene unit (Asp, Dap) are unable to form stable complexes. Complexes containing intermediate combined methylenes (5 or 6) display varying levels of stability, while complexes that contain seven or eight combined methylenes are extremely stable. The smaller stability differences exhibited by complexes with longer combined sidechains indicate that stability will not continue to increase with lengthening sidechains. Although the various stabilities found within these complexes are not sufficient to drive peptide partitioning, it is possible to govern complex assembly events. The capability for control of complex formation, coupled with other recent advances, bodes well for the future design of peptide structures.

3-7 Experimental Section

Peptide Synthesis. Amino acids were obtained from NovaBiochem (San Diego), with the exception of Boc-Dap(Bzl)-OH, Boc-Dab(Bzl)-OH and Boc-Orn(Bzl)-OH, which were obtained from Bachem (California). Peptides were prepared according to the in situ neutralization protocol developed by Kent,[10] except HGlu and HHGlu which were prepared by standard Fmoc solid phase methods. Each peptide was purified by reversed-phase HPLC (C-18 column, (solvent A) 1% CH_3CN in H_2O, 0.1% (v/v) CF_3CO_2H, (solvent B) 10% H_2O in CH_3CN, 0.07% (v/v) CF_3CO_2H), and

the identity of purified samples was confirmed by electrospray mass spectrometry (Finnegan LCQ Duo). All peptides are C-terminally amidated and N-Terminally acetylated; each contains an acetamidobenzoate group on the side chain nitrogen of Lys_{12} as a spectroscopic label ($\epsilon_{270} = 18069$).

CD Spectroscopy. All experiments were performed on an Aviv model 202 circular dichroism spectrometer, equipped with a Microlab 500 series automated titration assembly. Sample concentrations were measured by UV absorbance of the acetamidobenzoate label at 270 nm. Wavelength data are the average of three scans from 250 to 200 nm in 1 nm steps. Thermal denaturation experiments at 222 nm were run from 0 to 90 °C in 2 deg steps, at a 2 deg/min rate of increase with 1 min of equilibration and data averaging at each temperature. Tm values were obtained from the minima of the first derivatives of Θ vs 1/T plots. Guanidinium titrations were performed using the automated titration assembly. The signal at 222 nm was recorded for solutions of constant peptide concentration with guanidine hydrochloride concentrations varied from 0 to 5 M in 0.2 M increments. Data were collected for 1 min at each step, with 10 min equilibration times (solutions were stirred during equilibration but not data collection). Urea titrations were performed using identical conditions as guanidine titrations with the following exception: urea concentrations were varied from 0 to 8 M in 0.3 M increments.

Analytical Ultracentrifugation. Sedimentation equilibrium experiments were performed using a Beckman XL-I or Beckman XL-A analytical ultracentrifuge

equipped with an An60 Ti rotor or An50 Ti rotor. Data were collected using 12 mm path length six-sector centerpieces at 270 nm. Samples were dialyzed against the reference buffer at 4 °C overnight. Data were collected at 38000 and 48000 rpm at concentrations spanning 17-55 μM. Samples were judged equilibrated (in all cases equilibration was complete in 12 h) when three consecutive scans taken 1 h apart were indistinguishable. Solvent densities and partial molar volumes were calculated in the manner prescribed by Laue.[11] Data were analyzed using Ultrascan[12] (v. 7.1) and global fit to appropriate monomer dimer models.

Ni-NTA Affinity Tag Experiments (Figure 8). A 0.5 mL sample of a 50% slurry of Ni-NTA agarose (Qiagen) in an Eppendorf tube was centrifuged for 30 s, followed by removal of the supernatant. Peptide solution was added, and the tube was repeatedly inverted for 5 min. The sample was centrifuged (30 s), and the supernatant (flow-through fraction) was removed. The procedure was then repeated with 1 mL of buffer (wash fraction) and 1 mL of buffer containing 250 mM imidazole (elution fraction), except that the wash fraction was not agitated for 5 min. Solutions were analyzed by RP-HPLC. All solutions were 10 μM in total peptide, except for competition experiments, which used 20 μM and exchange experiments, in which each component peptide was 5 μM.

3-8 Literature Cited

1 (a) Guo, Z; Zhour, D.; Schultz, P.G. *Science* **2000,** *288*, 2042-2045. (b) Delano, W.L.; Ultsch, M.H.; De Vos, A.M.; Wells, J.A. *Science* **2000**, 287, 1279-1283.

2 (a) Micklatcher, C.; Chmielewski, J. *Curr. Opin. Chem. Biol.* **1999**, *3*, 724-729. (b) Degrado, W.F.; Summa, C.M.; Pavone, V.; Nastri, F.; Lombardi, A. *Annu. Rev. Biochem.* **1999**, *68,* 779-819. (c) Cooper, W.J.; Waters, M.L. *Curr. Opin. Chem. Biol.* **2005**, *9*, 627-631.

3 (a) Tang, Y.; Ghirlanda, G.; Vaidehi, N.; Kua, J.; Mainz, D.T.; Goddard, W.A. III; Degrado, W.F.; Tirrell, D.A. *Biochemistry* **2001**, *40*, 2790-2796. (b) Hill, R.B.; Hong, J.-K.; Degrado, W.F. *J. Am. Chem. Soc.* **2000**, *122*, 746-747. (c) Harbury, P.B.; Plecs, J.J.; Tidor, B.; Alber, T.; Kim, P.S. *Science* **1998**, *282*, 1462-1467. (d) Oakley, M.G.; Kim, P.S. *Biochemistry* **1998**, *37*, 12603-12610. (e) Harbury, P.B.; Zhang, T.; Kim, P.S.; Alber, T. *Science* **1993**, *262*, 1401-1407. (f) Gonzalez, L., Jr.; Woolfson, D.N.; Alber, T. *Nat. Struct. Biol.* **1996**, *3*, 1011-1018.

4 (a) Phelan, P.; Gorfe, A.A.; Jelesarov, I.; Marti, D.N.; Warwicker, J.; Bosshard, H.R. *Biochemistry* **2002**, *41*, 2998-3008. (b) Chana, M.; Tripet, B.P.; Mant, C.T.; Hodges, R.S. *J. Struct. Biol.* **2002**, *137*, 206-219. (c) Gurnon, D.G.; Whitaker, J.A.; Oakley, M.G. *J. Am. Chem. Soc.* **2003**, *125*, 7518-7519. (d) Schnarr, N.A.; Kennan, A.J. *J. Am. Chem. Soc.* **2003**, *125*, 667-671. (e) Schnarr, N.A.; Kennan, A.J. *J. Am. Chem. Soc.* **2004**, *126*, 14447-144451.

5 O'Shea, E.K.; Lumb, K.J.; Kim, P.S. *Curr Biol.* **1993**, *3*, 658-667.

6 Harbury, P.B.; Zhang, T.; Kim, P.S.; Alber, T. *Science* **1993**, *262*, 1401-1407.

7 Tm values were obtained according to the procedure outlined in: Cantor, C.R.; Schimmel, P.R. *Biophysical Chemistry of Macromolecules, Pt. 3*; W.H. Freeman: New York, NY, 1980, p1132.

8 Method modeled after: Brown, B.M.; Sauer, R.T. *Proc. Natl. Acad. Sci. U.S.A.* **1999**, *96*, 1983-1988.

9 (a) Santoro, M.M.; Bolen, D.W. *Biochemistry* **1988**, *27*, 8063-8068. (b) Becktel, W.J.; Schellman, J.A.; *Biopolymers* **1987**, *26*, 1859-1877. Monomer-dimer equilibrium modeled as in: (c) Jelesarov, I.; Lu, M. *J. Mol. Biol.* **2001**, *307*, 637-656. (d) Dueer, E.; Jelesarov, I. *Biochemistry* **2000**, *39*, 4472-4482.

10 Peptides were synthesized by standard solid phase methods, as in: Schnoelzer, M.; Alewood, P.; Jones, A.; Alewood, D.; Kent, S.B.H. *Int. J. Pept. Protein Res.* **1992**, *40*, 180-193.

11 Laue, T.M.; Shah, B.D.; Ridgeway, T.M.; Pelletier, S.L. in *Analytical Ultracentrifugation in Biochemistry and Polymer Science*; Harding, S.E., Rowe, A.J., Horton, J.C.m Eds.; The Royal Society of Chemistry: Cambridge, 1992; pp 90-125.

12 UltraScan (version 7.1) Developed by Borries Demeler, The University of Texas Health Science Center at San Antonio.

Appendix 1

NMR Spectra

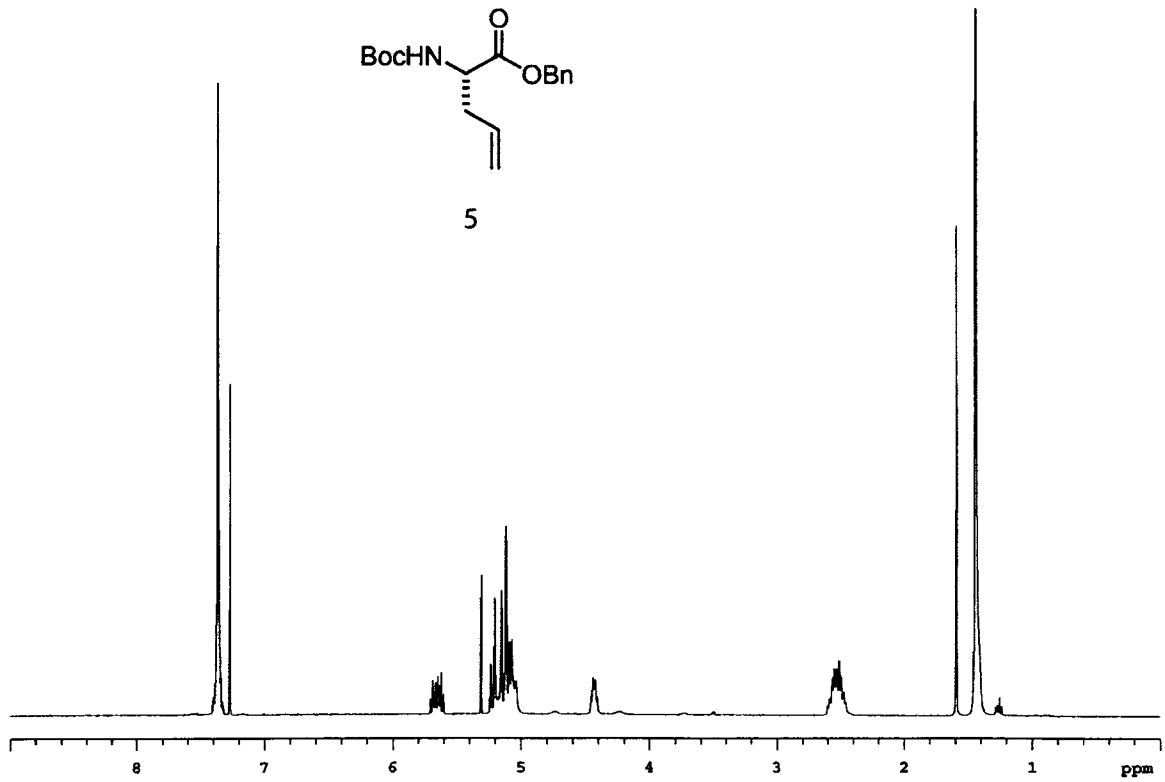

5

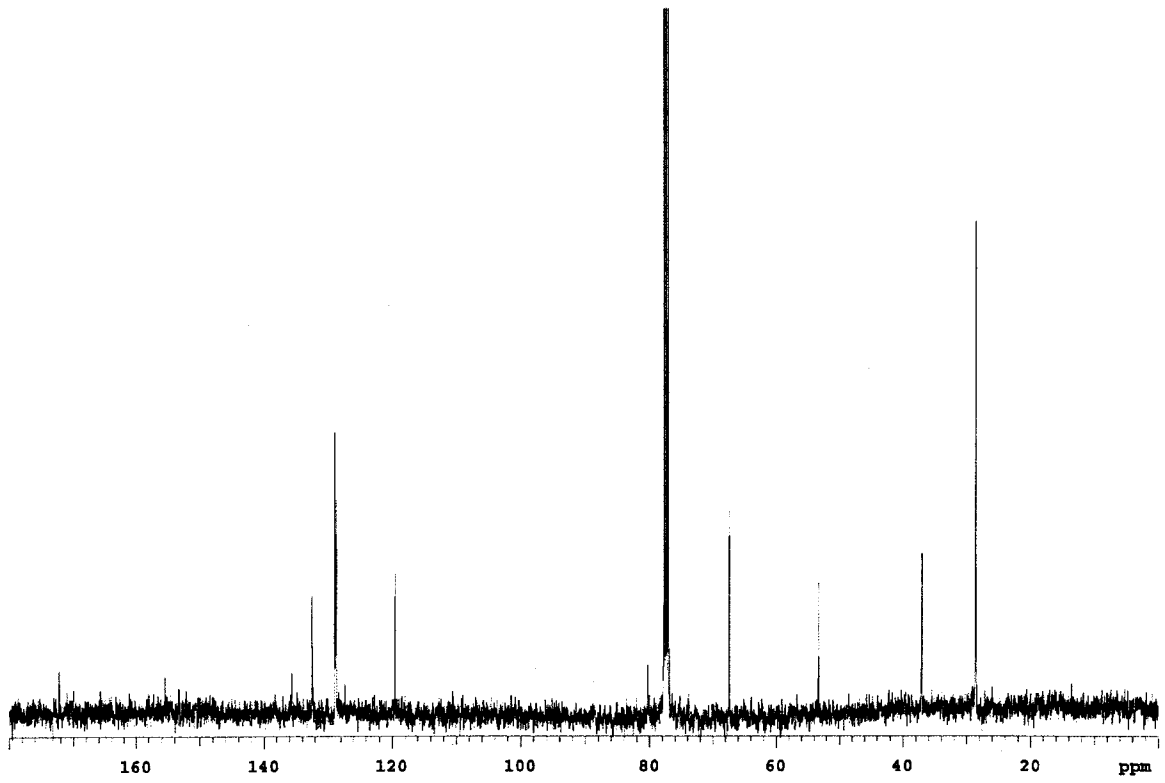

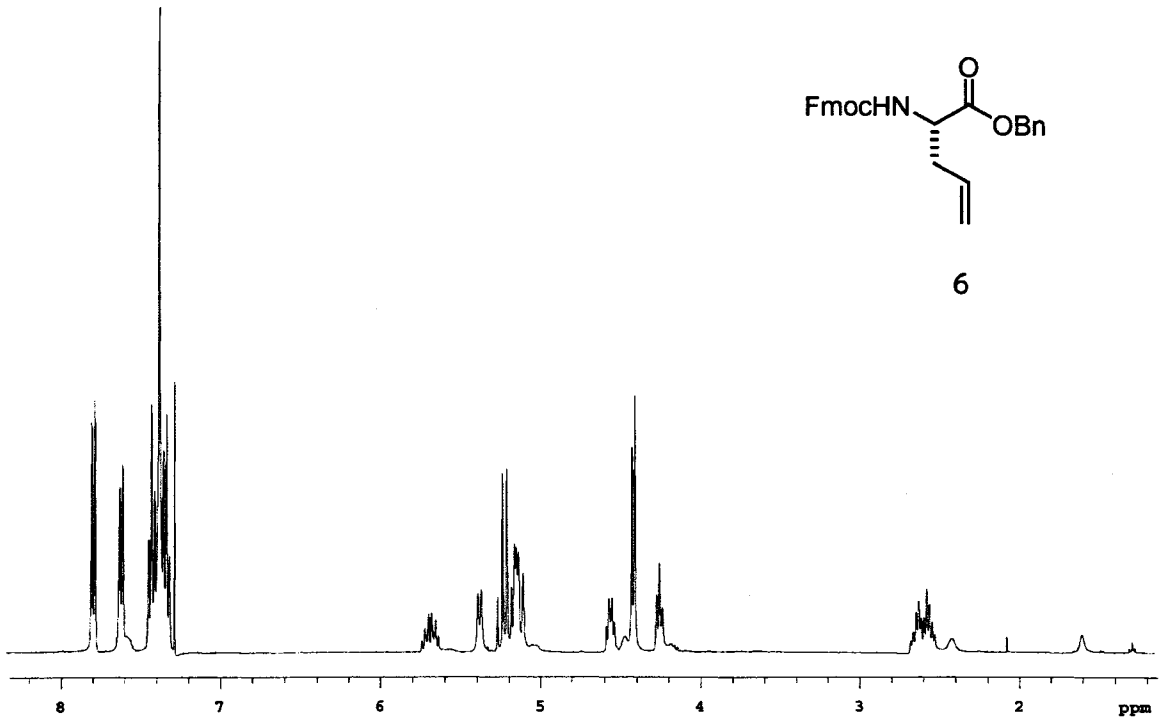

6

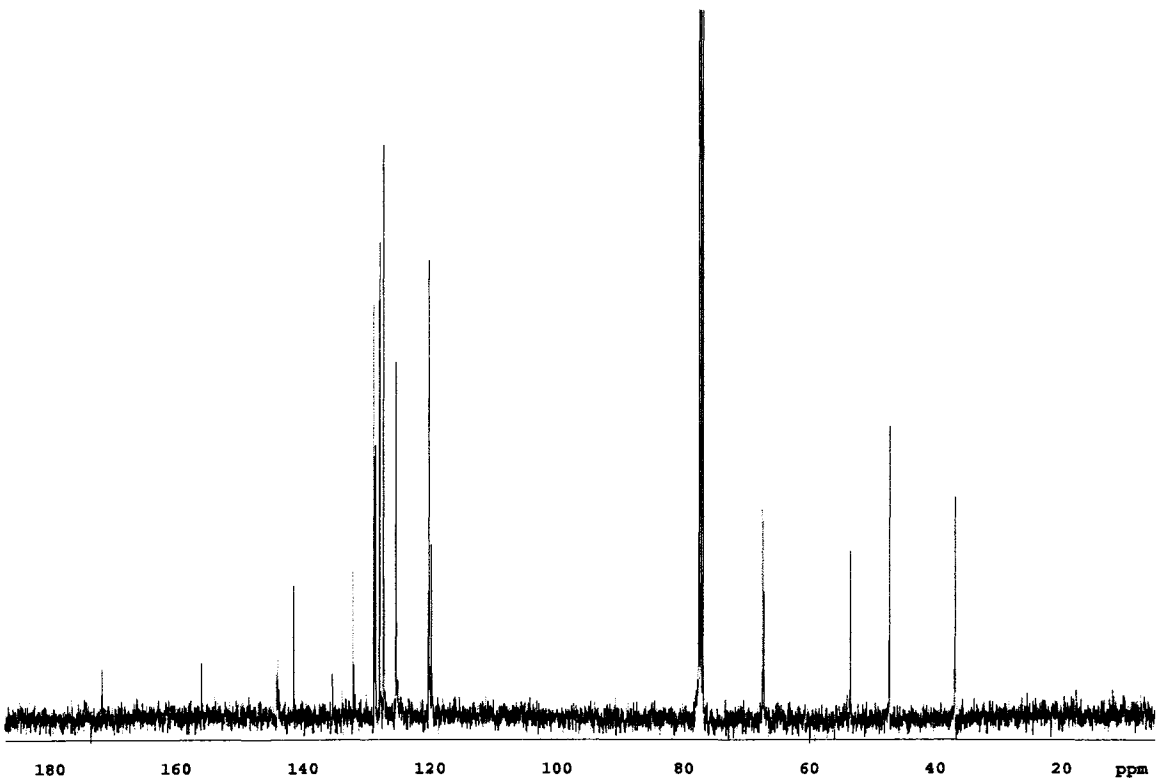

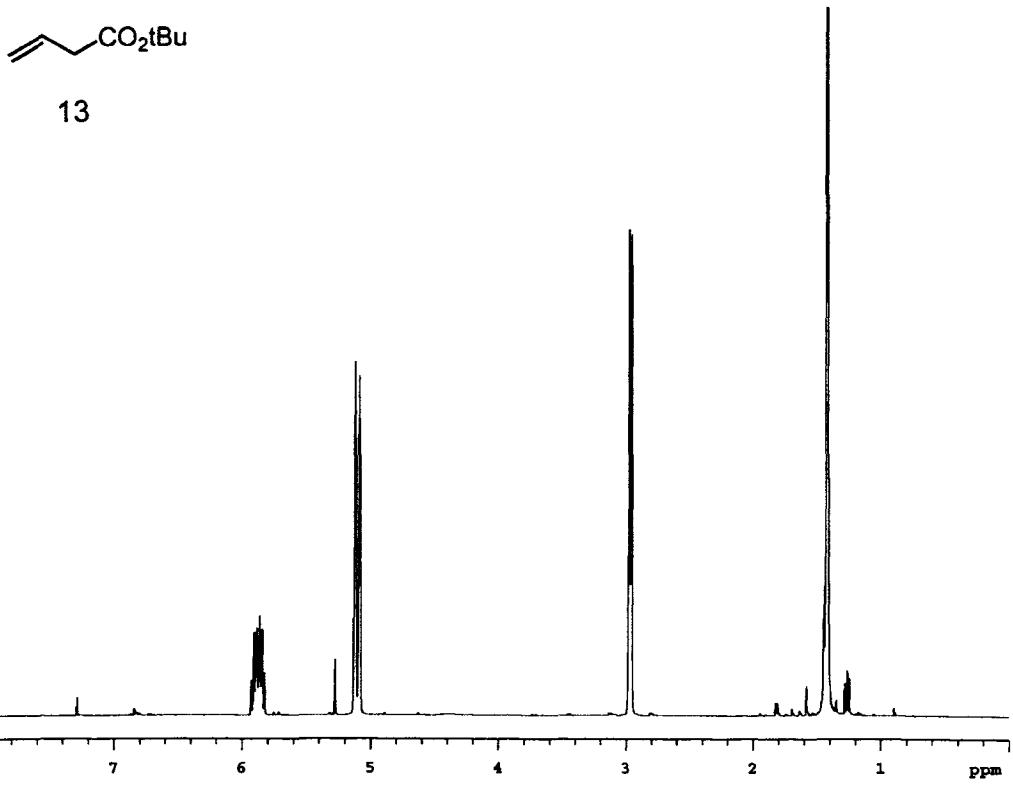

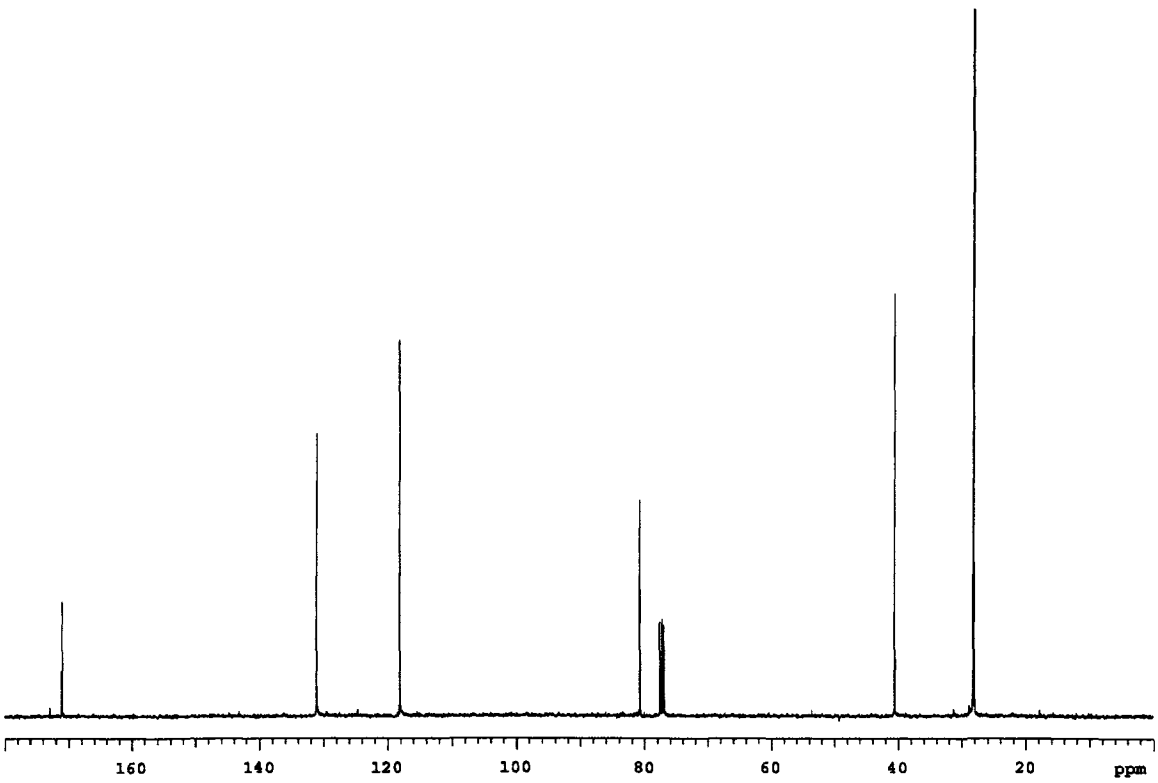

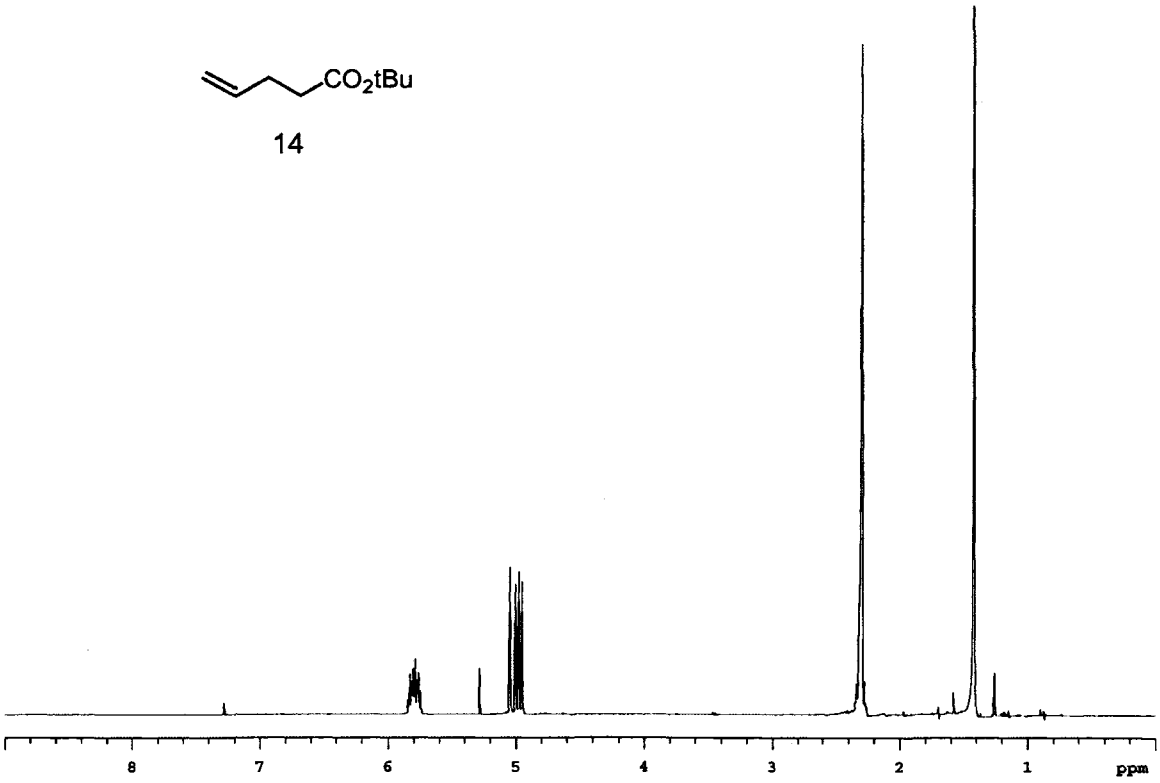

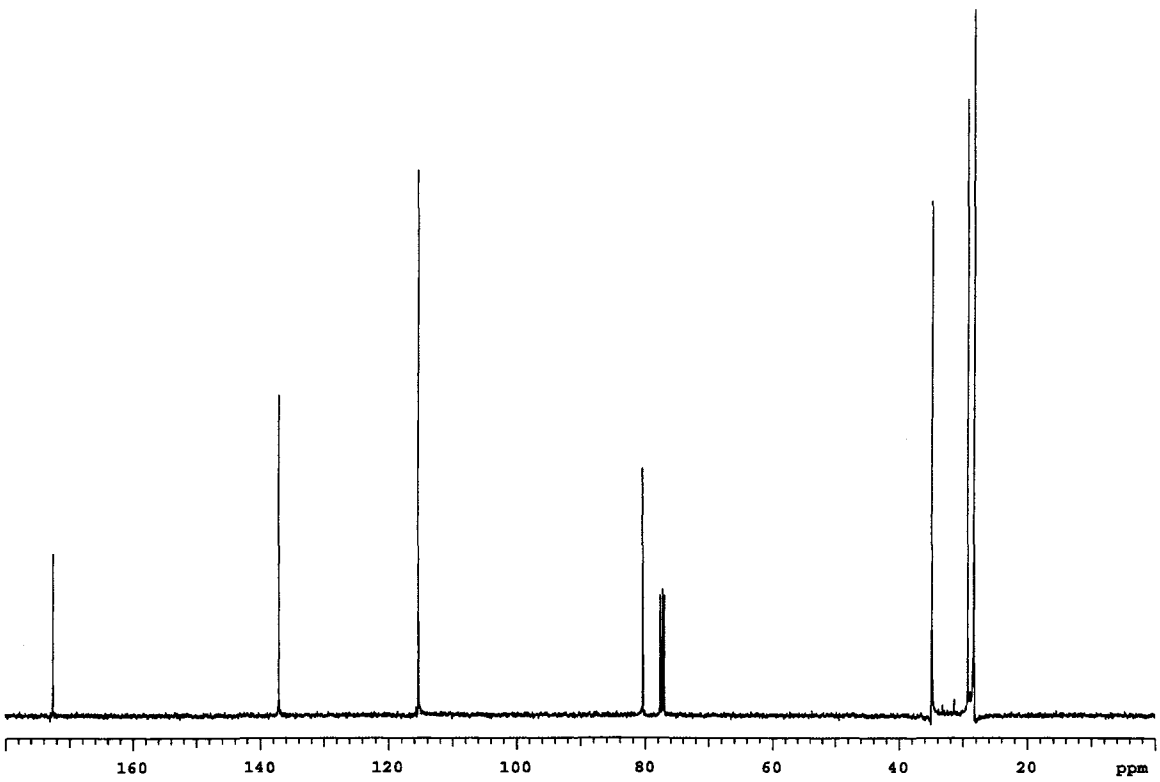

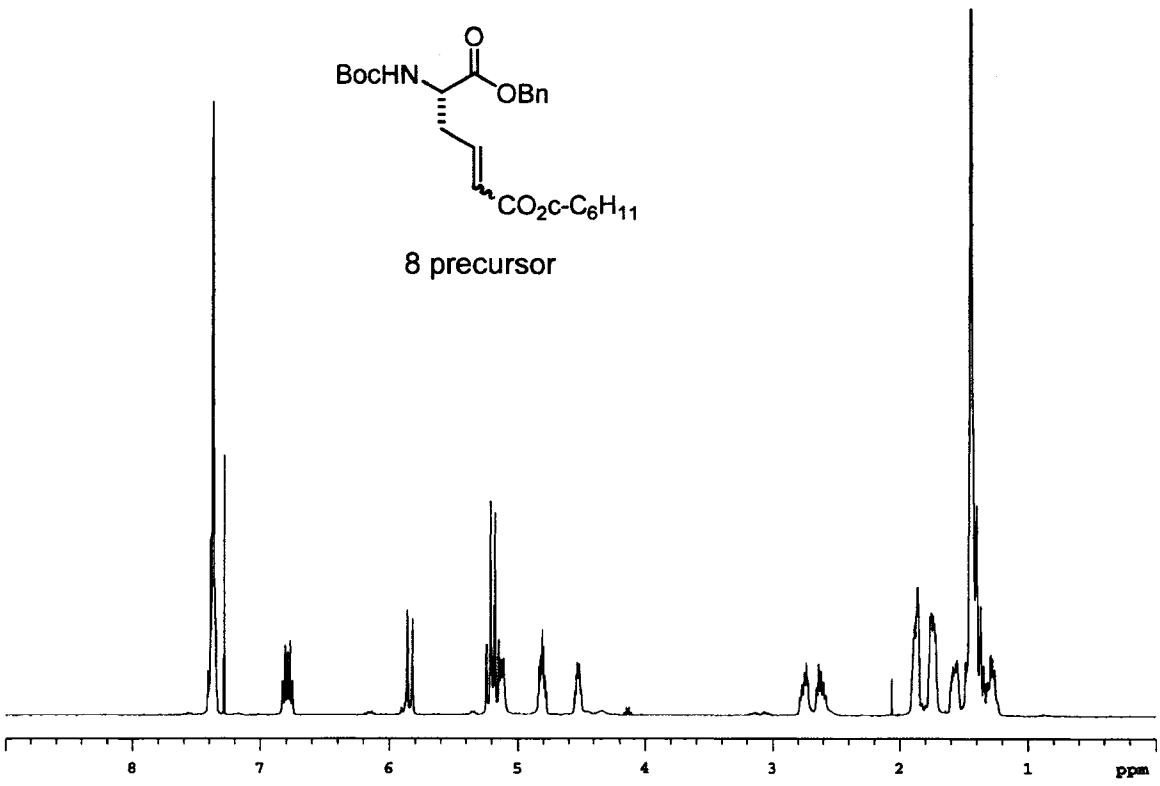

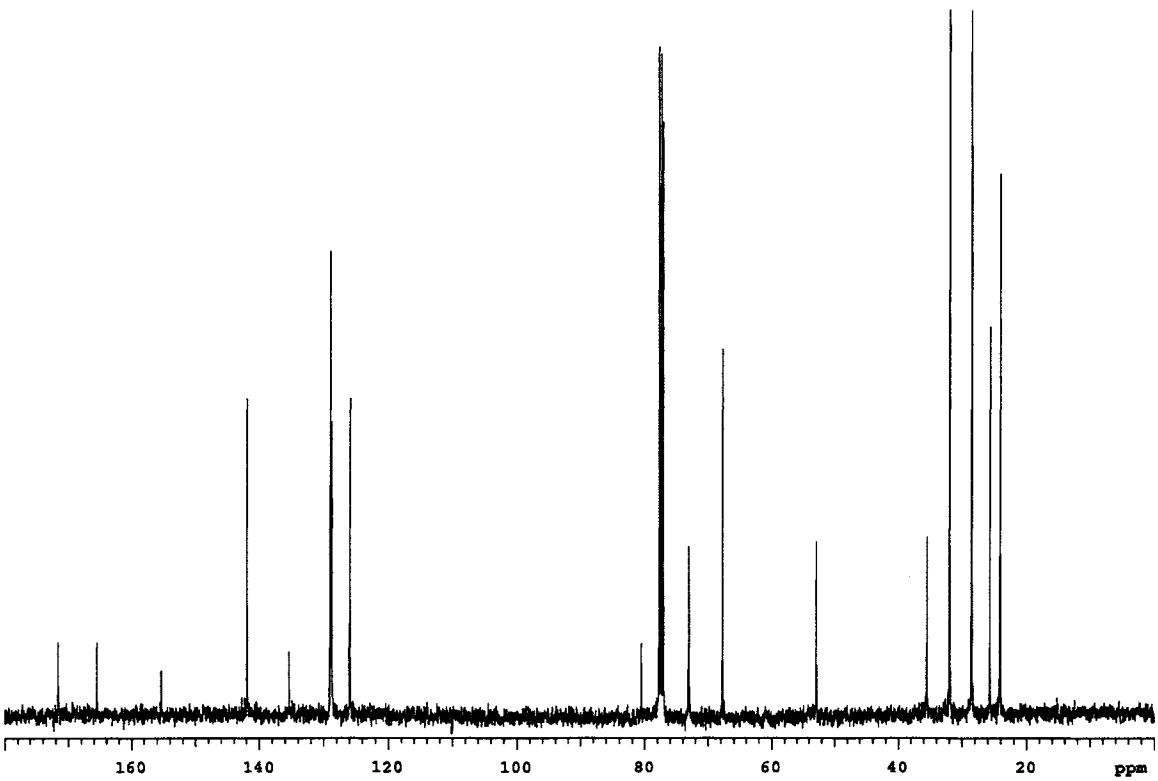

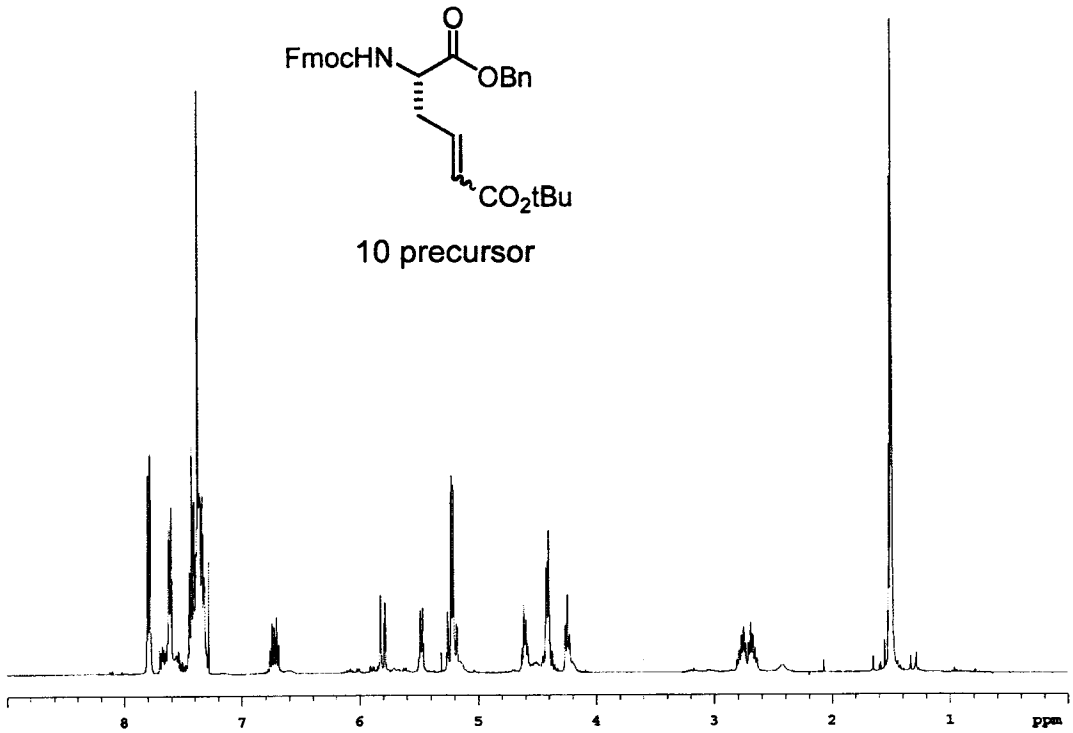

10 precursor

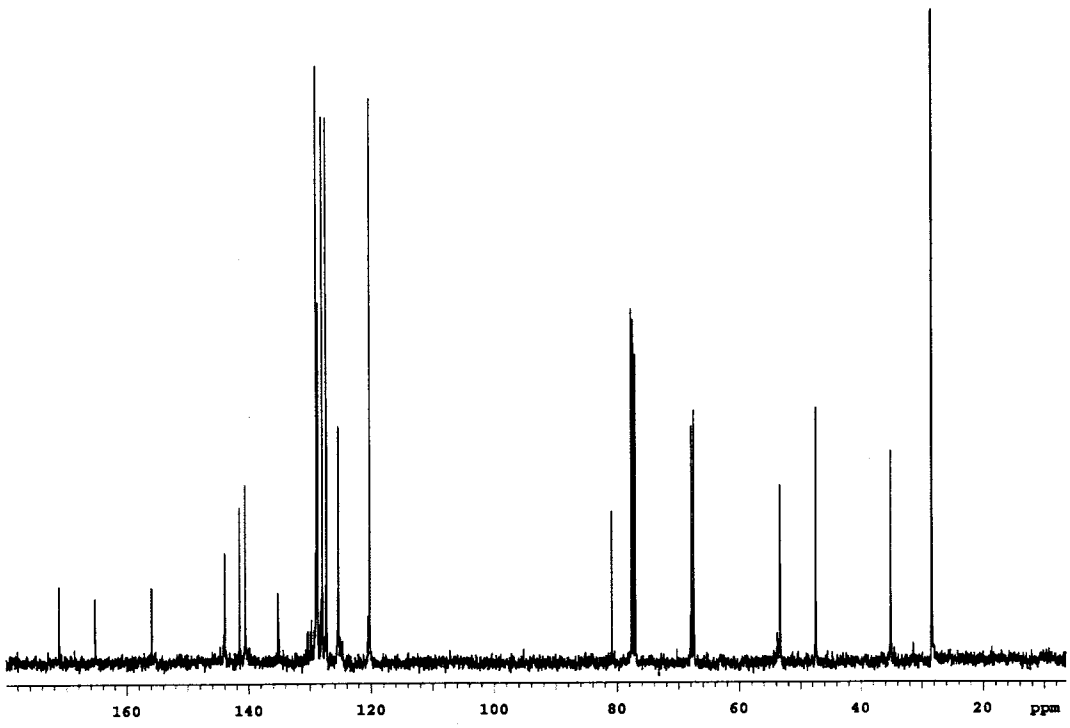

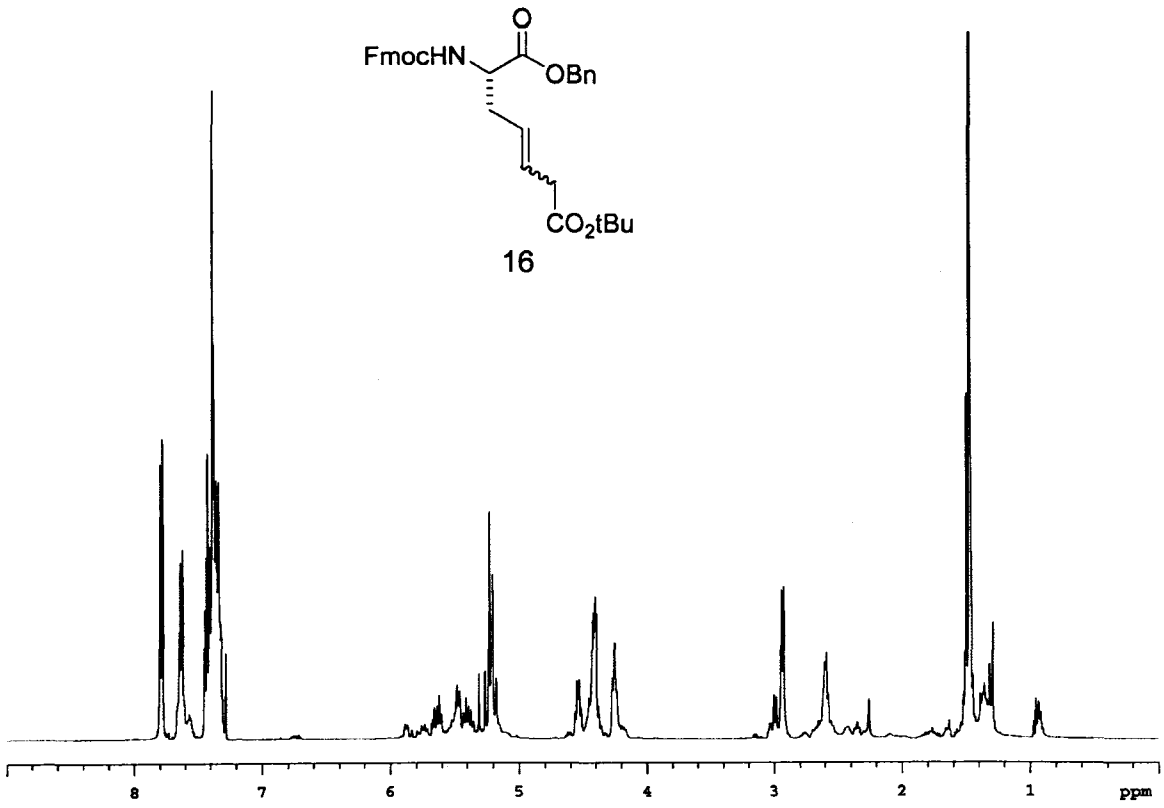

16

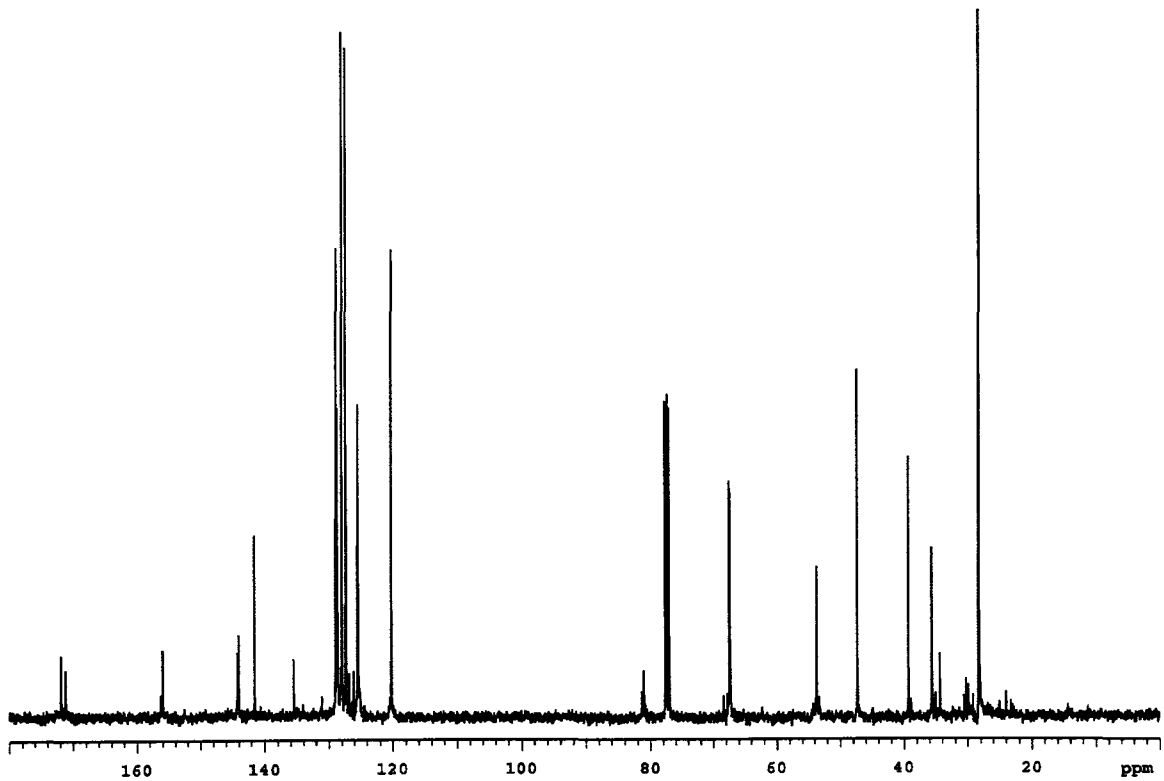

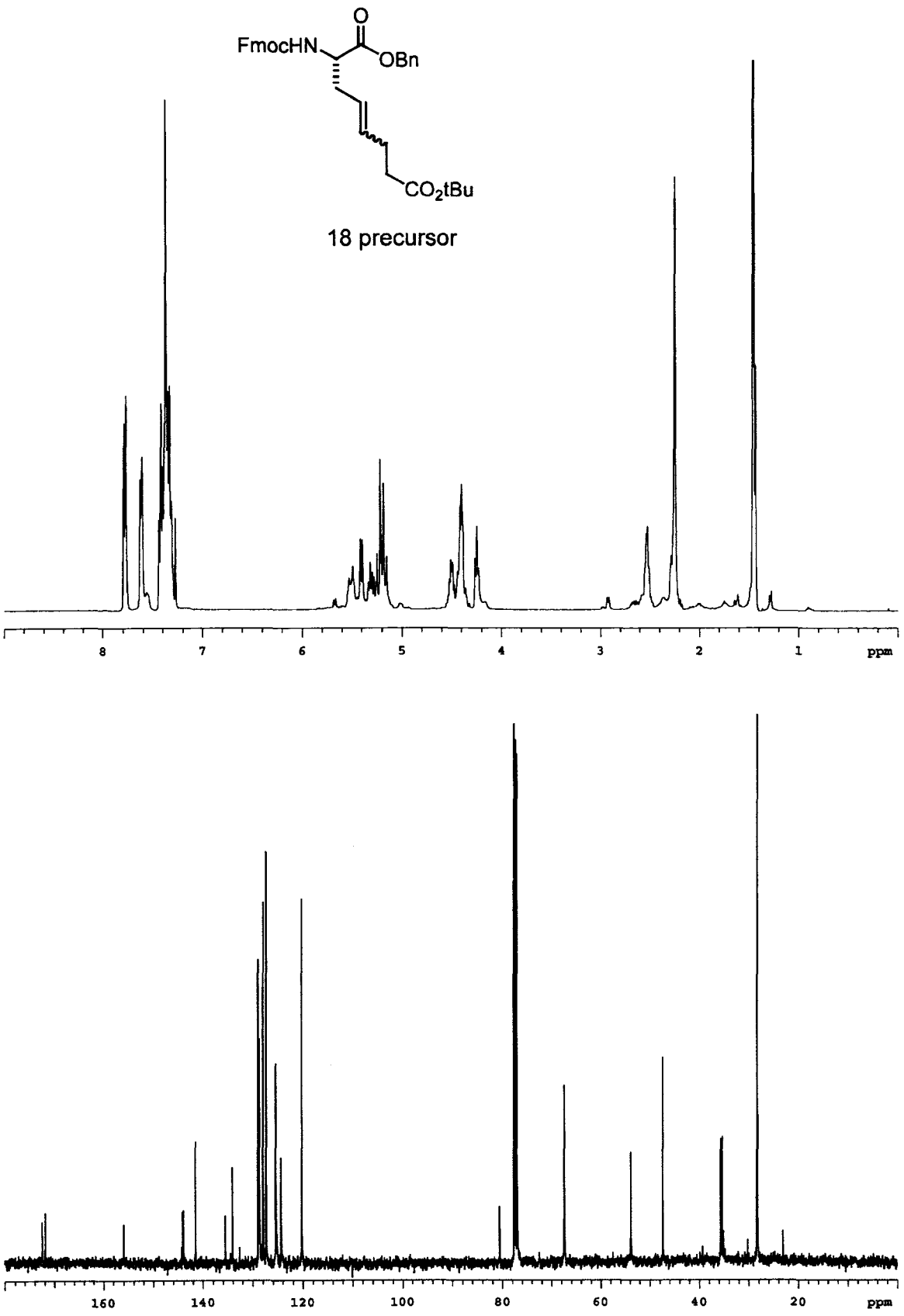

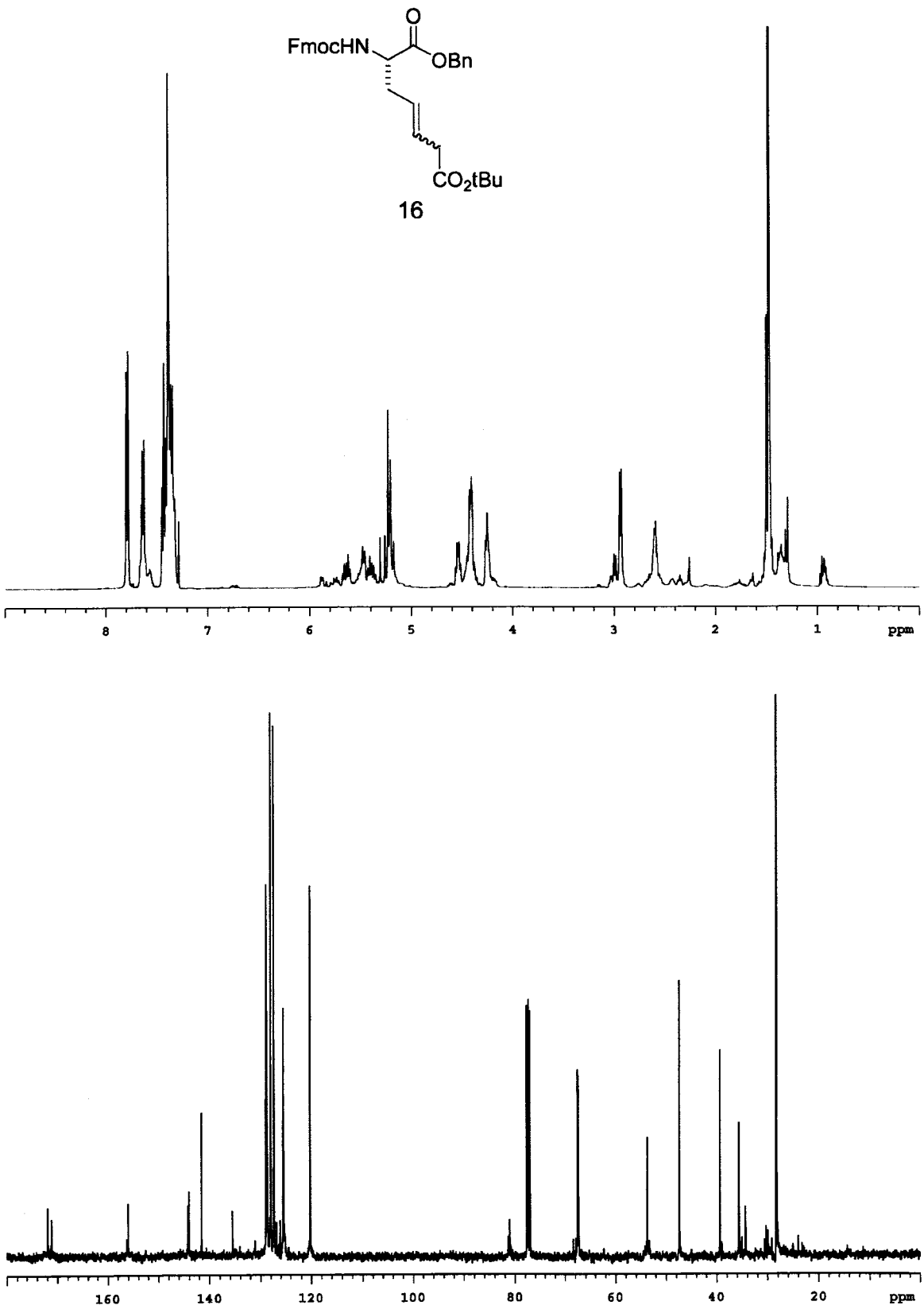

16

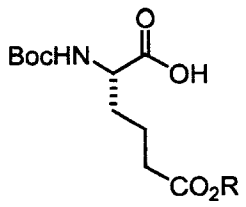

8

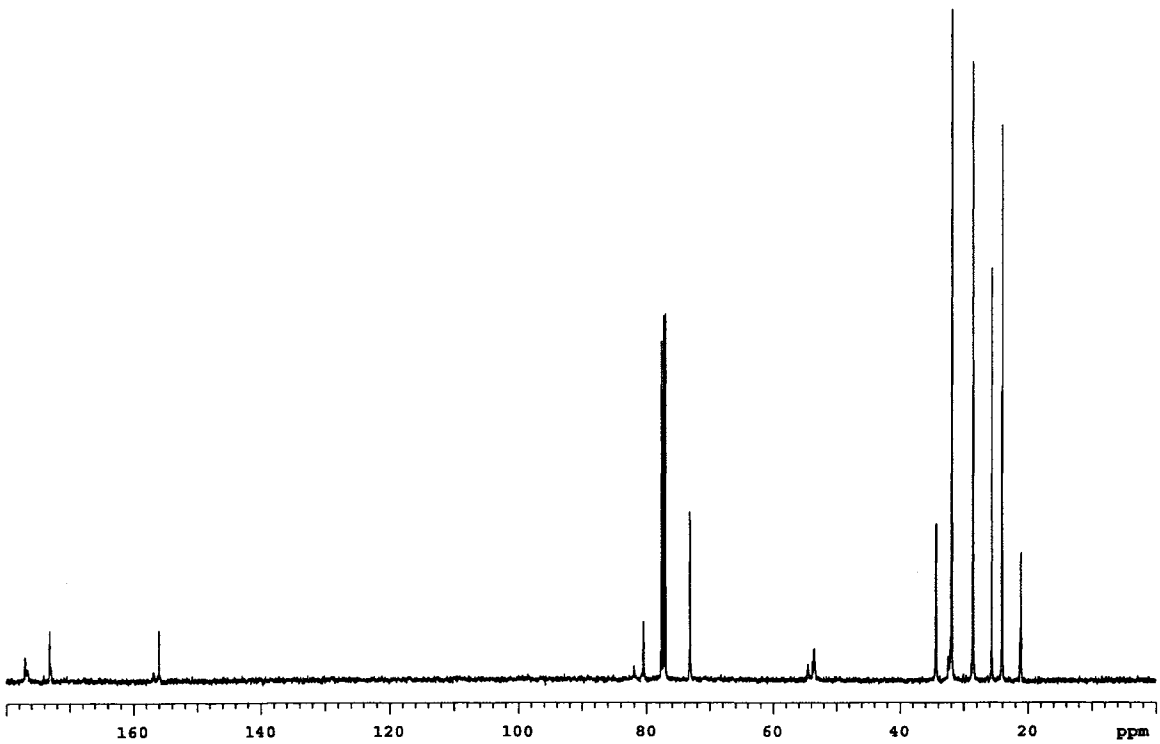

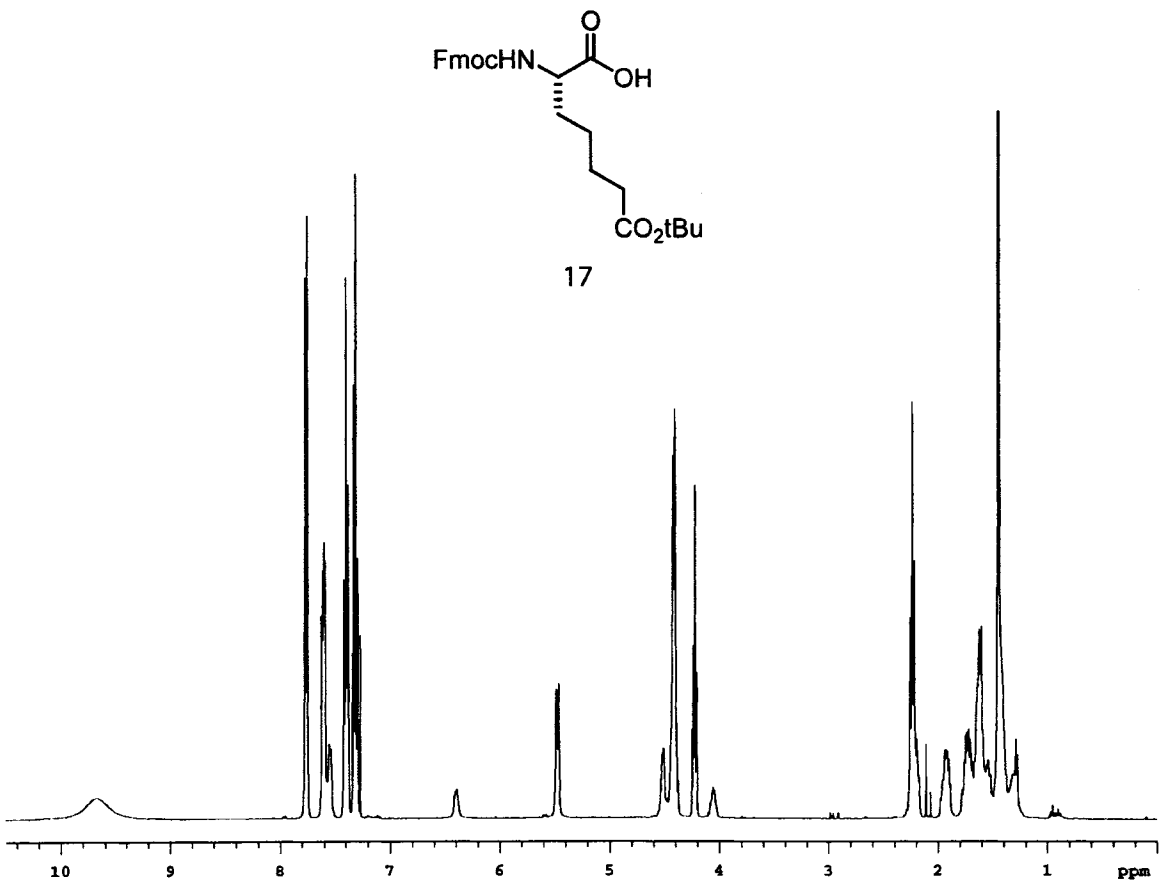

17

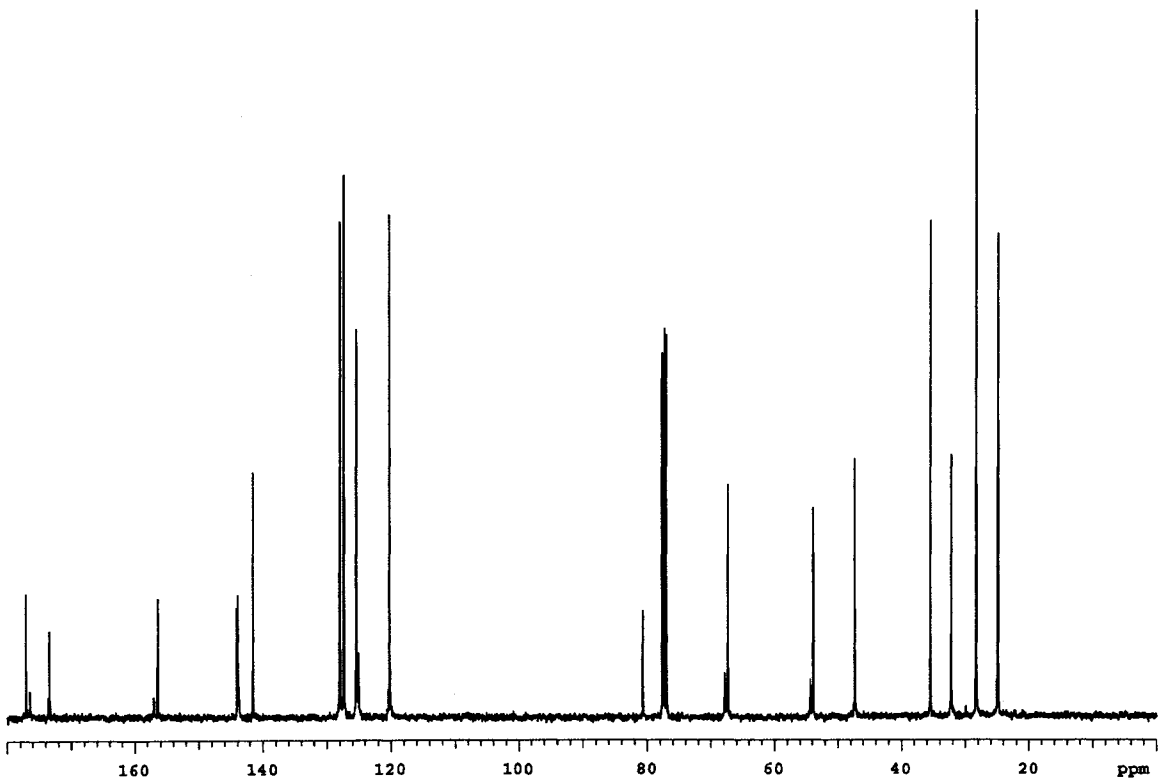

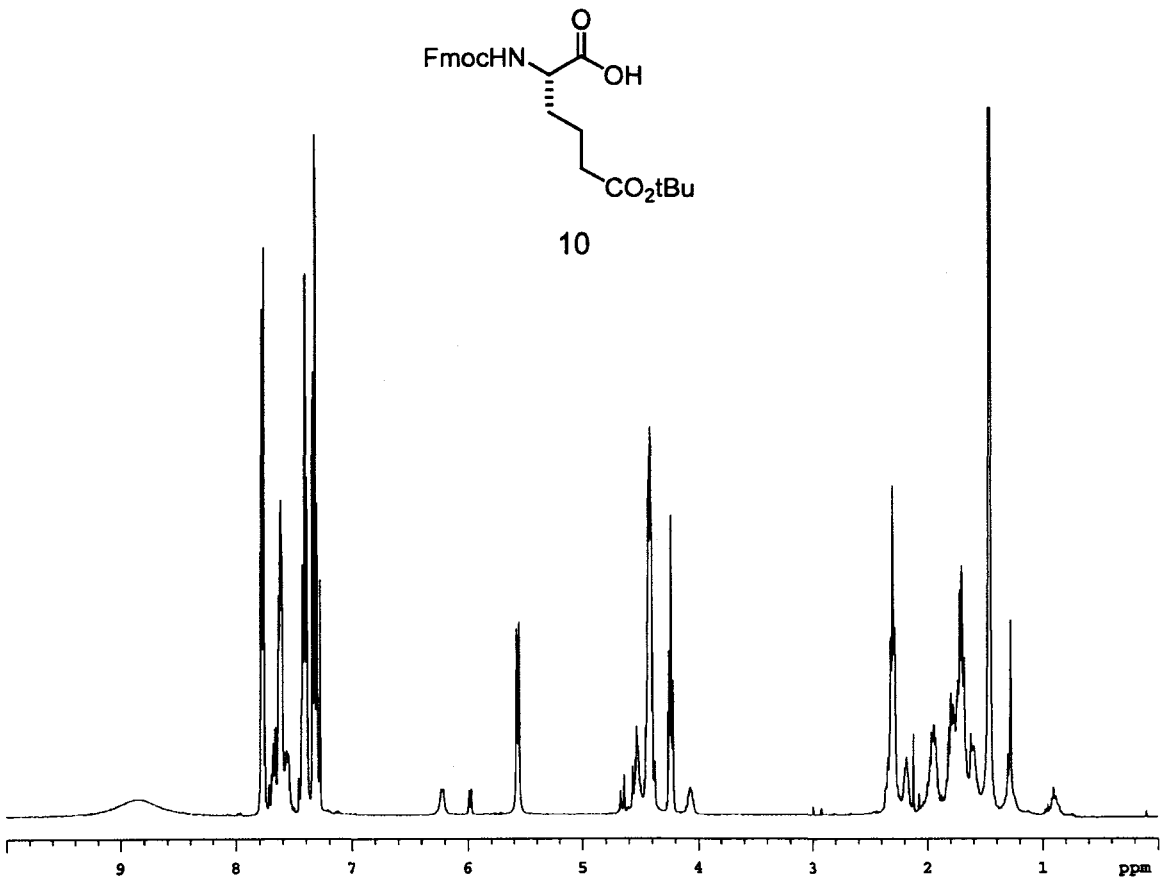

10

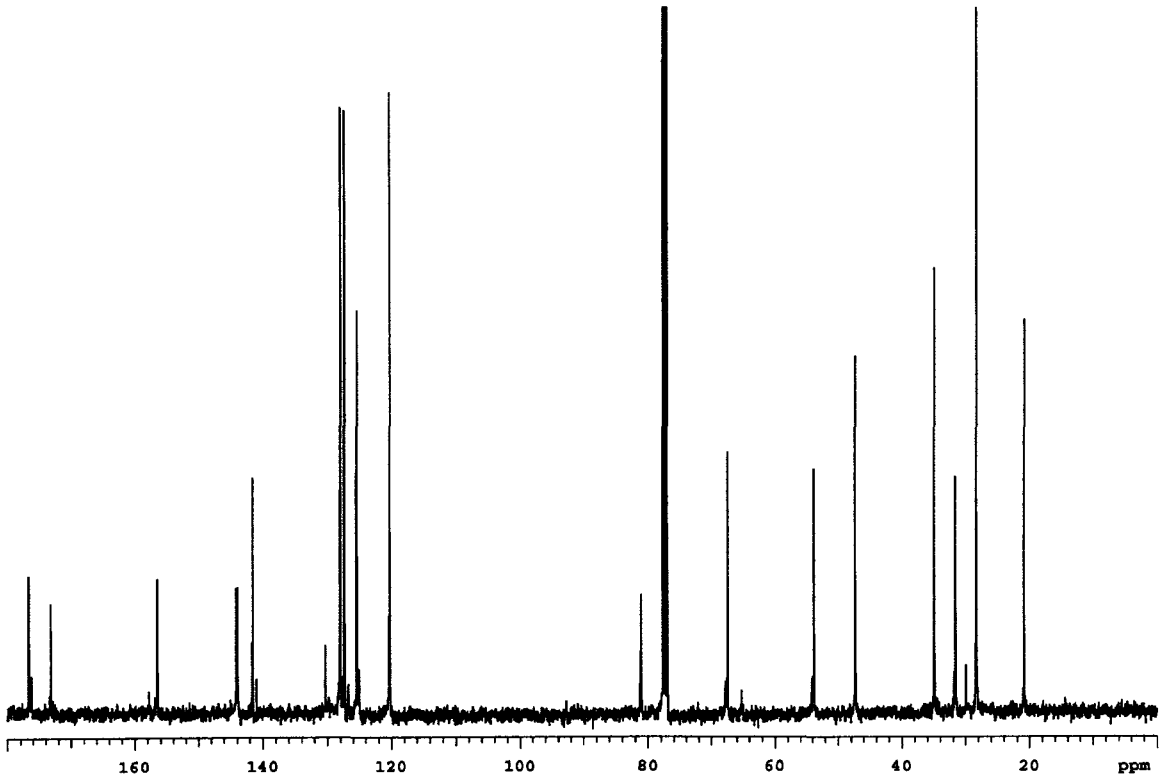

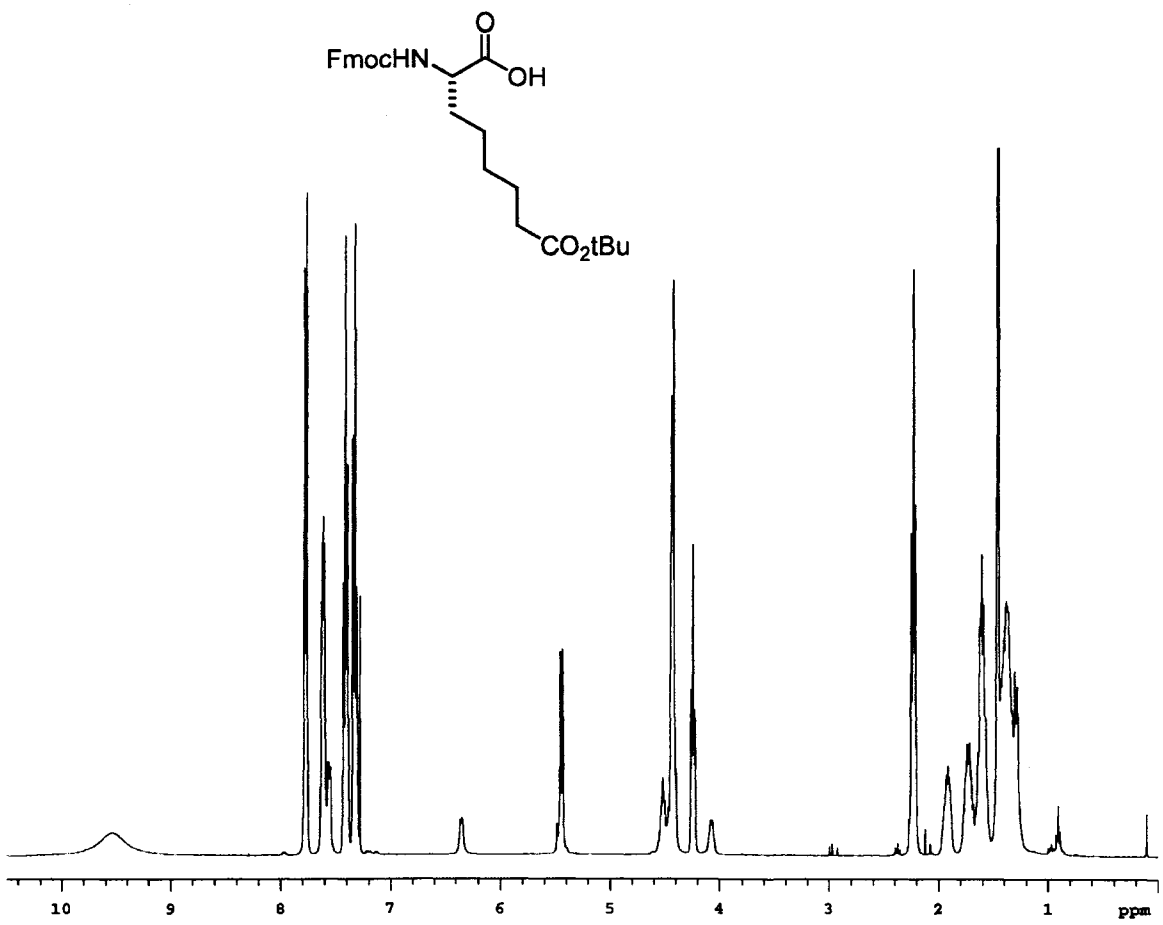

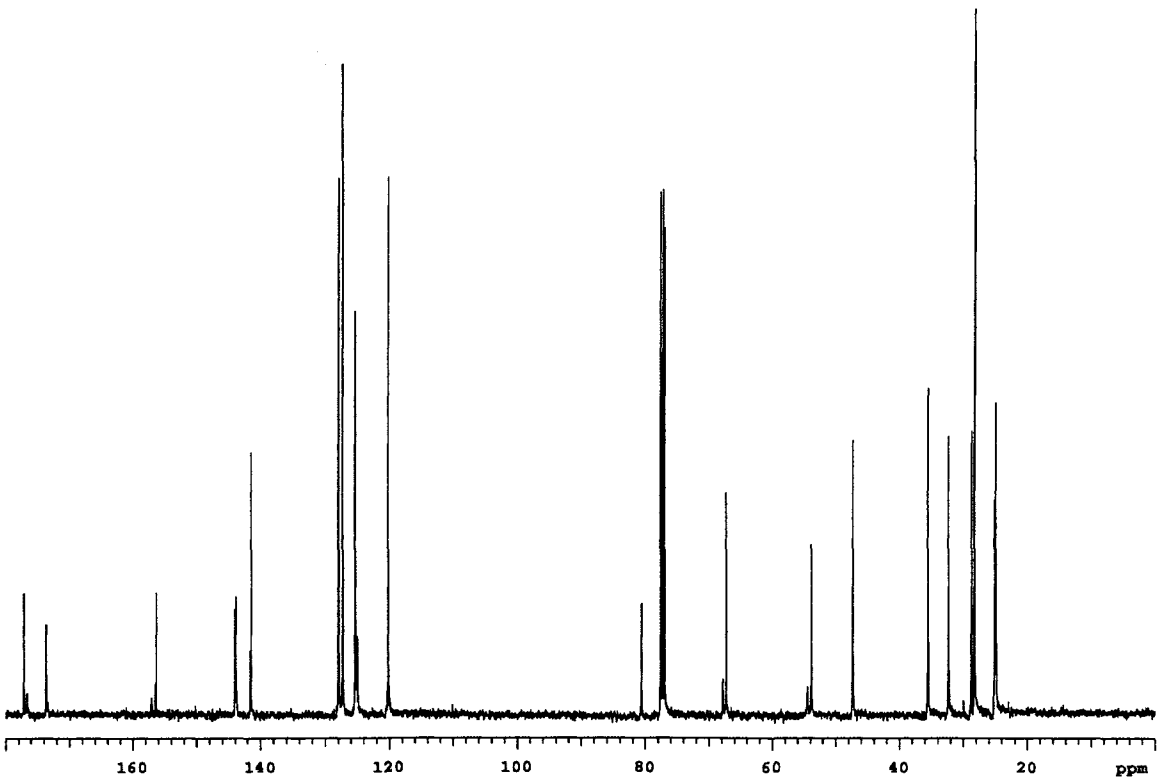

Appendix 2

Peptide Characterization

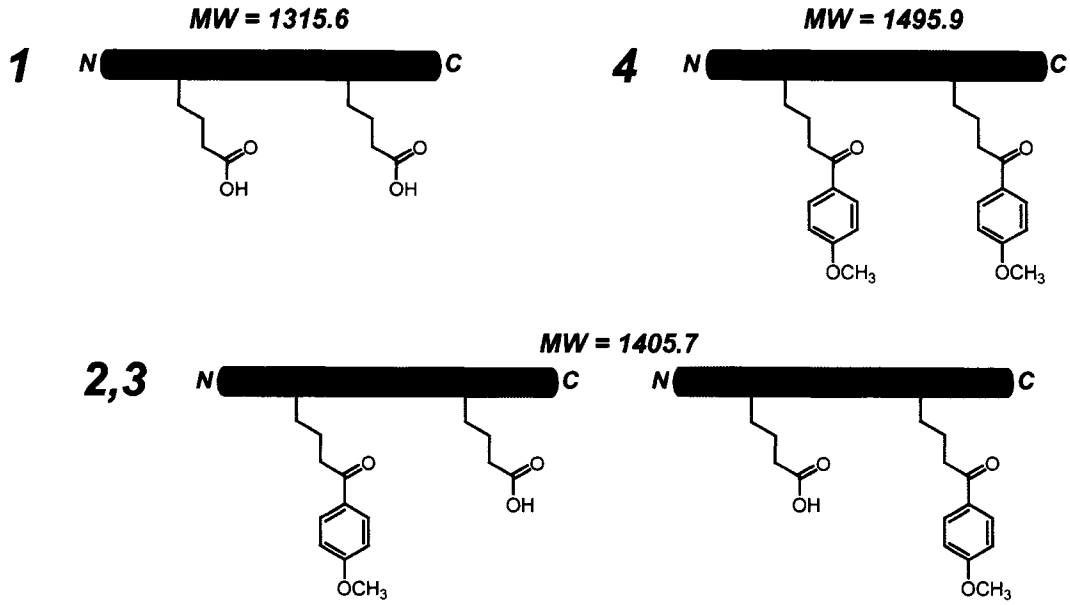

Figure 1. Chemical structures consistent with observed molecular weights for peaks 1-4 in crude HPLC traces Boc HGlu peptide (Chapter 2, Figure 2). Molecular weights are as calculated for the given structures, which correspond to the measured molecular weights in Figure S-3.

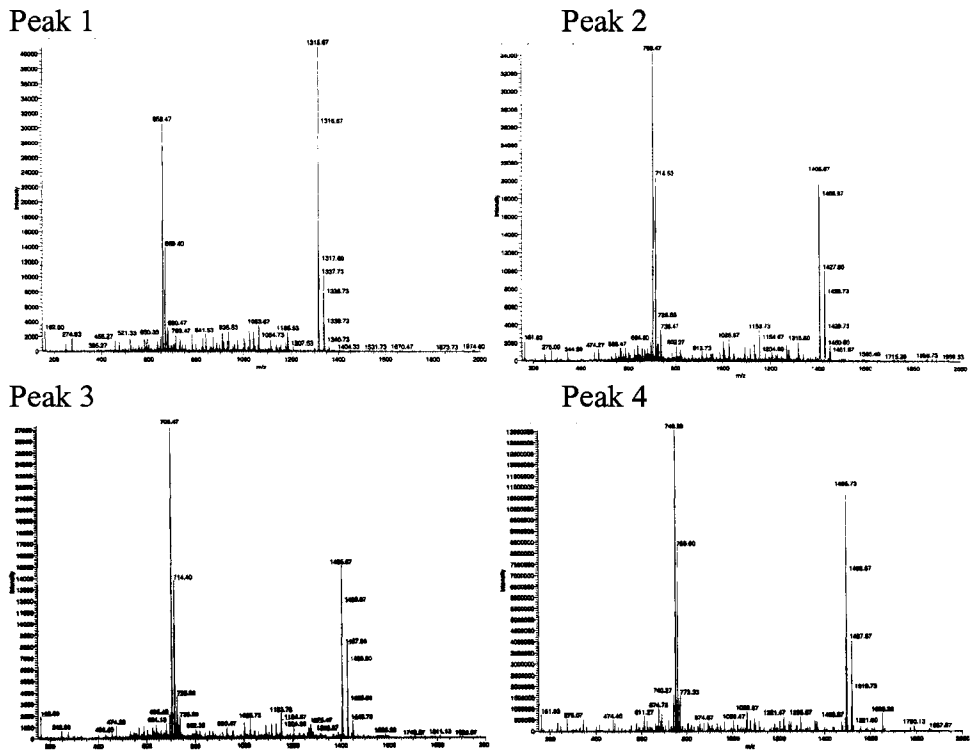

Figure 2. Electrospray mass spec data for peaks 1-4 isolated from crude HPLC traces of Boc HGlu test peptide (Chapter 2, Figure 2)

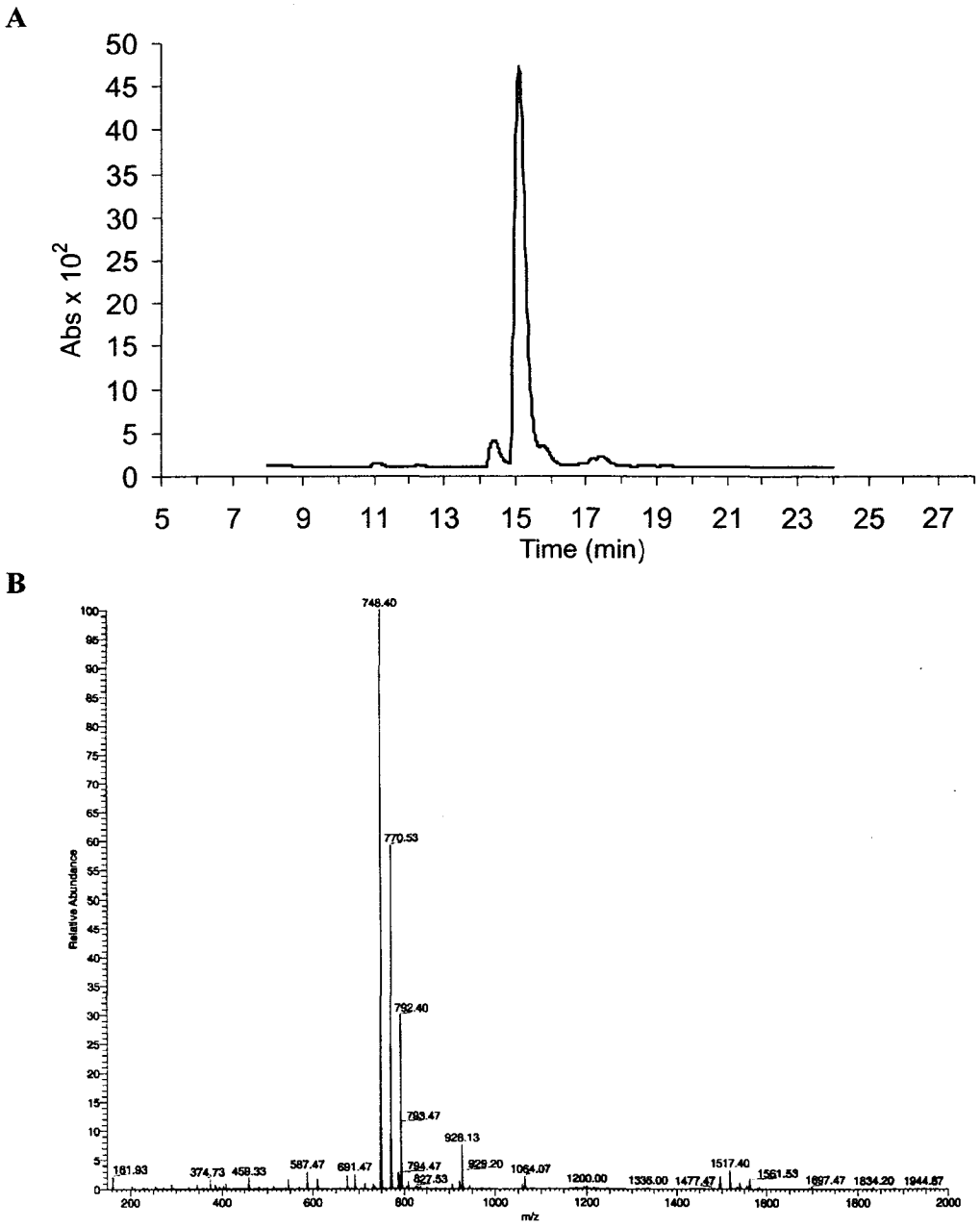

Figure 3. Characterization of Fmoc HGlu test peptide. (A) HPLC of crude peptide, (B) Electrospray mass spec data of purified material (MW_{calc} = 747.4, Chapter 2, Figure 4).

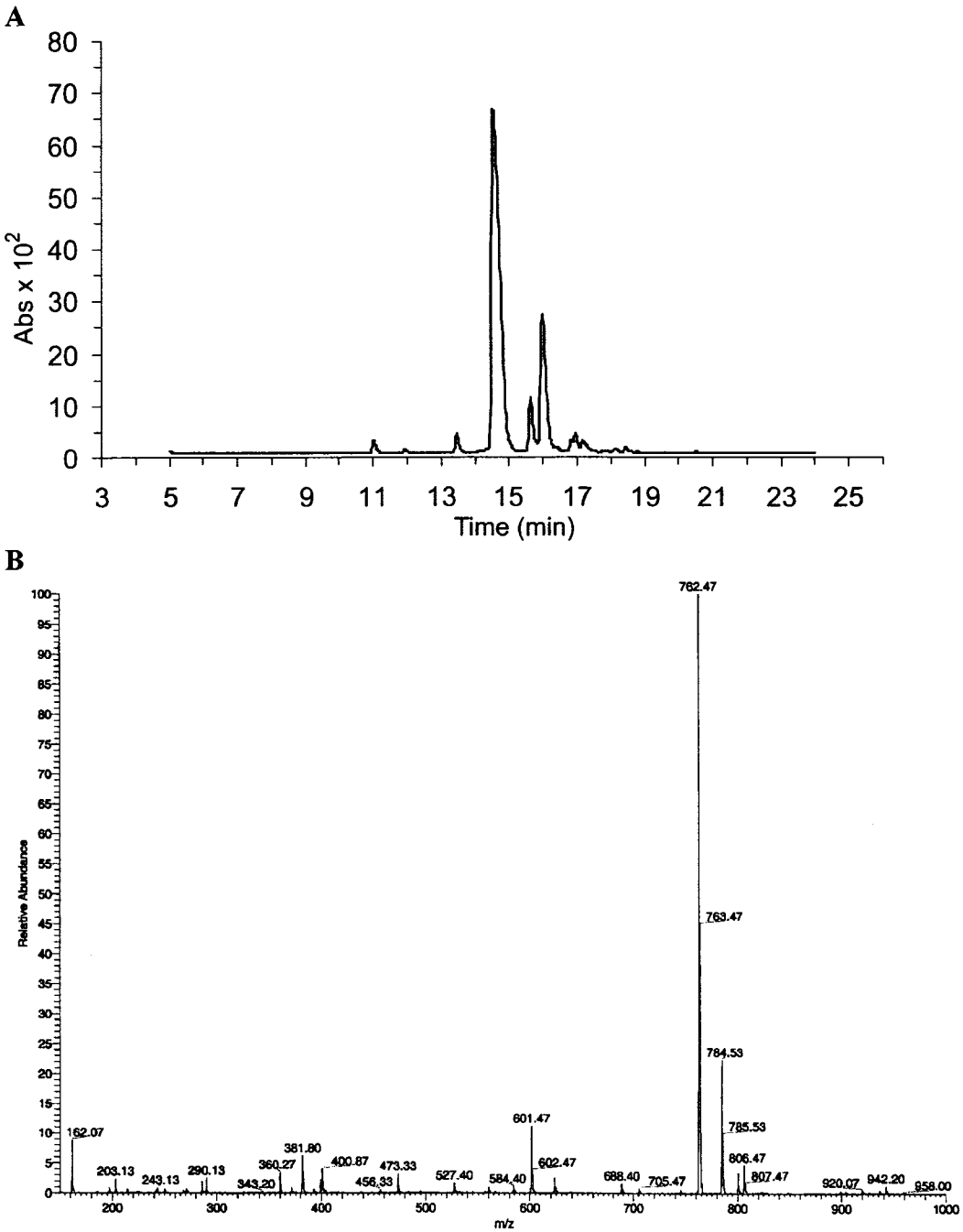

Figure 4. Characterization of Fmoc HHGlu test peptide. (A) HPLC of crude peptide, (B) Electrospray mass spec data of purified material (MW_{calc} = 761.4, Chapter 2, Figure 5).

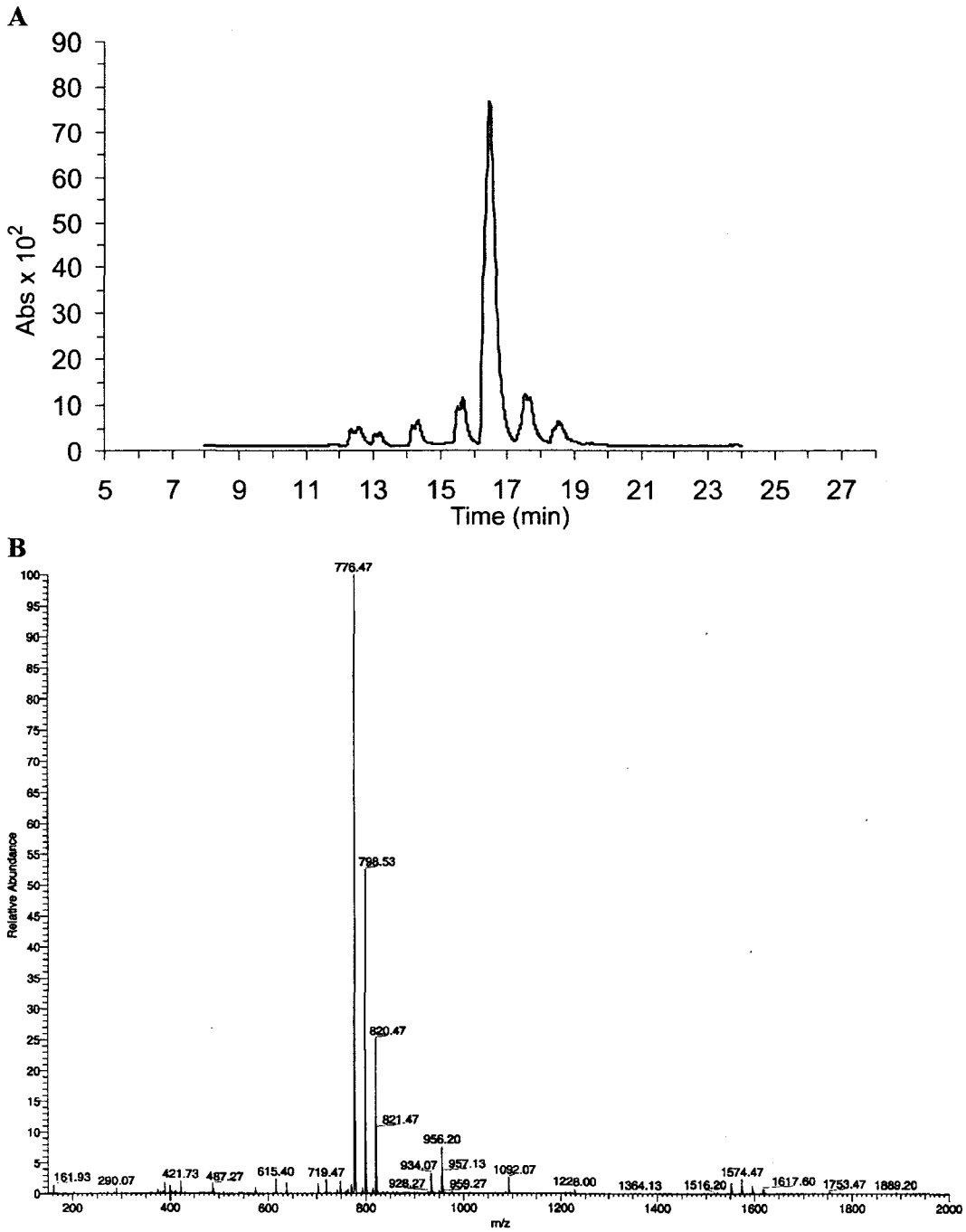

Figure 5. Characterization of Fmoc HHHGlu test peptide. (A) HPLC of crude peptide, (B) Electrospray mass spec data of purified material (MW_{calc} = 775.5, Chapter 2, Figure 5).

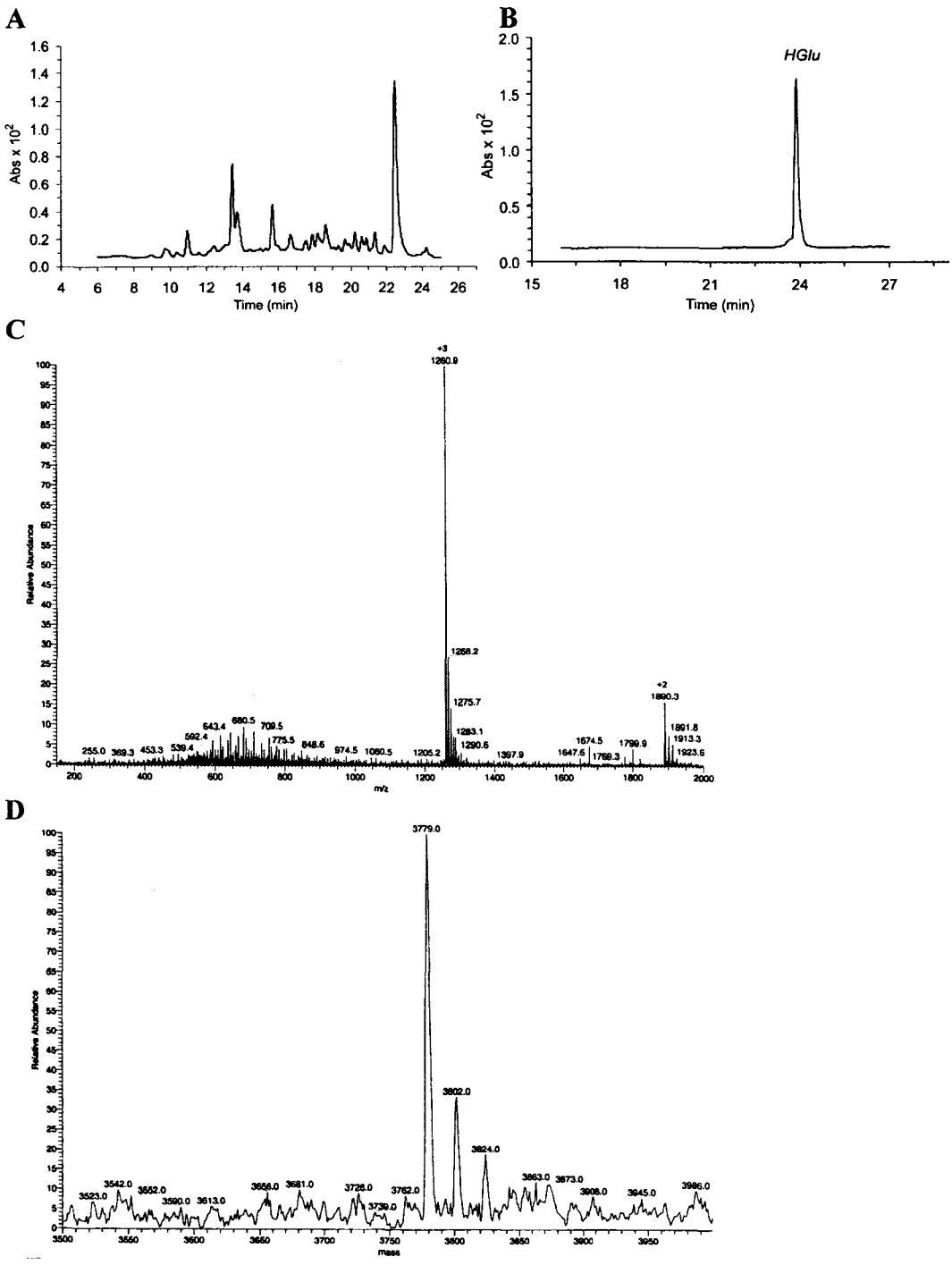

Figure 6. Characterization of full length HGlu peptide (Chapter 2, Figure 6 and Chapter 3, Figure 2). (A) HPLC of crude peptide, (B) HPLC of purified material (C, D) Electrospray mass spec raw (C) and deconvoluted (D) data for purified material (MW_{calc} = 3778.0).

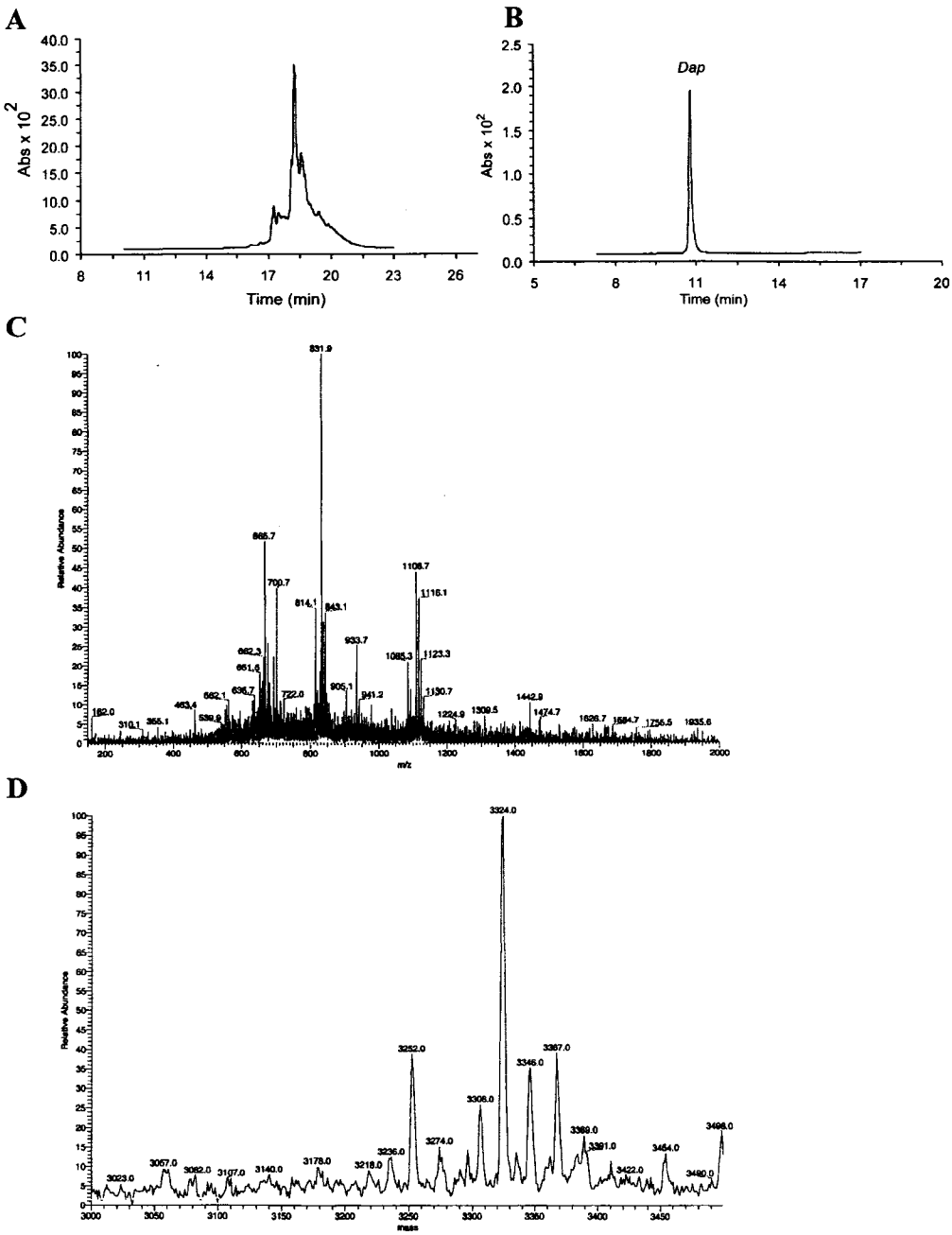

Figure 7. Characterization of full length Dap peptide (Chapter 3, Figure 2). (A) HPLC of crude peptide, (B) HPLC of purified material (C, D) Electrospray mass spec raw (C) and deconvoluted (D) data for purified material (MW_{calc} =3323.9)

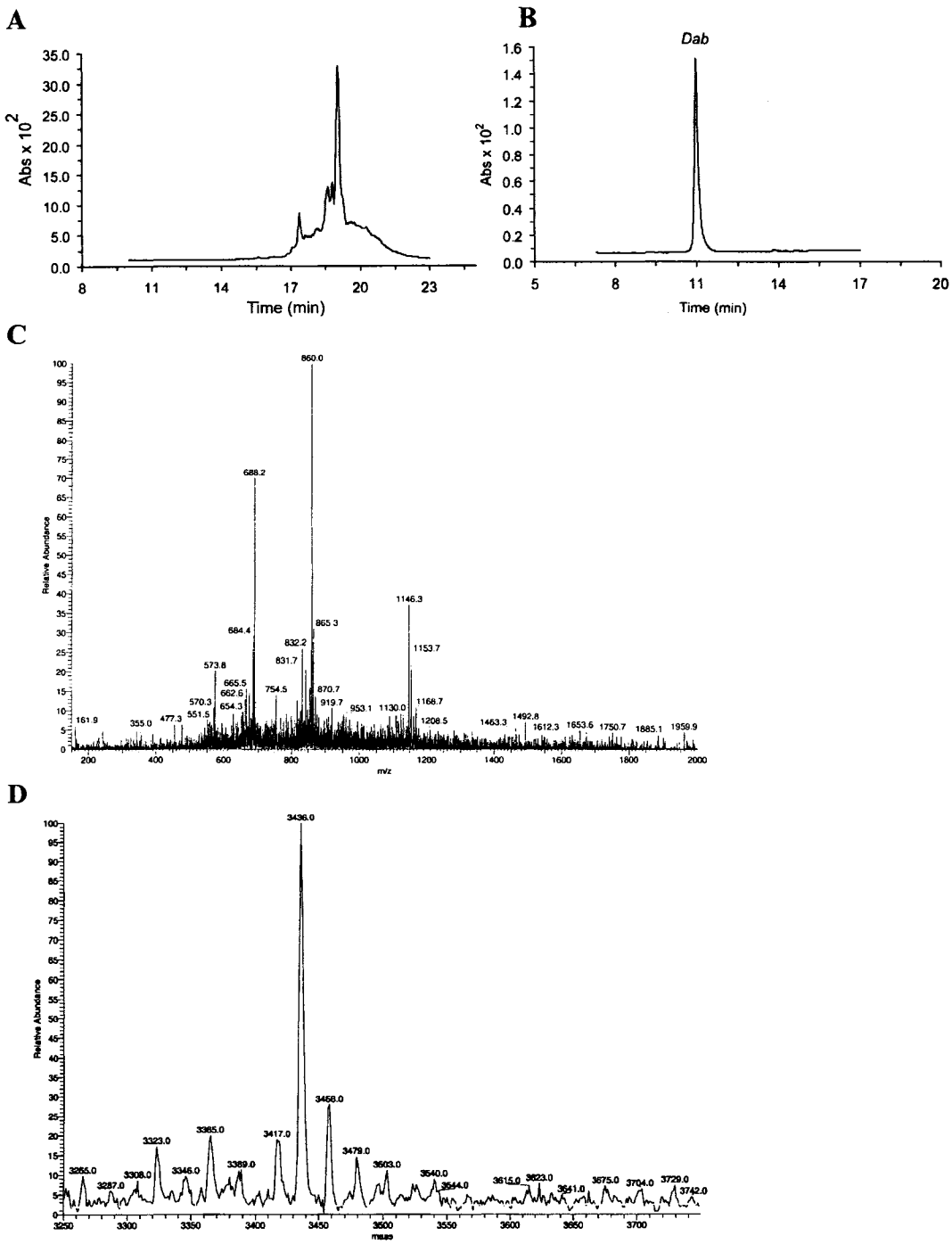

Figure 8. Characterization of full length Dab peptide (Chapter 3, Figure 2). (A) HPLC of crude peptide, (B) HPLC of purified material (C, D) Electrospray mass spec raw (C) and deconvoluted (D) data for purified material (MW_{calc} =3436.2)

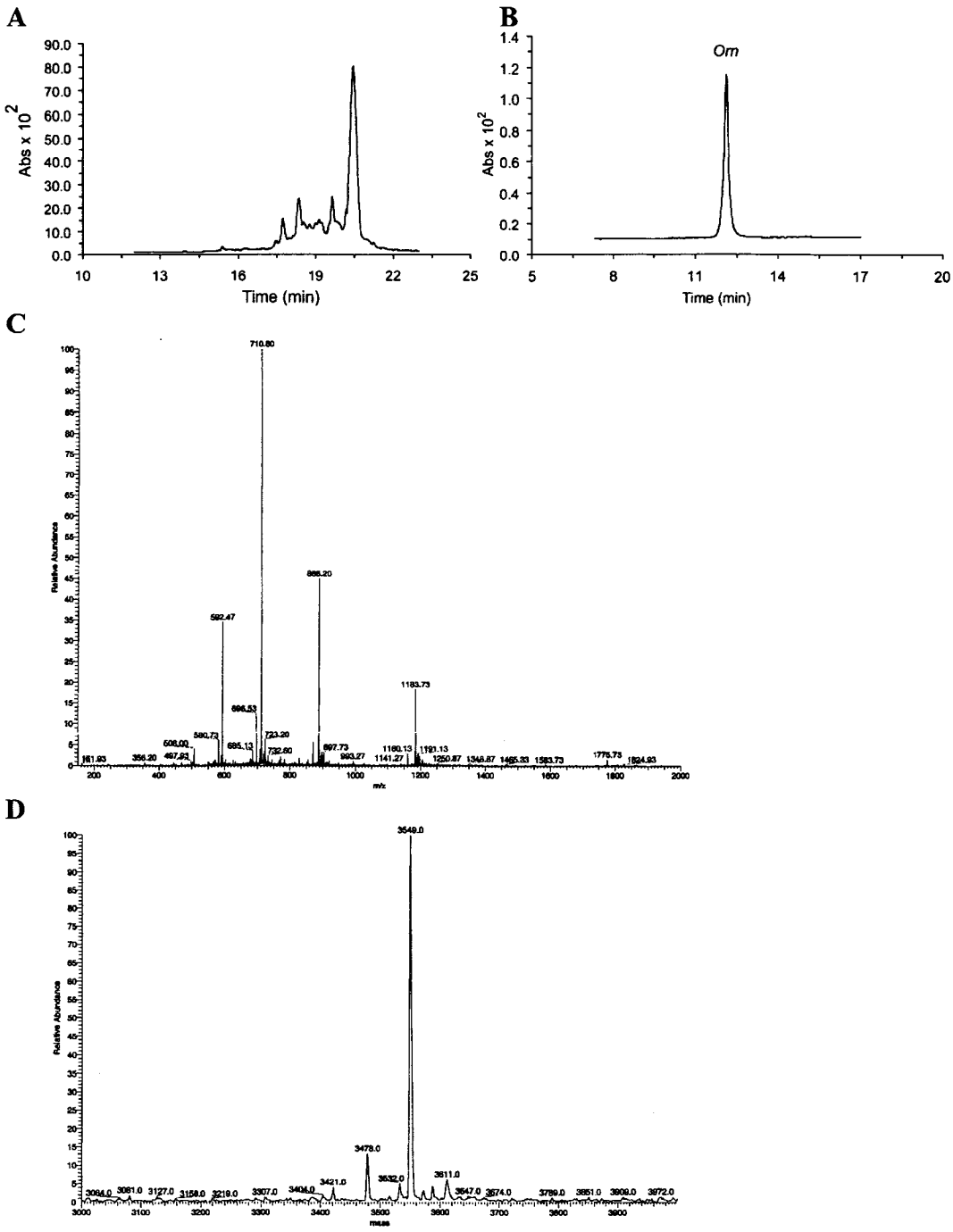

Figure 9. Characterization of full length Orn peptide (Chapter 3, Figure 2). (A) HPLC of crude peptide, (B) HPLC of purified material (C, D) Electrospray mass spec raw (C) and deconvoluted (D) data for purified material (MW_{calc} =3548.4)

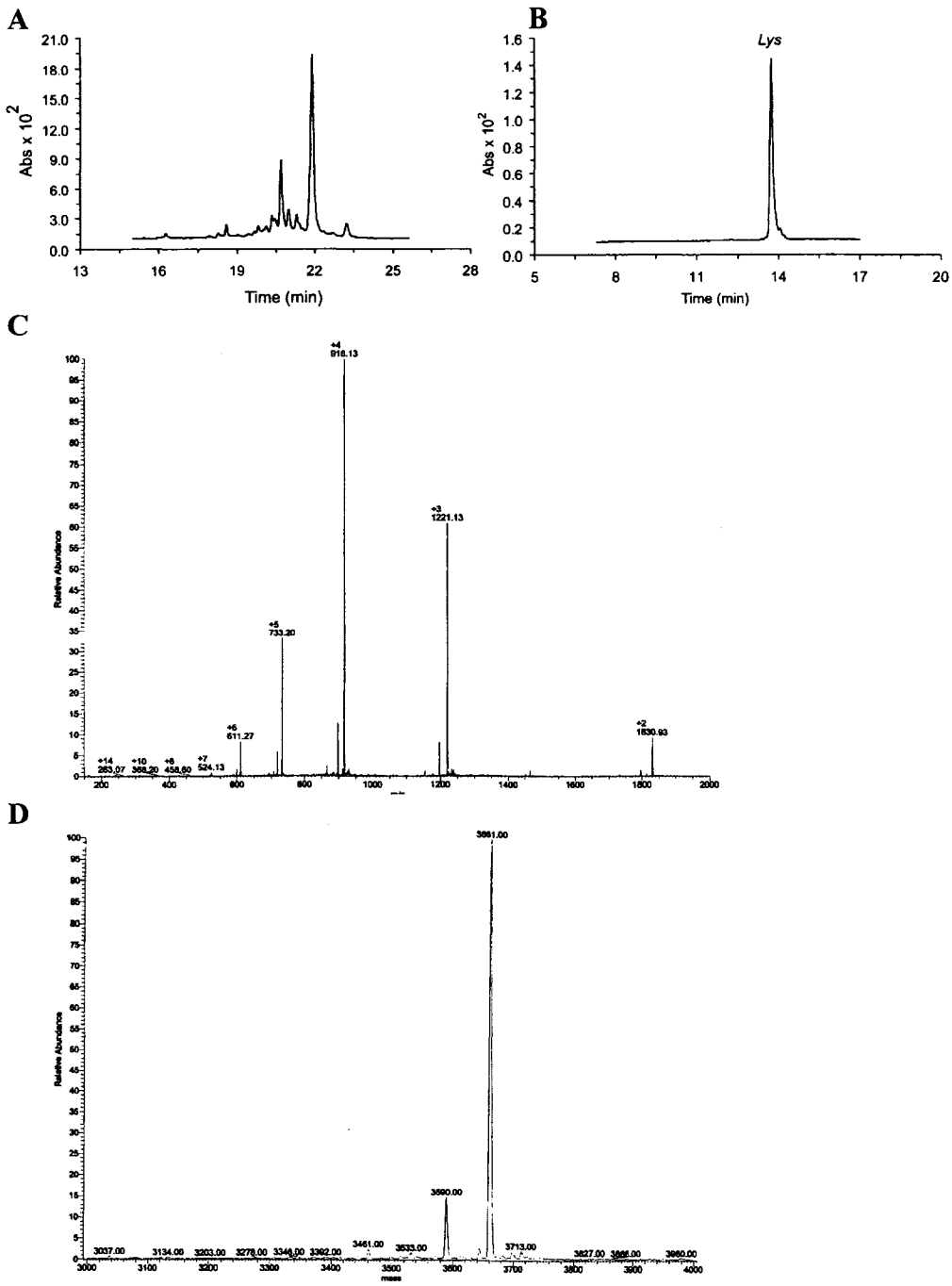

Figure 10. Characterization of full length Lys peptide (Chapter 3, Figure 2). (A) HPLC of crude peptide, (B) HPLC of purified material (C, D) Electrospray mass spec raw (C) and deconvoluted (D) data for purified material (MW_{calc} =3660.6)

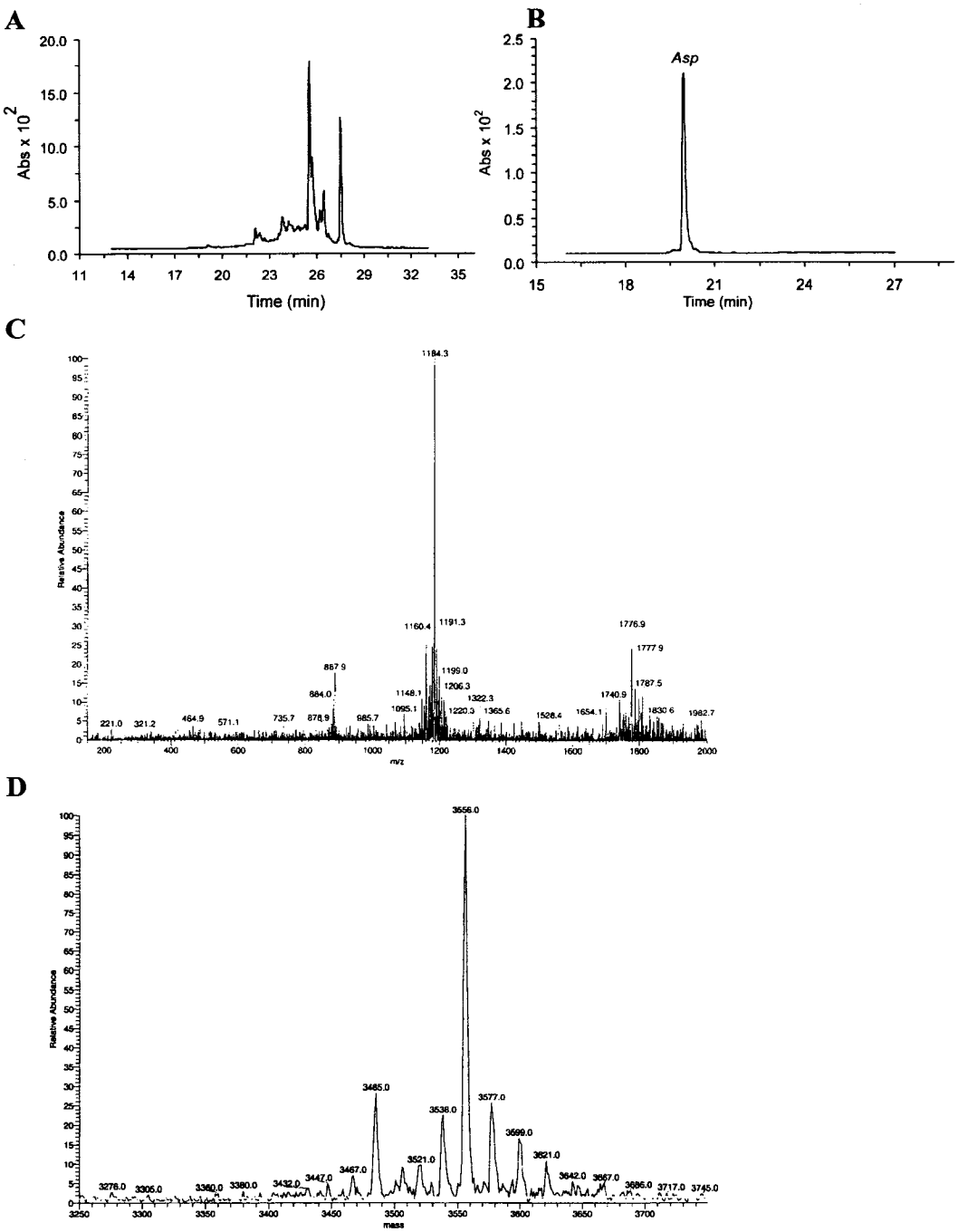

Figure 11. Characterization of full length Asp peptide (Chapter 3, Figure 2). (A) HPLC of crude peptide, (B) HPLC of purified material (C, D) Electrospray mass spec raw (C) and deconvoluted (D) data for purified material (MW_{calc} =3555.9)

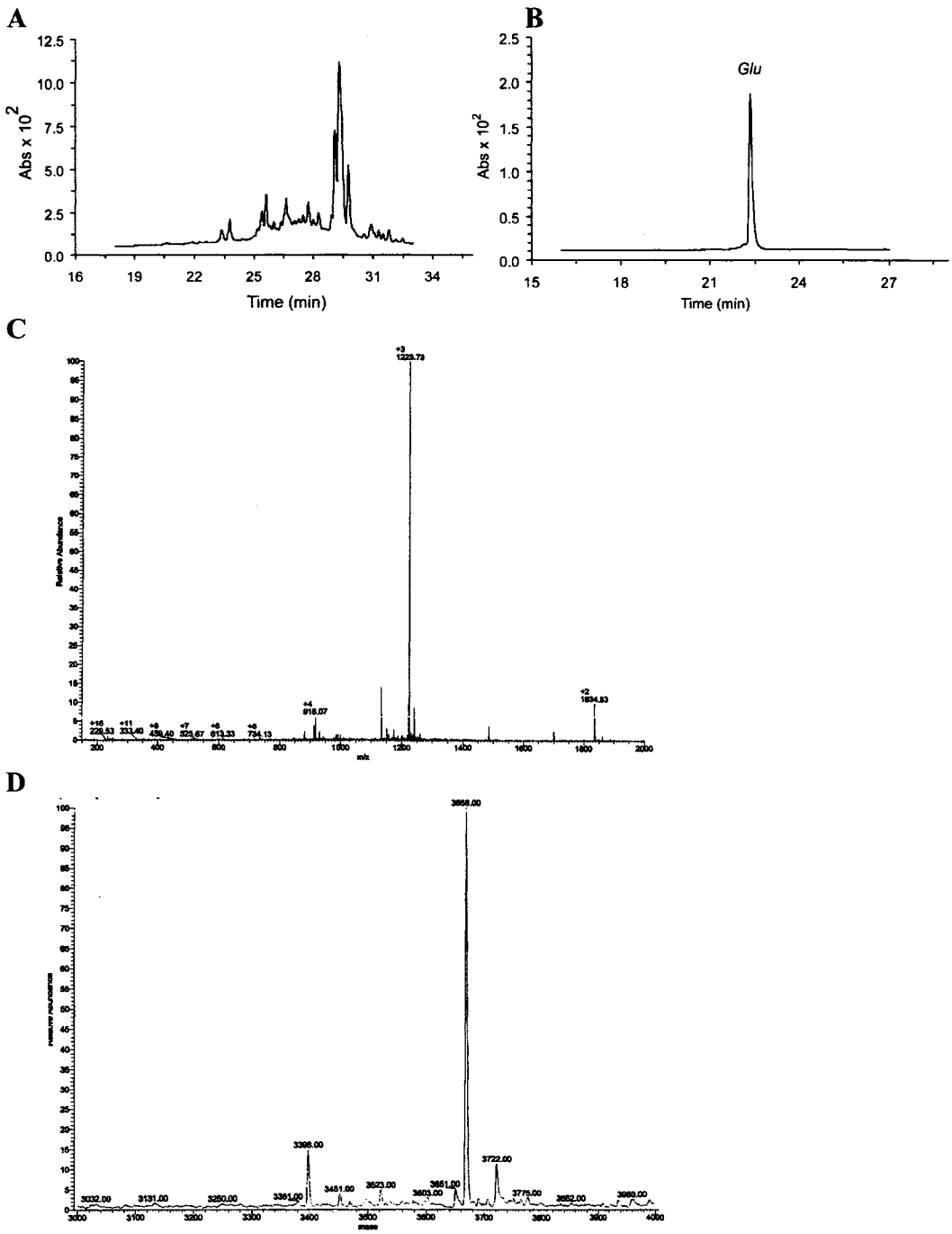

Figure 12. Characterization of full length Glu peptide (Chapter 3, Figure 2). (A) HPLC of crude peptide, (B) HPLC of purified material (C, D) Electrospray mass spec raw (C) and deconvoluted (D) data for purified material (MW_{calc} =3668.1)

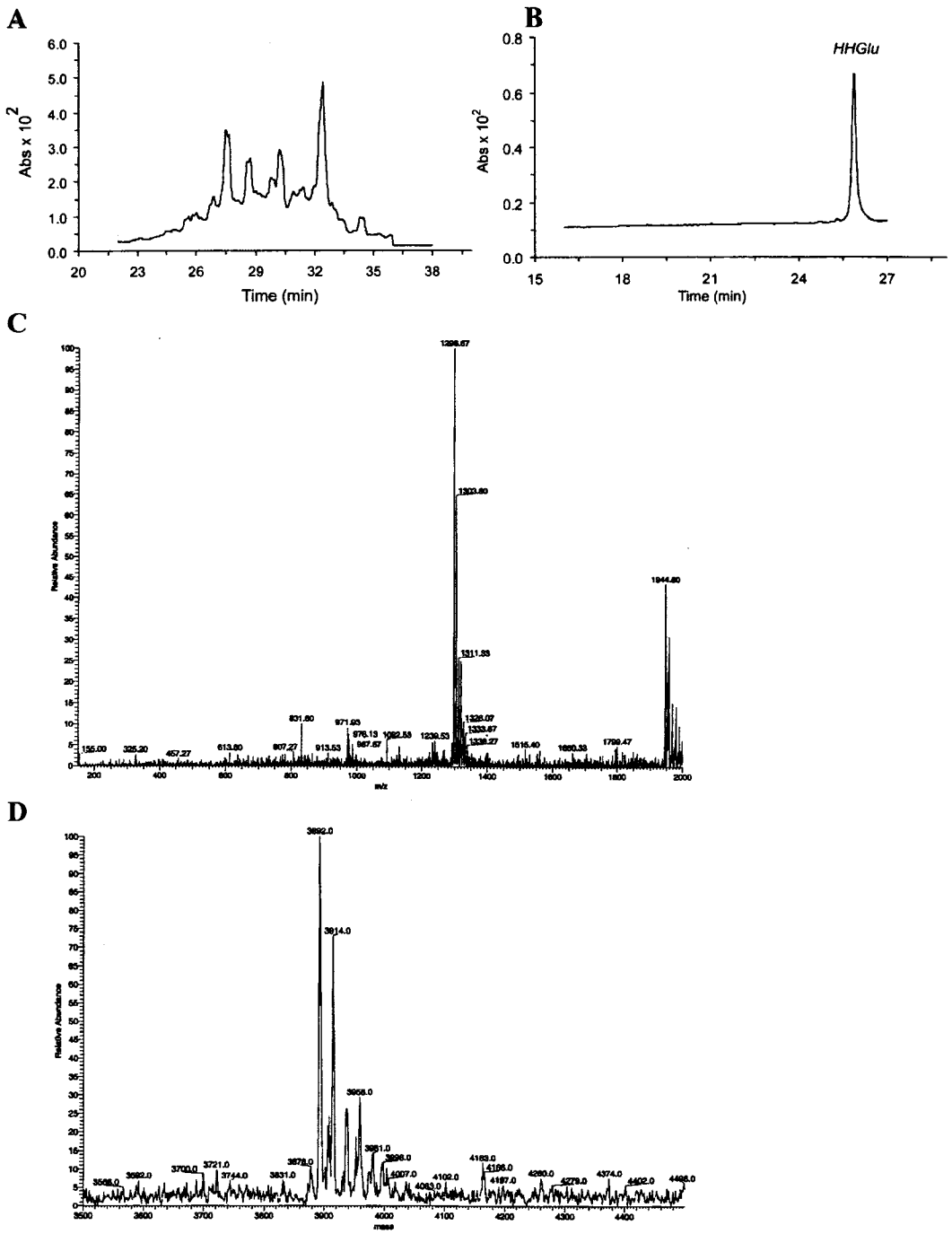

Figure 13. Characterization of full length HHGlu peptide (Chapter 3, Figure 2). (A) HPLC of crude peptide, (B) HPLC of purified material (C, D) Electrospray mass spec raw (C) and deconvoluted (D) data for purified material (MW_{calc} =3892.5)